A Study On The Improvement Of Surface Plasmon-Polariton (SPLP) Method For The Determination Of Compelx Dielectric Permittivity $\dot{\varepsilon}_2$ And Thickness h Of Thin Metal Films.

By
Shimeles Assefa

A thesis submitted in (part) fulfillment for the degree master of science in Physics in the Addis Ababa University.

June 1990

Dedicated to my father Assefa Alemu

and to my mother Yirgedu Zewdie.

ACKNOWLEDGEMENT

I am forever grateful to my advisor Dr. D.A.Letov for his attention, benevolence and effective help. I wish to express my appreciation to Dr. D.A. Letov for his initiation to the remarkable mofification of the exsiting SPLP method we devised and for the results obtained there of.

Finally, with a great sense of debt, I thank W/o. Birikty Paulos for her unfailing and unflagging efforts to cope with the typing of the thesis with its seemingly ceaseless revisions.

Shimeles Assefa

June 1990

ABSTRACT

The existing SPLP method for the determination of the complex dielectric permittivity and the thickness of metal film is reviewed. A close electrodynamic analysis of SPLP dispersion properties in very thin metal films is made. The analysis is based on the numerical solution of the exact dispersion equation using the 'Downhill' method and subsequent selection of physically reasonable results. The selection is performed via the comparison of the power flows through the boundaries of the metal film in the transverse direction.

The explicit expressions for the components of the power flow in the Kretschmann Prism-Metal Film-Air configuration have been derived.

Analysis made showed that splitting of the classical dispersion equation into two branches (ω^- mode and ω^+ mode) known in literature for the case of symmetric environment occurs also for the case of asymmetric environment, but the ω^+ mode branch is represented by a number of discrete points only. It was also shown that part of the ω^+ mode branch known in literature is physically unreal.

In addition to the two branches mentioned a third 'side' branch have been found, which turned out to be physically unreal.

The study of physically significant results revealed back-bending segments in the ω^- and ω^+ branches which demonstrate the phenomena of artificial anomalous dispersion.

The developed technique of the numerical solution of the exact dispersion equation allows to extend applicability of the SPLP method to the case of very thin metal films and puts no restrictions on the type of the environment.

C O N T E N T S

Introduction

Many of the fundamental properties (electronic) of the solid state can be successfully described by

(a) the analogy of single electron moving in the periodic array of atoms, and

(b) the plasma concept: the free electrons of a metal are treated as an electron liquid (or gas) of high density of about $10^{23} cm^{-3}$, ignoring the lattice in a first approximation. From this approach, it follows that longitudinal density fluctuations, plasma oscillations, will propagate through the volume of the metal. The quantum of these "Volume Plasmons" has an energy $\hbar\omega_{pe} = \hbar\left(\frac{4\pi n_e e^2}{m_e}\right)^{\frac{1}{2}} \sim 10eV$. An important extension of the plasmon physics has been accomplished by the concept of "Surface Plasmons". Their existence has been demonstrated in electron energy-loss experiments by Powell and Swan [11]. The electon charges on a metal boundary can perform Coherent fluctuations which are called surface Plasma Oscillations Ritchie [12].

Maxwell's theory shows that electromagnetic surface waves can propagate along semi-infinite metallic surface with a broad spectrum of eigen frequencies from $\omega=0$ to $\frac{\omega_p}{\sqrt{2}}$ depending on the wave vector $\vec{k}$. The frequency ω of these longitudinal oscillations is tied to its wave vector k_x by a dispersion relation $\omega(k_x)$. These charge fluctuations, which can be localized in the y (normal to interface) direction are accompanied by a mixed transversal and longitudinal electromagnetic field which disappears at $|y| \to \infty$, and has its maximum in the surface $y = 0$, typical for surface waves. This explains their sensitivity to surface properties.

The dispersion relation $\omega(k_x)$ for surface plasmons lies right of the light line which means that the surface

plasmons have a longer wave vector than light waves of the same energy $\hbar\omega$, propagating along the surface. This means that the surface plasmons (SP_s) cannot transform into light: it is a "nonradiative" surface plasmon (SP). Therefore on a semi-infinte metal surface, surface plasmons (SP_s) cannot couple with light.

In general, when an electromagnetic wave propagates through a condensed medium, its properties are modified by its coupling to the elementary excitations of the medium. The coupled excitation is frequently referred to as a polarition and consists of a photon coupled to a plasmon, optical phonon, magnon, etc. We refer to a photon coupled to a surface plasmon (SP) as surface plasmon-polarition (SPLP). In the literature the expression "surface plasmon-polarition" is often used which is identical to the term surface plasmon (SP). This excitation of SP modes with light needs special light-plasmon coupler known as prism coupler (ATR device). With the exitation of SP modes by light, a strong enhancement of the electromagnetic field in the surface (resonance amplification) is combined, which can be rather strong.

In an ATR (attenuated total refrection) device, the metal is in a form of a thin film deposited on the base of the prism surface.

Concentration of the electromagnetic field near the thin metal surface makes SPLP very sensitive to minor changes in characteristic quantities of intefacing media (like $\dot{\varepsilon}_2 = \varepsilon'_2 + i\varepsilon''_2$ of the film) and to the state of roughness of the boundary.

Therefore SPLP constitutes a highly sensitive non-destroying probe for measuring purposes, particularly in the optical and infrared range of frequencies.

Note: All complex quantities in the text are distingusished by a dot put above the character.

CHAPTER I

The Existing Method of Determination of Complex Dielectric Permittivity $\dot{\varepsilon}_2$ and Thickness h of a Thin Metal Film by SPLP Technique

1.1 Formation of SPLPs in an ATR Device.

The dispersion relation of SP_s propagating along semi-infinite metal surface boundering a dielectric medium ε_1 is given by [9]

$$\dot{k}_x^o = \frac{\omega}{c}\left(\frac{\varepsilon_1 \dot{\varepsilon}_2}{\varepsilon_2 + \dot{\varepsilon}_2}\right)^{1/2} \qquad (1.1)$$

With real ω and ε_1. Also $\dot{\varepsilon}_2 = \varepsilon_2' + i\varepsilon_2''$, under these conditions we obtain a complex $\dot{k}^o = k_x'^o + ik_{xo}'$ with

$$k_{xo}' = \left(\frac{\varepsilon_1 \dot{\varepsilon}_2}{\varepsilon_1 + \varepsilon_2'}\right)^{1/2} \cdot \frac{\omega}{c} \qquad (1.2)$$

and

$$k_{xo}'' = \frac{\omega}{c}\left(\frac{\varepsilon_1 \varepsilon_2'}{\varepsilon_1 + \varepsilon_2'}\right)^{3/2} \frac{\varepsilon_2''}{2(\varepsilon_2')^2} \qquad (1.3)$$

assuming $\varepsilon_2'' << |\varepsilon_2'|$. For eal k_{xo}' one needs $\varepsilon_2' < 0$ and $|\varepsilon_2'| > \varepsilon_1$. The medium with negative dielectric function is usually called "active medium". This expresses the fact that the coupling between the free electromagnetic field and the dipoles giving rise to SP_s occurs in this medium. Since a negative $\varepsilon_2'(\omega)$ implies an imaginary index of refraction in the absence of damping, the surface active medium is typically highly reflecting in the frequency range where SP_s propagate.

The DR (dispersion relation) of SP_s approaches the line $\frac{\omega}{c}\sqrt{\varepsilon_1}$ at small k_{xo}', but remains larger than $\frac{\omega}{c}\sqrt{\varepsilon_1}$, so that the SP_s cannot transform into light: it is a "non radiative" SP. At large k_{xo}', $\varepsilon_2' \to -\varepsilon_1$ and the value of ω approaches, assuming the metal as a free electron gas,

$$\omega_{sp} = \frac{\omega_p}{(1+\epsilon_1)^{\frac{1}{2}}} \qquad (1.4)$$

i.e., at small values of the wave vector, the surface polarition is primarily photon-like, whereas at large values of the wave vetor, it is primarily plasmon-like. In the latter case V_g and $V_{ph} \to 0$, so that the SP resembles a localized fluctuation of the electron plasma. The region of finite k'_{xo} (resonance region) is the region in which we expect surface plasmon (SP) - photon coupling to take place. By resonance we mean a condition in which the frequencies and wave vectors of both particle are approximately equal. The light line and the horizontal line at $0.707\omega_p$ are the dispersion relations for photons and surface plasmons in the absence of any coupling between them. The region of the crossover of these two curves is the resonance region. In reality, however, there always is coupling implicit in Maxwell's equations and expressed by the dielectric function. The dispersion curve given by the disperson eqn. (2) shows this implicit coupling.

The field amplitude of the SP_s decreases exponentially as exp $(-|\dot{k}yi||y|)$, normal to the surface. The value of the (skin) depth at which the field falls to 1/e, becomes

$$\hat{y}_i = \frac{1}{|\dot{k}_{yi}|} \qquad (1.5)$$

Where $\dot{k}_{yi}$ are given by

$$\dot{k}_{yi} = \left(\frac{\omega}{c}\right)^2 (\epsilon_1 - \dot{k}_{xo}^2)^{\frac{1}{2}} \qquad (1.6)$$

At large k'_{xo}, $\hat{y}_i$ is given by about $1|k'_{xo}$ leading to a strong concentration of the field near the surface in both media. At low k'_{xo} or large $|\epsilon'_2|$ values, the field in air has a strong (transverse) component E_y compared to the (longitudinal) component E_x, namely $E_y/E_x = -i|\epsilon'_2|^{\frac{1}{2}}$ and extends far into the air space- it resembles thus a guided photon field (Zenneck-Sommerfeld wave). In the metal, E_y is small against E_x since $E_y/E_x = i|\epsilon'_2|^{-\frac{1}{2}}$. These relations are derived from derived from $\text{div}\vec{E} = 0$, valid outside the surface air/metal.

At large k'_{xo} both components E_x and E_y become equal;

$$E_y = \pm iE_x \quad \text{(air : + i, metal : -i)}.$$

The intensity of SP_s propagating along a smooth surface decreases as $\exp(-2k''_{xo})$ with k''_{xo} from eqn.(3). The length Li after which the intensity decreases to 1/e is then given by

$$L_i = (2k''_{xo})^{-1} \tag{1.7}$$

The field of SP_s is described by

$$\vec{E} = \vec{E}^{+}_{o} \exp\left[+ i(k_{xo}x \pm k_{yi}y - \omega t)\right] \tag{1.8}$$

with + for $y \geq 0$, - for $y \leq 0$, and with imaginary k_y , which causes the exponential decay of the field E_y. The wave vector k_x lies parallel to the x direction - k_x lies parallel to the x direction - $k_x = \frac{2\pi}{\lambda p}$, where λp is the wave length of the plasma oscillation. Maxwell's equations yield the retarded dispersion relation given by eqn. (1).

The application of photons to excite SP_s meets the difficulty that the sispersion relation lies right from the light line ($k'_{xo} > \frac{\omega}{c}$). At a given photon energy $h\omega$ the wave vector $\frac{\hbar\omega}{c}$ has to be increased by a Δk_x value inorder to "transform" the photons into SP_s.
In an ATR device, its momentum becomes $(\frac{\hbar\omega}{c})\sqrt{\varepsilon_3}$, where ε_3 is the dielectric constant of the prism, instead of $\frac{\hbar\omega}{c}$ and its projection on the surface is

$$k'_x = \frac{\omega}{c}\sqrt{\varepsilon_3}\sin\theta_o \tag{1.9}$$

The dispersion relation given by eqn. (1) for SP_s propagating on the interface $\varepsilon_1 / \varepsilon_2$ (air/metal) can thus be satisfied between lines c, beyond which limit total reflection at an interface 3/2 takes place, and $C/\sqrt{\varepsilon_3}$. The excitation of SP is recognized as a minimum in the (totally reflected intensity (ATR minimum).

Another way to understand the formation of SP_s in this device (ATR): Since the excitation of SP_s occurs in the region of total reflection at the interface prism/metal, an evanescent light wave with a phase velocity

$$v_{ph} = \frac{\omega}{k'_x} = c/\sqrt{\varepsilon_3}\sin\theta_0, \text{ with}$$

$\sqrt{\varepsilon_3}\sin\theta_0 > 1$ propagates in the interface with $v_{ph} \leq c$.

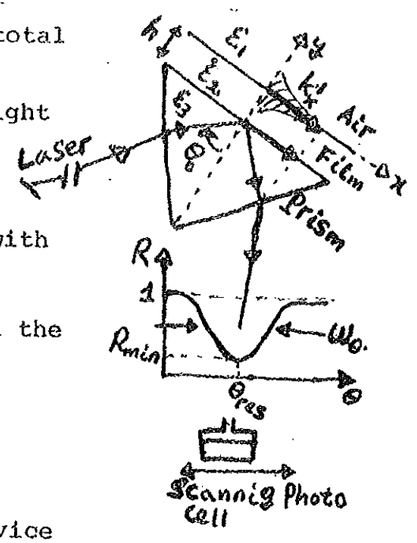

Fig. 1
ATR Device
(Kretschmann Configuration)

Since the light line $c/\sqrt{\varepsilon_3}$ in medium 3 (prism) lies to the right of the dispersion relation of SP_s up to certain k'_x, light can excite SP_s of frequencies ω below the crossing point of $c/\sqrt{\varepsilon_3}$ and DR of SP_s on the metal/air side. The SP_s on the interface 3/2 cannot be excited, since the DR of their SP_s lies to the right of $c/\sqrt{\varepsilon_3}$ because $\varepsilon_3 > 1$. This can be checked by replacing ε_1 by ε_3 in eqn. (1).

The resonance condition for SP_s is

$$v_{ph,SP_s} = v_{ph'\ evenescent\ wave} \qquad (1.10)$$

which implies

$$\frac{\omega}{k'_{xo}} = c\left(\frac{\varepsilon'_2\varepsilon_3}{\varepsilon_1+\varepsilon'_2}\right)^{1/2} = c/\sqrt{\varepsilon_3}\sin\theta_{res} \qquad (1.11)$$

can thus be fulfilled, particularly because the character of both waves is the same. The electromagnetic field of the evanesxcent wave decreases exponentially in the film and excites the SP_s on the metal/air interface.

1.2 Determination of $\dot{\varepsilon}_2$ and h of a thin metal film by SPLP technique.

The qvantitative description of the minimum of the reflected intensity R can be given by Fresnel's equations for the three-layer system 3/2/1: 3 dielectric medium, prism; 2 metal film of thickness h ; 1 dielectric, air or vacuum, etc. The reflectivity R for P-polarized light, with E_o the incoming and E_r the reflected field, is given by

$$R = |r_{321}|^2 = \left|\frac{E_r}{E_o}\right|^2 = \frac{r_{32} + r_{21}\exp(2ik_{2yh})}{1+r_{32}r_{21}\exp(2ik_{2yh})} \qquad (1.12)$$

with
$$r_{ik} = \left(\frac{k_{yi}}{\varepsilon_i} - \frac{k_{yk}}{\varepsilon_k}\right) / \left(\frac{k_{yi}}{\varepsilon_i} + \frac{k_{yk}}{\varepsilon_k}\right) \qquad (1.13)$$

where r_{iks} are the relative amplitudes of the reflected to incident waves on a given interface or Fresnel's reflection coefficients for plane polarized wave.

Under the special conditions $|\varepsilon_2'| >> 1$ and $|\varepsilon_2''| << |\varepsilon_2'|$ this dependence can be approximated in the region of the resonance by the Lorentzian type relation which reveals its physical meaning:

$$R \to R_{min}$$

$$R_{min} = 1 - \frac{4\eta}{(1+\eta)^2} \quad \text{with } \eta = \frac{k''_{xo}}{\Delta k''_x} \qquad (1.14)$$

$$\text{Using } \dot{k}_x = \dot{k}_{xo} + \Delta\dot{k}_x \qquad (1.15)$$

with k'_x given by eqn. (9) and k'_{xo} given by eqn. (2) the resonance wave vector $(\dot{k}_{xo} + \Delta\dot{k}_x)$ is different from eqn. (1), which is valid only for a semi-infinite metal;here we have a finite metal film of thickness h between two dielectrica. The term $\Delta\dot{k}_x$ can be approximated for $\exp(2i\dot{k}_{2yh}) << 1$ by

$$\Delta\dot{k}_x = \dot{r}_{32}^{o} \; 2 \left(\frac{\omega}{c}\right) \frac{1}{\epsilon_1 - \epsilon'_2} \left(\frac{\epsilon_1 \epsilon_2}{\epsilon_1 + \epsilon'_2}\right)^{3/2} \exp(2i\dot{k}_{2y}^{o} h) \tag{1.16}$$

or

$$\Delta k_x = \text{Const. } \dot{r}_{32} \; (k'_{xo}) \tag{1.17}$$

$\dot{r}_{32}$ is the coefficient of reflection

Its real part causes a displacement of the resonance position compared to k'_{xo} ,

$$\text{Re } [\Delta\dot{k}_x] = \text{Const. Re } [\dot{r}_{32}(k'_{xo})] \tag{1.18}$$

Its imaginary part gives an additional damping term,

$$\text{Im } [\Delta\dot{k}_x] = \text{Const. Im } [\dot{r}_{32}(k_{xo})] \tag{1.19}$$

which we call radiation damping, to the internal damping Im $(\dot{k}_{xo})$.

where r_{32} $(\dot{k}'xo)$ is given by

$$r_{32}(\dot{k}'xo) = \frac{(a^2 - \epsilon_3^2)}{a^2 + \epsilon_3^2} + i \frac{2a\epsilon_3}{a + \epsilon_3^2} \tag{1.20}$$

$$a^2 = [-\epsilon'_2 \; (\epsilon_3 - \epsilon_1) - \epsilon_3] \tag{1.21}$$

Equation (14) demonstrates that R passes a minimum which is zero for

$$\text{Im } [\dot{k}_{xo}] = \text{Im } [\Delta\dot{k}_x] \tag{1.22}$$

This matching condition fixes the thickness h_{opt} of the metal film at a given λ. However, the value of h_{opt} (optimum value of the thickness) depends on the dielectric function $\dot{\epsilon}_2$. Since it is not known exactly h_{opt} varies at least by 10%. The experimental arrangement (ATR device) is shown in Fig.1 This device is used for the determination of

of experimental variables θ_{res} , R_{min} , and ω_θ i.e; the resonance angle, minimum or reflectivity, and half-width of the reflection minimum.

The physics giving rise to the reflectivity minimum: the light wave, having passed the prism (ε_3), is partially reflected at the interface 3/2. Partially it traverses the film as an exponentially decaying wave. At interface 2/1 it induces excitations which radiate light back into the film. If the thickness h increases, the back scattered field disappears due to Im $[\Delta\dot{k}_x] \to 0$, so that R approaches the value unity.

For decreasing thickness h the back-scattered field increases. Since it is in antiphase with the incoming wave, see eqn. (12), the two interfere distructively thus reducing R. At $h = h_{opt}$ they even compensate each other and R becomes zero.

The antiphase radiation field, captured in the metal film, is converted into heat. In the resonance case $R = 0$ the total damping amounts to 2 Im $[\dot{k}_{xo}]$. This value determines the half-width of the reflection minimum. A further decrease of h leads to increasing Im $[\Delta\dot{k}_x]$ and has the effect that R assumes again a value close to unity.

From resonance condition eqn. (11), we have [13]

$$\xi'(\theta_{res}) = \frac{\varepsilon_1 \varepsilon_3 \sin^2\theta_{res}}{\varepsilon_1 - \varepsilon_3 \sin^2\theta_{res}} \qquad (1.23)$$

Note that eq (23) assumes $k'_x \approx k'_{xo}$.

The reflectance has a lorentz dip at $\theta_o = \theta_{res}$ with a half-width ω_θ (when Im $[\dot{k}_x] < R_e[\dot{k}_x]$)

$$\frac{\omega\theta}{2} = \frac{\text{Im}\,[\dot{k}_x]\cos\theta_{res}}{k_3} \qquad (1.24)$$

with $k_3 = \frac{\omega}{c}\sqrt{\varepsilon_3} = k_o\sqrt{\varepsilon_3}$ and

$$\theta_{res} = \arcsin\left[\frac{\mathrm{Re}[\dot{k}_x]}{k_3}\right] \tag{1.25}$$

Moreover,

$$\mathrm{Im}[\dot{k}_x] = \mathrm{Im}[\dot{k}_{xo}] + \mathrm{Im}[\Delta\dot{k}_x]$$
$$= \mathrm{Im}[\Delta\dot{k}_x][\eta + 1] \tag{1.26}$$

With

$$\eta = \frac{1 \pm \sqrt{R_{min}}}{1 \mp \sqrt{R_{min}}} \tag{1.27}$$

The choice of algebraic signs in eqn. (1.27) should be based upon the physical sense of which is clear from eqn (1.14). In the limiting case $h \to \infty$ $\mathrm{Im}[\Delta\dot{k}_x]$ should vanish, giving $\eta \to \infty$. This result can be achieved from eqn. (1.27) if the upper signs (both in the numerator and the denominator) are used with $R_{min} \to 1$. This case would be denoted as η_+. In the other limiting case $h \to 0$, the perturbation $\mathrm{Im}[\Delta\dot{k}_x]$ prevails over $\mathrm{Im}[\dot{k}_{xo}]$, therefore $\eta \to 0$. this result follows from eqn. (1.27) if the lower signs are used, with $R_{min} \to 1$. This case would be denoted as η_-.

This consideration of the limiting cases suggest that there must be a switch from the upper case to the lower case as h change from ∞ to 0. this abrupt change occurs at $h = h_{opt}$, when $R_{min} \to 0$.

From eqn. (1.26), we have

$$\mathrm{Im}[\dot{k}_x] = \mathrm{Im}[\dot{k}_{xo}]\left[\frac{\eta+1}{\eta}\right] \tag{1.28}$$

where Im $(\dot{k}_{xo})$ is given by

$$\text{Im}\left[\dot{k}_{xo}\right] = k_o \left(\frac{\varepsilon_1 \varepsilon_2'}{\varepsilon_1 + \varepsilon_2'}\right)^{3/2} \frac{\varepsilon_2''}{2(\varepsilon_2')^2} \qquad (1.29)$$

Using eqns. (27) through (29), we arrive at

$$\varepsilon_2''\,(R_{min}, \theta_{res}, \omega\theta) = \frac{\omega\theta}{2}\,(1 \pm \sqrt{R}_{min})\,\frac{\varepsilon_1^2\,\varepsilon_3\,\tan\theta_{res}}{(\varepsilon_1 - \varepsilon_3 \sin^2\theta_{res})^2} \qquad (1.30)$$

From the above eqns. after a few steps one arrives at

$$\text{Im}\left[\Delta\dot{k}_x\right] = k_3 \frac{\omega\theta}{4\cos\theta_{res}}\,(1 \mp \sqrt{R}_{min}) \qquad (1.31)$$

Which is the experimentally measured value of $\text{Im}[\Delta\dot{k}_x]$. The numerical solution of the eqn:

$$\left[\text{Im}[\Delta k_x(h)]\right]_{theoretical} = \left[\text{Im}[\Delta k_x]\right]_{experimental} \qquad (1.32)$$

Gives the experimetally determined value of h(thickness of the metal film) L.h.S of Eqn. (1.32) is given by eqn. (1.16).

Writing eqn.(1.32) explicitly, we have

$$\text{Im}\left[\frac{2k_o}{\varepsilon_1 - \varepsilon_2'}\left(\frac{\varepsilon_1 \varepsilon_2'}{\varepsilon_1 + \varepsilon_2'}\right)^{3/2} \dot{r}_{32}^{o} \exp\left[2i\dot{k}_{2o_y} h\right]\right]$$

$$= \frac{k_3\,\omega_\theta}{4\cos\theta_{res}}\,(1 \mp \sqrt{R}_{min}) \qquad (1.33)$$

Eqn. (33) determines the value of h, from experimentally determined value of R_{min}, θ_{res} and ω_θ.

The experimental value of ε_2'' given by eqn. (30) is very sensitive to the experimental conditions compared to ε_2' given by eqn. (23). So the value of hopt is even more sensitive to experimental conditions since it depends on both ε_2' and ε_2''.

For a series of evaluations the knowledge of $\dot{\varepsilon}_2(\omega)$ is needed. Since data of $\dot{\varepsilon}_2(\omega)$ found in literature shown fluctuations due to unknown preparation (experimental) conditions, it is therefore important that photometric measurement of the reflection minimum allows determination of $\dot{\varepsilon}_2(\omega)$ of the film surface in situ very accurately. By fitting Fresnel's eqn. (14) with the observed ATR curve, ε_2' , ε_2'' , and h of the metallic film can be obtained with an accuray ranging from 0.5% to 2.5%.

.3 The Phenomenon of Splitting SP_s into Symmetric and Anti-Symmetric modes for the case of Symmetric Environment ($\varepsilon_1 = \varepsilon_3$)

We have seen that surface plasmons (SP_s) propagate on smooth surfaces of semi-infinite metals. Surface plasmons exist on thin films, too. Their properties depend on the film thickness and the dielectric medium on both sides of the film. As we have seen, the metal film between asymmetric dielectrica, e.g., prism/metal film/ air allows the excitation of SP_s by irradiation with light. If ε_3 is close in value to ε_1 (nearly symmetric environment) and if ε_1 and ε_3 propagate envanescent waves, the dispersion relation for SP_s at the two surfaces $\varepsilon_1/\varepsilon_2$ and $\varepsilon_1/\varepsilon_3$ is obtained by writing that the Fresnel coefficient for P-polarized light in the three media ($\varepsilon_1/\varepsilon_2/\varepsilon_3$) configuration has a pole, see eqn. (12). The denominator of eqn. (12) is thus a classical thin film dispersion eqn.

From the classical thin film formula one obtains the condition

$$\dot{k}_{2y}\dot{\varepsilon}_2\left[\varepsilon_1\dot{k}_{3y}+\varepsilon_3\dot{k}_{1y}\right]+\left[\varepsilon_1\varepsilon_3\dot{k}_{2y}^2+\dot{\varepsilon}_2^2\,\dot{k}_{1y}\dot{k}_{3y}\right]\tanh\left(\frac{\dot{k}_{2yh}}{i}\right)=0 \qquad (1.34)$$

For large thickness h, $\tanh\left(\frac{\dot{k}_{2yh}}{i}\right) = 1$ and eqn. (34) becomes

$$\left(\frac{\dot{k}_{1y}}{\varepsilon_1}+\frac{\dot{k}_{2y}}{\dot{\varepsilon}_2}\right)\cdot\left(\frac{\dot{k}_{3y}}{\varepsilon_3}+\frac{\dot{k}_{2y}}{\dot{\varepsilon}_2}\right)=0 \qquad (1.35)$$

We recover the two modes corresponding to SP_s (surface electromagnetic waves) at each interface: $\varepsilon_1/\varepsilon_2$ and $\varepsilon_2/\varepsilon_3$, which are totally decoupled. By putting each bracket in eqn. (35) equal to zero.

For smaller values of h, we obtain from eqn. (34) or classical thin film formula a dispersion curve with two branches. For $k'_x \to \infty$, their asymptotic values correspond to $\varepsilon_1 + \dot{\varepsilon}_2 = 0$ and $\varepsilon_3 + \dot{\varepsilon}_2 = 0$.

There will be two resonances in the R curves for scanning either at fixed θ and variable ω or at fixed ω and variable θ. The important point to notice is that for not too small values of h/λ, $\tanh\left(\frac{\dot{k}_{2yh}}{i}\right)$ is not very different from unity and the two resonances are practically decoupled[10].

When the active film is relatively thin (thickness below about $1000A^{o}$ at optical frequencies and is surrounded by the same medium (symmetric environment) on both sides ($\varepsilon_3=\varepsilon_1$), the two resonances are associated with short-and long-range SP_s, see Sarid [6].

The symmetric environmenton both sides of the metal film has interesting properties, especially if the thickness of the metal film becomes small, more exactly $\dot{k}_{2y}h \ll 1$. The symmetry causes the SP - frequency to be the same on both sides of the film, so that in the case of a thin film the electromagnetic fields of both surfaces interact and the

frequency splits into $\omega\pm$, a high-frequency mode ω^+(electric field symmetric to the plane y = 0) and a low - frequency mode ω^-(electric field asymmetric to the plane y = 0). The values of ω^+ and ω^- depend therefore on $\dot{k}_x$ as well as on h, the thickness of the metal film, (see fig. 2).

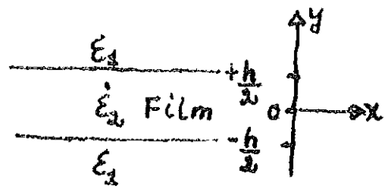

Fig. 2. A symmetric Layer System
$\varepsilon_1/\dot{\varepsilon}_2/\varepsilon_1$. $\dot{\varepsilon}_2$: dielectric function of the metal film. y = 0 is the plane of symmetry.

4 Splitting of the Dispersion Equation into Two Branches.

The classical thin film dispersion equation for the metal film between asymmetric dielectrica is given by

$$\dot{r}_{32}\dot{r}_{21}\, e^{2i\dot{k}_{2y}h} + 1 = 0 \qquad (1.36)$$

For the symmetric environment, $\varepsilon_3 = \varepsilon_1$

$$\dot{r}_{32} \to \dot{r}_{12}$$

This implies that

$$\dot{r}_{12}\dot{r}_{21}\, e^{2i\dot{k}_{2y}h} + 1 = 0 \qquad (1.37)$$

but $\dot{r}_{12} = -\dot{r}_{21}$ and eqn. (37) can be written as

$$1 - (\, r_{21}\, e^{i\dot{k}_{2y}h})^2 = 0 \qquad (1.38)$$

and hence

$$1 + \dot{r}_{21}\, e^{i\dot{k}_{2y}h} = 0 \qquad (1.39)$$

$$1 - \dot{r}_{21}\, e^{i\dot{k}_{2y}h} = 0 \qquad (1.40)$$

where $\dot{r}_{21}$ is Fresnel's reflection coefficient for P-polarized light, given by

$$\dot{r}_{21} = \left(\frac{\dot{k}_{2y}}{\dot{\varepsilon}_2} - \frac{\dot{k}_{1y}}{\varepsilon_1}\right) \Big/ \left(\frac{\dot{k}_{2y}}{\dot{\varepsilon}_2} + \frac{\dot{k}_{1y}}{\varepsilon_1}\right) \qquad (1.41)$$

Putting eqn. (41) into eqns. (39) and (40), we arrive at

$$\dot{\varepsilon}_2\dot{k}_{1y} + \varepsilon_1\dot{k}_{2y} \tanh\left(-\frac{i\dot{k}_{2y}h}{2}\right) = 0 \qquad (1.42)$$

$$\dot{\varepsilon}_2\dot{k}_{1y} + \varepsilon_1\dot{k}_{2y} \operatorname{Ctgh}\left(-\frac{i\dot{k}_{2y}h}{2}\right) = 0 \qquad (1.43)$$

It can be shown that

$$\frac{-i\dot{k}_{2y}h}{2} = \frac{\dot{k}_{2y}h}{2i} \qquad (1.44)$$

and hence eqns: (42) and (43) can be rewritten as

$$\omega^{+}:\ L^{+} = \dot{\varepsilon}_2\dot{k}_{1y} + \varepsilon_1\dot{k}_{2y} \tanh\left(\frac{\dot{k}_{2y}h}{2i}\right) = 0 \qquad (1.45)$$

$$\omega^{-}:\ L^{-} = \dot{\varepsilon}_2\dot{k}_{1y} + \varepsilon_1\dot{k}_{2y} \operatorname{ctgh}\left(\frac{\dot{k}_{2y}h}{2i}\right) = 0 \qquad (1.46)$$

Eqns. (45) and (46) represent the splitting of the dispersion equation into two branches for the symmetric environment with very thin metal films. This is valid for P-polarized light.

For strict derivation of eqns. (45) and (46) see appendix A

For large k'_x ($\dot{k}_{2y} = \dot{k}_{1y} = ik'_x$) eqn. (45) becomes

$$\dot{\varepsilon}_2 + \varepsilon_1 \tanh\left(\frac{k'_x h}{2}\right) = 0 \qquad (1.47)$$

Rearranging and solving eqn. (1.47) becomes

$$\frac{\varepsilon_1 + \dot{\varepsilon}_2}{\varepsilon_1 - \dot{\varepsilon}_2} = + e^{-k'_x h} \qquad (1.48)$$

This is for the ω^+ mode. Similarly for the ω^- mode, we have

$$\frac{\varepsilon_1 + \dot{\varepsilon}_2}{\varepsilon_1 - \dot{\varepsilon}_2} = - e^{-k'_x h} \qquad (1.49)$$

Combining eqns. (48) and (49), we get

$$\frac{\varepsilon_1 + \dot{\varepsilon}_2}{\varepsilon_1 - \dot{\varepsilon}_2} = \pm e^{-k'_x h} \qquad (1.50)$$

The Drude form for the dielectric function of a free electron gas is

$$\varepsilon'_2(\omega) = 1 - \frac{\omega_p^2}{\omega^2} \text{(neglecting absorption)} \qquad (1.51)$$

Where ω_p is the electron plasma frequency:

$\omega_p^2 = \dfrac{4\pi n_e e^2}{m_e}$ with n_e = electron density, e = electron charge, m_e = electron (effective) mass and with $\varepsilon_1 = 1$, eqn. (50) becomes

$$\omega^{\pm} = \frac{\omega_p}{\sqrt{2}} \left(1 \pm e^{-k'_x h}\right)^{\frac{1}{2}} \qquad (1.52)$$

This eqn. demonstrate the splitting in the nonretarded region and in addition the relation $\omega^+ > \omega^-$ for finite h. For $k'_x h > 1$

we obtain eqn. (4) i.e.

$\omega_{sp} = \frac{\omega_p}{\sqrt{2}}$ for case $\varepsilon_1 = 1$. That is for large k'_x and h

$\omega^+ = \omega^- = \omega_{sp}$, (no splitting of the dispersion equation).

If

$\varepsilon_1 > 1$ then $\omega_{sp} \to \frac{\omega_p}{\sqrt{1+\varepsilon_1}}$, lowering the upper limit

(Maximum allowed) frequency of surface plasmons.

This theoretical prediction has been confirmed by electron -loss spectroscopy with freely supported Al foils of $\approx$ 200 A^o thickness [9]. From [9] one sees that besides the 15ev loss, the excitation of the volume plasmons $\hbar\omega p$, the SP_s split into 4.9 and 9.4 ev. The 4.9 ev loss refers to the excitation of the lower mode $\hbar\omega^-$, and the 9.4ev loss refers to the excitation of the upper mode $\hbar\omega^+$. The 4.9 and 9.4ev loss shows the splitting of 7ev SP. The Al foil was covered with a very thin oxyd film which reduces the 10ev excitation of a clean Al surface to about 7ev. However, it is not convenient to reach the region of small k'_x with electrons, fast or slow, since the aperture of the electron beam cannot be sufficiently reduced due to intensity reasons: A value of the aperture of 5×10^{-5} rad with $\lambda el = 0.05 A^o$ (50 kev) gives an experimental k_x ($k_x = kel\theta, \theta$ is the scattering angle) width (Δk_x) of $3x10^{-3} A^{o-1}$ which is comparable with the extension of the whole retarded region of the dispersion relation. this demonstrates that fast and slow electrons are not suitable, as yet, for studying the SP properties at very low k'_x values. The reverse is valid for light: a laser beam with a divergence of 10^{-3} rad at $6000 A^o$ gives a Δk_x of about $10^{-6} A^{o-1}$ and allows thus to

Probe the SP dispersion relation down to very low k_x' values. It has not yet been possible to reach the region of larger k_x' with photons. Thus, it is obvious that this splitting has also been studied with optical means since the observations in the region of light line are less difficult than those with electron-loss spectroscopy and give more details in the low k_x' region.

Fukui and Normandian [9] found in a study of the symmetric system, that the damping of the high-frequency mode ω^+ decreases with decreasing thickness h and the reverse of ω^- mode. This result has been confirmed by Sarid [6]. This behavior of ω^+ mode attracted the attention of subsequent researchers, since the decrease of damping imply longer propagation lengths it is called long-range SP(LRSP). The strong field enhancement i.e., larger intensity of the field than SP_s of single boundary and of ω^- mode, makes this mode (ω^+) suitable for the study of surfaces. In the cases just mentioned the resonant excitation of SP_s has been produced in the ATR device and the dielectrica on both sides are symmetric concerning the refractive index.

The physical reason for the decrease of the damping with decrease of film thickness h (case of ω^+mode) is the decrease of the field in the film which is pushed out of it with decreasing h, so that the Joule heat per cm^3diminishes. In the case of ω^- mode as h decreases the damping increases because of the increase of the field in the film. This mode (ω^-) is suitable for the determination of $\epsilon_2(\omega)$ and h of the film.

1.5 Derivation of Cycle-Average Power flow in the Kretschmann Prism - Metal Film - Air Configuration.

While $\vec{E}$ and $\vec{H}$ are written as complex vectors it is the real part that has physical significance. Thus the poynting vector is given by

$$S = R_e\vec{E} \times R_e\vec{H} = \tfrac{1}{2} (\vec{E} + \vec{E}^*) \times \tfrac{1}{2} (\vec{H} + \vec{H}^*)$$

This implies

$$\vec{S} = \frac{1}{4} \left[\vec{E}\times\vec{H} + \vec{E}^*\times\vec{H} + \vec{E}\times\vec{H}^* + \vec{E}^*\times\vec{H}^* \right] \qquad (1.53)$$

Where the asterisks denote complex conjugates.
We are interested in the mean value of S over one cycle of oscillation since the time of measurement is usually much longer than a period T, i.e., in

$$\langle\vec{s}\rangle = \frac{1}{T}\int_0^T \vec{s}\,dt' ,$$

Where T is the period of oscillation, being equal to $\frac{2\pi}{\omega}$. The terms $\vec{E}\times\vec{H}$ and $\vec{E}^*\times\vec{H}^*$ in the expression for $\vec{S}$ eqn. (1.53) contain exponential time factors exp $(\mp 2i\omega t')$. As

$$\frac{1}{T}\int_0^T e^{\mp 2i\omega t'}\,dt' = 0 ,$$

these terms do not contribute to $\langle\vec{s}\rangle$. On the other hand, the remaining terms $\vec{E}^*\times\vec{H}$ and $\vec{E}\times\vec{H}^*$ do not contain any time factor are not affected by averaging. Hence

$$\langle\vec{s}\rangle = \frac{1}{4} (\vec{E}^*\times\vec{H} + \vec{E}\times\vec{H}^*) = \frac{1}{4} \left[(E\times H^*)^* + (E\times H^*) \right]$$

This implies

$$\langle\vec{s}\rangle = \frac{1}{2} R_e \, (\vec{E}\times\vec{H}^*) \qquad (1.54)$$

Applying eqn. (1.54) to surface electromagnetic waves on thin metallic film bounded by dielectric media.

Suppose a TM polarization, $\vec{H} = \vec{H}_z$, wave incident on the film.

Now eqn. (1.54) becomes

$$\langle \vec{s} \rangle = \frac{1}{2} R_e \, (\vec{E} \times \vec{H}^*) = \frac{1}{2} R_e \, (-E_x H_z^* \hat{j} + E_y H_z^* \hat{i})$$

and

$$\langle s_x \hat{i} + s_y \hat{j} \rangle = \frac{1}{2} R_e \, (E_y H_z^*) \hat{i} - \frac{1}{2} R_e (E_x H_z^*) \hat{j}$$

Resolving gives

$$\langle s_x \rangle = \frac{1}{2} R_e \, (E_y H_z^*) \tag{1.55}$$

$$\langle s_y \rangle = -\frac{1}{2} R_e \, (E_x H_z^*)$$

Maxwell's eqn. which relate $\vec{H}$ to $\vec{E}$ is

$$\vec{\nabla} \times \vec{H} = \varepsilon \frac{\partial \vec{E}}{\partial t} \tag{1.56}$$

assuming $J_{ext} = 0$.

The magnetic field distribution in the film is assumed to be

$$\dot{H}_{z2} = (\dot{A}_2 \, e^{i\dot{k}_{2y}y} + \dot{B}_2 \, e^{-i\dot{k}_{2y}y}) \, e^{i(\dot{k}_x x - \omega t)} \tag{1.57}$$

The field distributions in the bounding dielectrica are

$$\dot{H}_{z1} = \dot{A}_1 \, e^{i\dot{k}_{1y}y + i(\dot{k}_x x - \omega t)} \quad \text{in air} \tag{1.58}$$

$$\dot{H}_{z3} = \dot{A}_3 \, e^{-i\dot{k}_{3y}y + i(\dot{k}_x x - \omega t)} \quad \text{in prism} \tag{1.59}$$

From the above three eqns. one gets using eqn.(1.56) the respective electric field distributions, and using eqn. (1.55) we have for the three media

$$\langle s_{xj} \rangle = \frac{1}{2} R_e \frac{\dot{k}_x}{\omega \varepsilon_j} |H_{zj}|^2 \quad \text{where } j = 1,2,3 \tag{1.60}$$

and

$$\langle s_{1y} \rangle = \frac{1}{2} R_e \frac{\dot{k}_{1y}}{\omega \varepsilon_1} |\dot{H}_{z1}|^2 \tag{1.61}$$

$$\langle S_{2y} \rangle = -\frac{1}{2} R_e \frac{\dot{k}_{2y}}{\omega \dot{\varepsilon}_2} \left[-|\dot{A}_2|^2 e^{-2k''_{2y} y} + |\dot{B}_2|^2 e^{2k''_{2y} y} + \right.$$

$$\left. + B_2 A_2^* e^{-2ik'_{2y} y} - \dot{A}_2 \dot{B}_2^* e^{2ik'_{2y} y} \right] e^{-2k''_x x} \tag{1.62}$$

$$\langle S_{3y} \rangle = -\frac{1}{2} R_e \frac{\dot{k}'_{3y}}{\omega \varepsilon_3} |\dot{H}_{z3}|^2 \tag{1.63}$$

Now we need to express the amplitudes $\dot{A}_1$, $\dot{A}_2$, $\dot{B}_2$ interms of $\dot{A}_3$, the amplitude of the incident wave. This is accomplished using boundary conditions at y = 0 (metal/air) interface gives

$$\dot{r}_{21} = \frac{\dot{B}_2}{\dot{A}_2} \tag{1.64}$$

and

$$\dot{A}_1 = \dot{A}_2 + \dot{B}_2 \tag{1.65}$$

where $\dot{r}_{21}$ is the Fresnel reflection coefficient given by eqn. (1.13)

The boundary conditions at y = -h (prism/metal) interface, together with eqn.64,

$$\dot{r}_{21}\, \dot{r}_{32}\, e^{2i\dot{k}_{2y} h} + 1 = 0 \tag{1.66}$$

which is the thin metal film dispersion equation. Where $\dot{r}_{32}$ is the Fresnel reflection coefficient given by eqn. (1.13) at prism/metal interface.

Using eqns. (1.64) through (1.66), we can express $\dot{A}_1$, $\dot{A}_2$, and $\dot{B}_2$ interms of $\dot{A}_3$. Hence

$$\dot{A}_1 = \frac{\dot{A}_3\, e^{i\dot{k}_{3y} h} \left[\dot{r}_{23}\, e^{i\dot{k}_{2y} h} + e^{-i\dot{k}_{2y} h} \right]}{\dot{r}_{23} + 1} \tag{1.67}$$

$$\dot{A}_2 = \frac{\dot{r}_{23}\dot{A}_3\, e^{i(\dot{k}_{2y} + \dot{k}_{3y})h}}{\dot{r}_{23} + 1} \qquad (1.68)$$

$$\dot{B}_2 = \frac{A_3\, e^{i(\dot{k}_{3y} - \dot{k}_{2y})h}}{\dot{r}_{23} + 1} \qquad (1.69)$$

Note: For strict derivation of the above and following results see appendix B.

Using eqn. (1.60) the x-components of the average power flow for the three media can be written as

$$\langle s_{1x} \rangle = \frac{k'_x\, e^{-2k''_{3y}h}}{2\omega\varepsilon_1 [\,|\dot{r}_{23}|^2 + 2r'_{23} + 1]} \cdot$$

$$\cdot \left[\, |r_{23}|^2\, e^{-2k''_{2y}h} + e^{2k''_{2y}} + 2(r'_{23}\cos(2k'_{2y}h) - \right.$$

$$\left. - r''_{23}\sin(2k'_{2yh}))\right] \cdot e^{-2k''_{1y}y} \qquad (1.70)$$

$$\langle s_{2x} \rangle = \frac{(k'_x\varepsilon'_2 + k''_x\varepsilon''_2)\cdot e^{-2k''_{3y}h}}{2\omega\,|\dot{\varepsilon}_2|^2(|\dot{r}_{23}|^2 + 2r'_{23} + 1)} \cdot$$

$$\cdot \left[\, |\dot{r}_{23}|^2\, e^{-2k''_{2y}(h+y)} + e^{2k''_{2y}(h+y)} + 2(r'_{23}\cos[2k'_{2y}(h+y)]\right.$$

$$\left. - r''_{23}\sin[2k'_{2y}(h+y)])\right] \qquad (1.71)$$

$$\langle s_{3x} \rangle = \frac{k'_x\, e^{2k''_{3y}y}}{2\omega\varepsilon_3} \qquad (1.72)$$

assuming $|\dot{A}_3|^2 = 1$ and at $x = 0$. The field intensity falls as $e^{-2k''_x x}$ in the x - direction. The same assumption is used for the y-components.

Using eqns. (1.61) through (1.63), the y-components of the average power flow for the three media can be written as

$$\langle s_{1y} \rangle = \frac{k'_{1y}\, e^{-2k''_{3y}h}}{2\omega\epsilon_1 \left[|\dot{r}_{23}|^2 + 2r'_{23} + 1 \right]} \cdot$$

$$\cdot \left[|\dot{r}_{23}|^2 e^{-2k''_{2y}h} + e^{2k''_{2y}h} + 2(r'_{23} \cos[2k'_{2y}h] - r''_{23} \sin[2k'_{2y}h]) \right] e^{-2k''_{1y}y} \qquad (1.73)$$

$$\langle s_{2y} \rangle = \frac{e^{-2k''_{3y}h}}{2\omega|\dot{\epsilon}_2|^2 \left[|\dot{r}_{23}|^2 + 2r'_{23} + 1 \right]} \left[(k'_{2y}\epsilon'_2 + k''_{2y}\epsilon''_2) \times \right.$$

$$\left(|\dot{r}_{23}|^2 e^{-2k''_{2y}(h+y)} e^{2k''_{2y}(h+y)} \right) + 2(k'_{2y}\epsilon''_2 - k''_{2y}\epsilon'_2) \times$$

$$\left. (r'_{23} \sin[2k'_{2y}(h+y)] + r''_{23} \cos[2k'_{2y}(h+y)]) \right] \qquad (1.74)$$

$$\langle s_{3y} \rangle = \frac{-k'_{3y}\, e^{2k''_{3y}y}}{2\omega\epsilon_3} \qquad (1.75)$$

Integrating, over y from $-\infty$ up to $+\infty$, the x-comonents of the power flow, the total cycle-average power flow in each medium comes out as

$$\langle P_{1x} \rangle = \int_0^\infty \langle s_{1x} \rangle \, dy$$

assuming $|\dot{A}_3|^2 = 1$ and at $x = 0$. The field intensity falls as $e^{-2k''_x x}$ in the x - direction. The same assumption is used for the y-components.

Using eqns. (1.61) through (1.63), the y-components of the average power flow for the three media can be written as

$$\langle s_{1y} \rangle = \frac{k'_{1y}\, e^{-2k''_{3y}h}}{2\omega\varepsilon_1 \left[|\dot{r}_{23}|^2 + 2r'_{23} + 1 \right]} \cdot$$

$$\cdot \left[|\dot{r}_{23}|^2 e^{-2k''_{2y}h} + e^{2k''_{2y}h} + 2(r'_{23} \cos[2k'_{2y}h] - r''_{23} \sin[2k'_{2y}h]) \right] e^{-2k''_{1y}y} \qquad (1.73)$$

$$\langle s_{2y} \rangle = \frac{e^{-2k''_{3y}h}}{2\omega|\check{\varepsilon}_2|^2 \left[|\dot{r}_{23}|^2 + 2r'_{23} + 1 \right]} \left[(k'_{2y}\varepsilon'_2 + k''_{2y}\varepsilon''_2) \times \right.$$

$$\left(|\dot{r}_{23}|^2 e^{-2k''_{2y}(h+y)} e^{2k''_{2y}(h+y)} \right) + 2(k'_{2y}\varepsilon''_2 - k''_{2y}\varepsilon'_2) \times$$

$$\left. (r'_{23} \sin[2k'_{2y}(h+y)] + r''_{23} \cos[2k'_{2y}(h+y)]) \right] \qquad (1.74)$$

$$\langle s_{3y} \rangle = \frac{-k'_{3y}\, e^{2k''_{3y}y}}{2\omega\varepsilon_3} \qquad (1.75)$$

Integrating, over y from $-\infty$ up to $0 + \infty$, the x-comonents of the power flow, the total cycle-average power flow in each medium comes out as

$$\langle P_{1x} \rangle = \int_0^{\infty} \langle s_{1x} \rangle \, dy$$

$$= \frac{k'_x \, e^{-2k''_{3y}h}}{4\omega\varepsilon_1 k''_{1y}\left[\,|r_{23}|^2 + 2r'_{23} + 1\right]} \left[\,|r_{23}|^2 \, e^{-2k''_{2y}h} + e^{2k''_{2y}h} + 2(r'_{23}\cos(2k'_{2y}h) - r''_{23}\sin(2k'_{2y}h))\right]$$

$$\langle P_{2x}\rangle = \int_{-h}^{0} \langle s_{2x}\rangle dy \qquad (1.76)$$

$$= \frac{(k'_x\varepsilon'_2 + k''_x\varepsilon''_2)\, e^{-2k''_{3y}h}}{2\omega|\dot{\varepsilon}_2|^2\left[\,|\dot{r}_{23}|^2 + 2r'_{23} + 1\right]} \left[\frac{1}{2k''_{2y}}\left[\left(e^{2k''_{2y}h} - 1\right) - |\dot{r}_{23}|^2\left(e^{-2k''_{2y}h} - 1\right)\right] + \frac{1}{k'_{2y}}\left[r'_{23}\sin(2k'_{2y}h) + r''_{23}\left(\cos(2k'_{2y}h) - 1\right)\right]\right] \qquad (1.77)$$

$$\langle P_{3x}\rangle = \int_{-\infty}^{-h} \langle s_{3x}\rangle \, dy$$

$$= \frac{k'_x \, e^{-2k''_{3y}h}}{4\omega\varepsilon_3 k''_{3y}} \qquad (1.78)$$

Note: The above relations for the power flows are derived or worked out by my advisor and my self. We haven't come across these relations in literature.

The poynting vector P(x) of the SP_s, integrated over y from $-\infty$ up to $+\infty$, contains the field intensity $|E_{sp}(0^+)|^2$ of the SP_s just at the metal surface. At resonance or R = 0 the power of the SP_s is lost exclusivly by internal absorption in the metal or

$$\frac{-dP(x)}{dx} = 2k''_{xo}P(x) \qquad (1.79)$$

with k''_{xo}, according to (1.3). This loss is compensated for by the power of the incoming light $|E_3|^2$ which radiates on the unit surface area. Both have to be equal in the steady state. Thus one obtains the quotient $|E_{sp}(0^+)|^2 / |E_3|^2$ as a function of the experimental parameters as the angle of incidence, the dielectic function, etc. Thus the maximum enhancement of the electric-field intensity is obtained from

$$\left[\frac{|H_{z1}(1/2)|^2}{|H_{z3}(3/2)|^2}\right]_{max} = \frac{\varepsilon_1}{\varepsilon_3} \frac{|E(1/2)|^2}{|E_3(3/2)|^2} = \frac{\varepsilon_1}{\varepsilon_3} T^{el}_{max} \tag{1.80}$$

where

$$T^{el}_{max} = \frac{1}{\varepsilon_1} \frac{2|\varepsilon'_2|^2}{\varepsilon''_2} \frac{a}{|\varepsilon'_2|+\varepsilon_1} \tag{1.81}$$

with $a^2 = |\varepsilon'_2| (\varepsilon_3 - \varepsilon_1) - \varepsilon_3$. where $|E(1/2)|^2 = |E_{sp}(0^+)|^2$ is the field intensity on the metal surface at the air side, and $|E_3|^2$ is the incoming field intensity in the prism(ε_3) for p-polarized light.

The strong light intensity in the resonance case indicates a strong electromagnetic field in the boundary air/metal (field enhancement).

CHAPTER 2

Exact Numerical Solutions of the thin metal film dispersion equation in asymmmetric and symmetric environments

2.1 Preparation of the thin film dispersion equation in a form to be solved by the computer for the asymmetric and symmetric environments

The classical thin film dispersion equation for the asymmetric environment is

$$\dot{r}_{21}\dot{r}_{23}\, e^{2i\dot{k}_{2y}h} - 1 = 0 \qquad (2.1)$$

Resolving this complex equation into real and imaginary parts

$$\dot{r}_{21}\dot{r}_{23}e^{2i\dot{k}_{2y}h} - 1 = R_e\left[\dot{r}_{21}\dot{r}_{23}\, e^{2i\dot{k}_{2y}h} - 1\right] + i\ \mathrm{Im}\left[\dot{r}_{21}\dot{r}_{23}\, e^{2i\dot{k}_{2y}h}\right] \qquad (2.2)$$

Let

$$F_1(k_x', k_x'') = R_e\left[\dot{r}_{21}\dot{r}_{23}\, e^{2i\dot{k}_{2y}h} - 1\right] \qquad (2.3)$$

For eqn. (2.1) to be satisfied

$$F_1(k_x', k_x'') = 0 \qquad (2.4)$$

and the imaginary part should also vanish.

To find explict relations for the terms in eqn. (2.2) we write

$$\dot{r}_{21} = r'_{21} + ir''_{21}$$

$$\dot{r}_{23} = r'_{23} + ir''_{23} \qquad (2.5)$$

$$e^{2i\dot{k}_{2y}h} = e^{-2k''_{2y}h}\,[\cos(2k'_{2y}h) + i \sin(2k'_{2y}h)]$$

Putting eqns. (2.5) into eqn.(2.3) yields

$$F_1(k'_x,k''_x) = e^{-2k''_{2y}h}\,[(r'_{21}r'_{23} - r''_{21}r''_{23})\cos(2k'_{2y}h) - (r'_{21}r''_{23} + r''_{21}r'_{23})\sin(2k'_{2y}h)] - 1 \qquad (2.6)$$

Let

$$A = r'_{21}r'_{23} - r''_{21}r''_{23} \qquad (2.7)$$

$$B = r'_{21}r''_{23} + r''_{21}r'_{23} \qquad (2.8)$$

$$C = 2k'_{2y}h \qquad (2.9)$$

Using the relations in eqns. (2.7) through (2.9) in eqn. (2.6) we have

$$F_1(k'_x,k''_x) = e^{-2k''_{2y}h}(A\cos C - B\sin C) - 1 \qquad (2.10)$$

The imaginary part of eqn. (2.1) comes out as

$$\text{Im}\,[\dot{r}_{21}\dot{r}_{23}\,e^{2i\dot{k}_{2y}h} - 1] = e^{-2k''_{2y}h}\,[A\sin C + B\cos C] \qquad (2.11)$$

eqn. (2.1) requires that

$$A \sin C + B \cos C = 0$$

This implies

$$A = \frac{-B \cos C}{\sin C} \qquad (2.12)$$

Putting eqn. (2.12) into eqn. (2.10) gives

$$F_f\ (k'_x, k''_x) = B\ e^{-2k''_{2y}h} + \text{Sin } C \qquad (2.13)$$

The modulus of eqn. (2.1) is

$$|\dot{r}_{21}\dot{r}_{23}\ e^{2ik_{2y}h}_{-1}|^2 = |\dot{r}_{21}\dot{r}_{23}|^2\ e^{-4k''_{2y}h}_{-2R_e}$$

$$\cdot[\dot{r}_{21}\dot{r}_{23}\ e^{2ik'_{2y}h}] + 1 \qquad (2.14)$$

but

$$R_e\ (\dot{r}_{21}\dot{r}_{23}\ e^{2ik_{2y}h}) = e^{-2k''_{2y}h}\ (A \cos C - B \sin C)$$

(2.15)

Using eqn. (2.12), this can be written as

$$R_e\ (\dot{r}_{21}\dot{r}_{23}\ e^{2ik_{2y}h}) = \frac{B\ e^{-2k''_{2y}h}}{\sin C} \qquad (2.16)$$

It can also be shown that

$$|\dot{r}_{21}\dot{r}_{23}|^2 = A^2 + B^2 \qquad (2.17)$$

Thus rewriting eqn. (2.14) yields

$$|\dot{r}_{21}\, r_{23}\, e^{2ik'_{2y}h}_{-1}|^2 = (A^2 + B^2)\, e^{-4k''_{2y}h} - 1$$

$$\cdot \frac{2}{\sin C}(B\, e^{-2k''_{2y}h} + \sin C) \qquad (2.18)$$

From eqn. (2.13) we see that

$$F_1 = B\, e^{-2k''_{2y}h} + \sin C$$

Hence

$$|\dot{r}_{21}\, \dot{r}_{23}\, e^{2ik_{2y}h}_{-1}|^2 = \left[(A^2 + B^2)\, e^{-4k''_{2y}h} - 1\right]$$

$$+ \frac{2}{\sin C} F_1 = 0 \qquad (2.19)$$

Since $F_1 = 0$. We see that

$$(A^2 + B^2)\, e^{-4k''_{2y}h} - 1 = 0$$

Let

$$F_2(k'_x, k''_x) = (A^2 + B^2)\, e^{-4k''_{2y}h}_{-1} \qquad (2.20)$$

Now for eqn. (2.1) to be satisfied

$$F_1(k'_x, k''_x) = 0 \qquad (2.21)$$

and

$$F_2(k'_x, k''_x) = 0$$

Using eqn.s (2.13) and (2.20) we solve numerically the dispersion equation by the Downhill Method.

For the symmetric environment ($\varepsilon_3 = \varepsilon_1$) , we have seen that the dispersion equation splits into two branches, i.e.,

$$\omega^+ : L^+ = \dot{\varepsilon}_2 \dot{k}_{1y} + \varepsilon_1 \dot{k}_{2y} \tan h \left(\frac{\dot{k}_{2y} h}{2i} \right) = 0 \qquad (2.22)$$

$$\omega^- : L^- = \dot{\varepsilon}_2 \dot{k}_{1y} + \varepsilon_1 \dot{k}_{2y} \operatorname{ctgh} \left(\frac{\dot{k}_{2y} h}{2i} \right) = 0 \qquad (2.23)$$

To use the Downhill method we write the above eqns. in a form (by resolving into real and imaginary parts)

$$F_1 (k_x' , k_x'') = 0 \qquad (2.24)$$

$$F_2 (k_x' , k_x'') = 0$$

If eqn. (2.24) is for eqn. (2.22). then we can write for eqn. (2.23)

$$F_3 (k_x' , k_x'') = 0 \qquad (2.25)$$

$$F_4 (k_x' , k_x'') = 0$$

Thus for both environments we get numerical results for k_x' and k_x''. It should also be noted that the approximate analytical solution of the dispersion equation developed in chapter 1 for the asymmetric environment is not applicable to the symmetric environment since the perturbation term ($\Delta\dot{k}_x$) becomes very large and the perturbation losses meaning. Moreover, analytical solution for the symmetric environment is only applicable for the case of very thin metal films or more exactly $\frac{\dot{k}_{2y} h}{2i} << 1$.

.2 Results obtained for Symmetric ($\varepsilon_3 = \varepsilon_1$) and Asymmetric ($\varepsilon_3 \neq \varepsilon_1$) environments

Exact numerical results for both environments have been obtained after a series of computer programs which involve the Downhill method. These results are obtained for different cases:

a) big thickness of the metal film and strong absorption i.e., relaxation time, τ(tau), small.

b) big thickness of the metal film and weak absorption i.e., relaxation time, τ(tau), large.

c) small thickness of the metal film and strong absorption.

d) small thickness of the metal film and weak absorption.

The results are displayed here in graphs and tables. The graphs and tables show the attenuation and propagation properties of SPLPs. The physical description of SPLP properties is through field distributions and power flows.

For all cases the exact results are compared with the approximate analytical results obtained from SPLP method found in literature.

.21 Results obtained for Symmetric Environment ($\varepsilon_3 = \varepsilon_1$).

In the case of $\varepsilon_3 = \varepsilon_1$, for the lower ($\omega$-) branch fig. (2.1), in the case of big h and strong absorption, shows that the exact solution is close to the dispersion relation of semi-infinite metal boundarying dielectric medium whereas the approximate solution is very far from these curves and lies almost horizontally at very small frequencies. For the same mode fig. (2.3), in the case of big h and weak absorption, shows almost similar behavior to the previous case.

For both cases just mentioned figs.(2.2,4)display the exact solution for the imaginary part of k_x is close to that of semi-infinite metal whereas the approximate analytical solution for k_x'' is about 6 orders different in magnitude. The approximate solution increases k_x'' by about 6 orders of magnitude beyond the exact value. Therefore for the symmetric environment the approximate solution fails for both k_x' and k_x'' . We suppose this to

be true for smaller thicknesses of the metal film.

:.22 Results obtained for Asymmetric Environment ($\varepsilon_3 \neq \varepsilon_1$).

a) For case of big film thickness h and strong absorption fig. (2.5) displays that the exact solution has got maximum allowed frequency ω^* and real wave vector $k_x'^*$. The approximate solution almost coincides with the dispersion curve of semi-infinite metal and lies to the left of the exact solution without showing maximum allowed real wave vector $k_x'^*$. As can be seen from the figure the approximate solution for k_x' fails with increasing frequency.

For the same case fig (2.6) shows that the exact solution for the imaginary part of k_x almost coincides with that of the approximate solution. The approximate solution for k_x'' is satisfactory and improving with increasing frequency.

b) For case of big film thickness h and weak absorption (fig.(2.7) displays the exact solution has got maximum allowed frequency ω^* and real wave vector $k_x'^*$. But in this case both ω^* and $k_x'^*$ are increased compared to the case of strong absorption.

The difference between the exact and approximate solutions is considerable compared to previous case (a)

For this same case fig. (2.8) shows that the exact solution for the imaginary part of k_x is close to that of semi-infinite metal whereas the approximate solution for k_x'' is about 8 orders different in magnitude. The

approximate solution increases k_x'' by about 8 orders of magnitude beyond the exact value. Therefore the approximate solution fails for both k_x' and k_x'' .

c) For case of small film thickness h and strong absorption fig. (2.9) displays that the exact solution has got maximum (upper cutoff) allowed frequency ω^* and real wave vector $k_x'^*$. In this case both ω^* and $k_x'^*$ are increased compared to the above two cases. The dispersion curve of the exact solution also shows back-bending which is due to absorption. As can be seen from the figure the approximate solution for k_x' fails.

For this case fig. (2.10) shows that the exact solution for k_x'' lies to the right of the approximate solution which is almost similar to the case (a) discussed above. The approximate solution for k_x'' is satisfactory, improving with increasing fequency.

d) For case of small film thickness h and weak absorption fig . (2.11) displays that the exact and approximate solutions are far removed from each other with the usual peculiarity of the exact solution i.e., it has got maximum (upper cut off) allowed frequency ω^* and $k_x'^*$ but slightly lowered compared to that of case (c). From Fig. (2.12) one can see that the difference between exact and approximate solutions for k_x'' is about 8 orders of magnitude.

The approximate solution increases k_x'' by about 8 orders of magnitude beyond the exact value. Therefore the approximate solution fails for both k_x' and k_x'' .

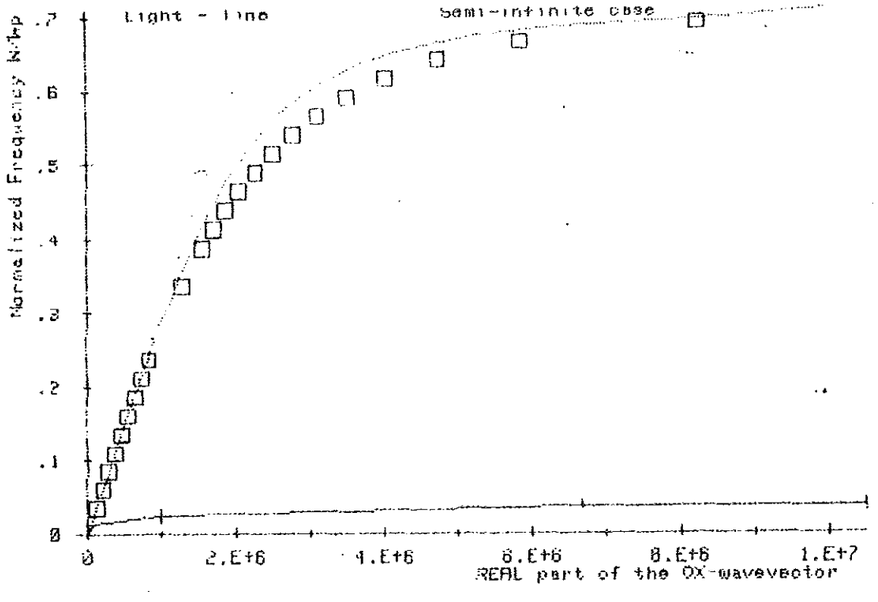

Fig 2.1 .(L39). Graphs for the REAL part of the wavevector versus w/Wp: - solution of the approximate dispersion eq. - (-I-I-I- line type), - solution of the exact dispersion eq. - line with squares in the PMA str E1= 1 , E3= 1.00000001 , Wp= 1.E+15 Hz, H= 5000 'A', Tau= 1.E-13 *ep

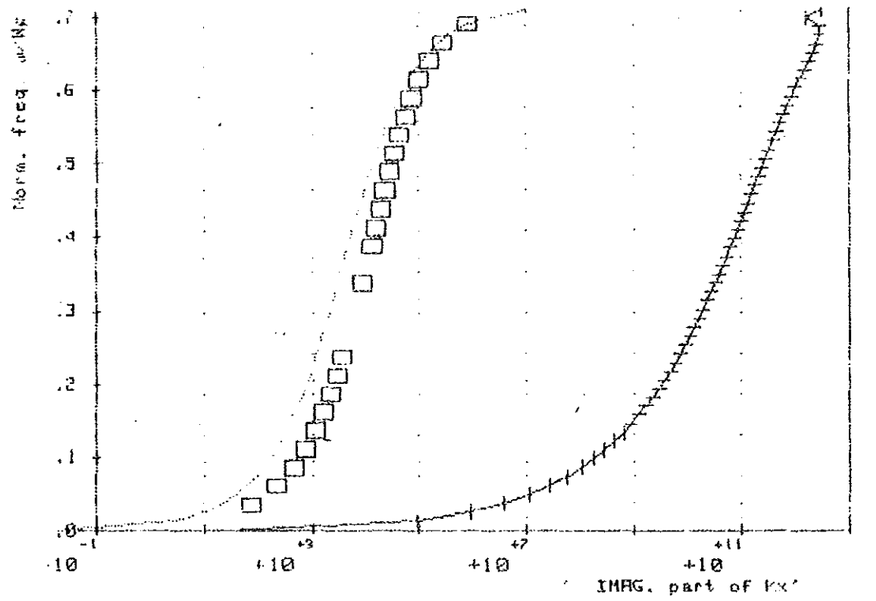

Fig. 2.2 .(L39). Graph for the IMAG. part of the wave vector versus w/Wp:- solution of the approximate disp.eq. - (-I-I-I- line type), - solution of the exact disp. eq. - line with squares in the PMA-str. E1 = 1 , E3 = 1.00000001 , H = 5000 A, Wp = 1.E+15 Hz, Tau = 1.E-13

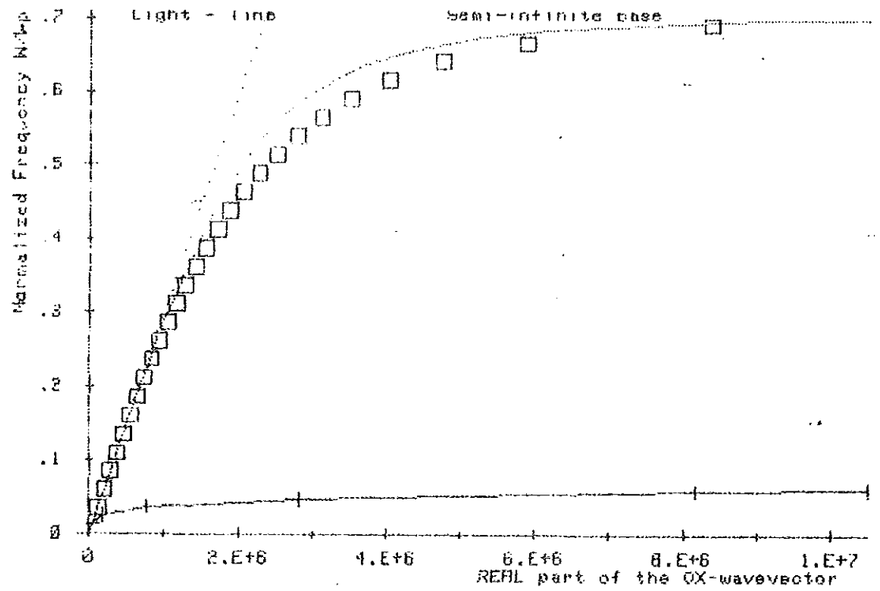

Fig 2.3 .(L40). Graphs for the REAL part of the wavevector versus w/Wp: - solution of the approximate dispersion eq. - (-I-I-I- line type), - solution of the exact dispersion eq. - line with squares in the PMA str E1= 1 , E3= 1.0000001 , Wp= 1.E+15 Hz, H= 5000 'A', Tau= .001 sec*

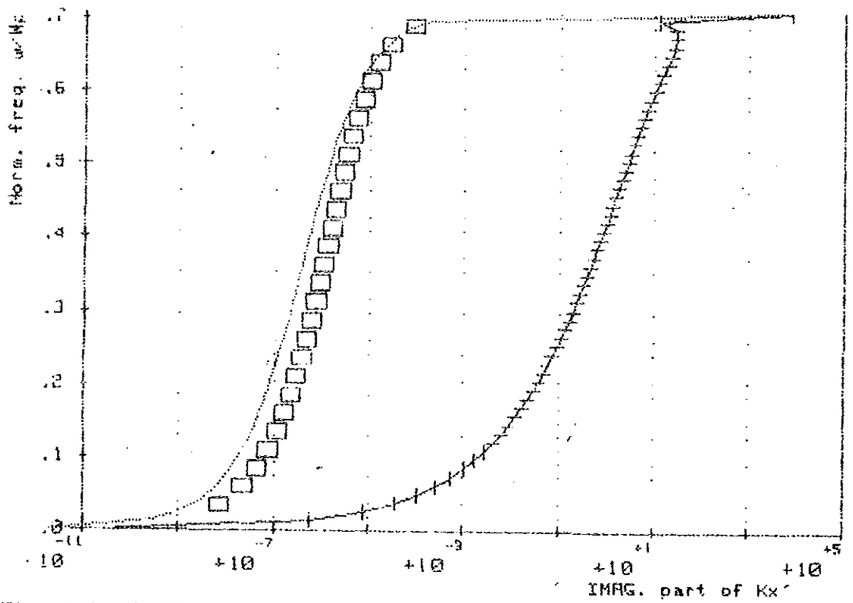

Fig. 2.4 .(L40). Graph for the IMAG. part of the wave vector versus w/Wp:- solution of the approximate disp.eq. - (-I-I-I- line type), - solution of the exact disp. eq. - line with squares in the PMA-str. E1 = 1 , E3 = 1.0000001 , H = 5000 A, Wp = 1.E+15 Hz, Tau = .001 sec

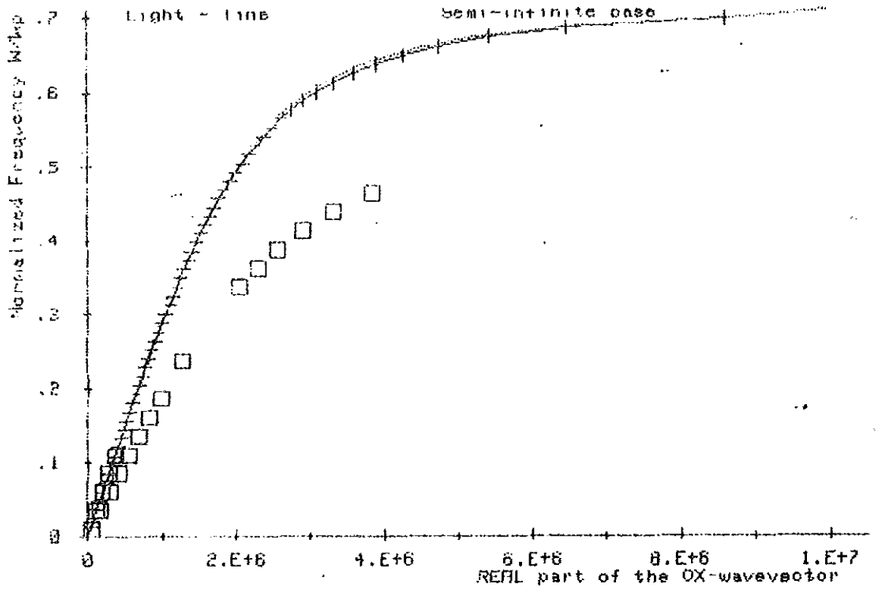

Fig 2.5 ,(L3B). Graphs for the REAL part of the wavevector versus w/Wp: - solution of the approximate dispersion eq. - (-I-I-I- line type), - solution of the exact dispersion eq. - line with squares in the PMA str E1= 1 , E3= 2.25 , Wp= 1.E+15 Hz, H= 5000 'A', Tau= 1.E-13 sec. *

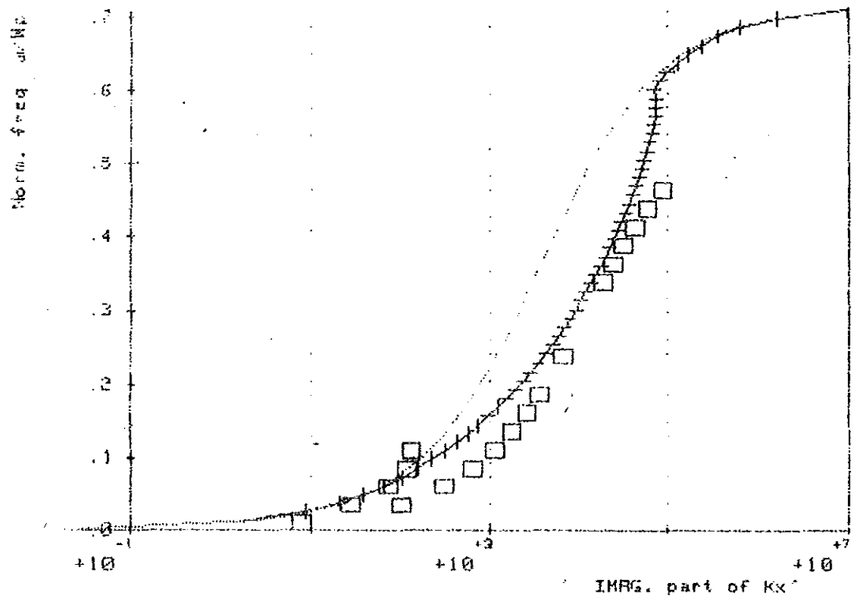

Fig. 2.6 ,(L3B). Graph for the IMAG. part of the wave vector versus w/Wp: solution of the approximate disp.eq. - (-I-I-I- line type), - solution of the exact disp. eq. - line with squares in the PMA-str. E1 = 1 , E3 = 2.25 , H = 5000 A, Wp = 1.E+15 Hz, Tau = 1.E-13 sec .

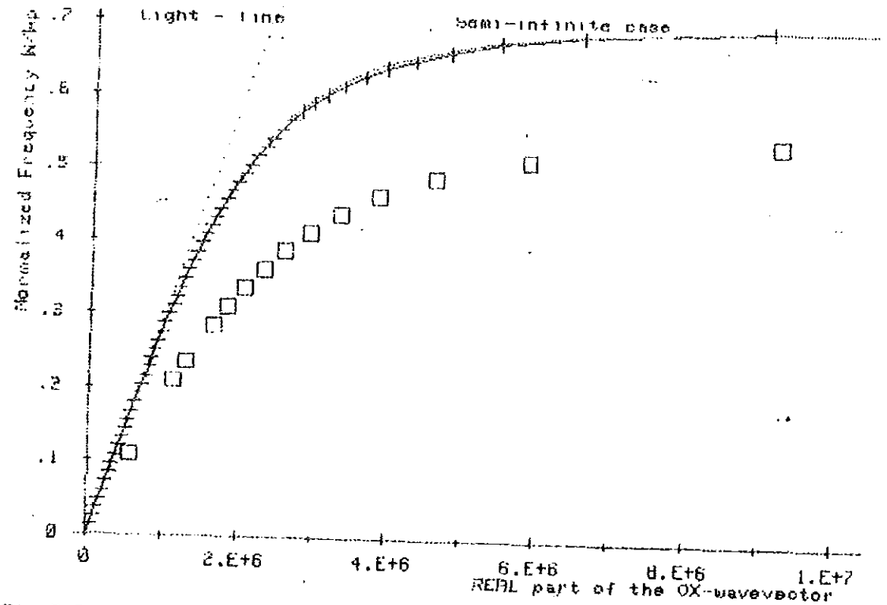

Fig 2.7 .(L27). Graphs for the REAL part of the wavevector versus w/Wp: - solution of the approximate dispersion eq. - (-I-I-I- line type), - solution of the exact dispersion eq. - line with squares in the PMA str E1= 1 , E3= 2.25 , Wp= 1.E+15 Hz, H= 5000 A/, Tau= .001 sec. *

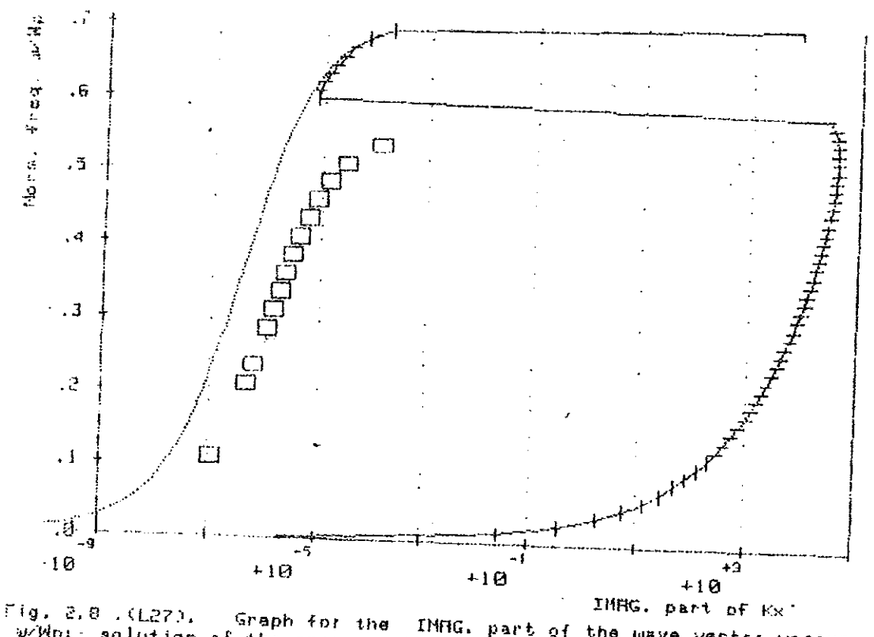

Fig. 2.8 .(L27). Graph for the IMAG. part of the wave vector versus w/Wp: solution of the approximate disp.eq. - (-I-I-I- line type), - solution of the exact disp. eq. - line with squares in the PMA-str. E1 = 1 , E3 = 2.25 , H = 5000 A, Wp = 1.E+15 Hz, Tau = .001 sec *

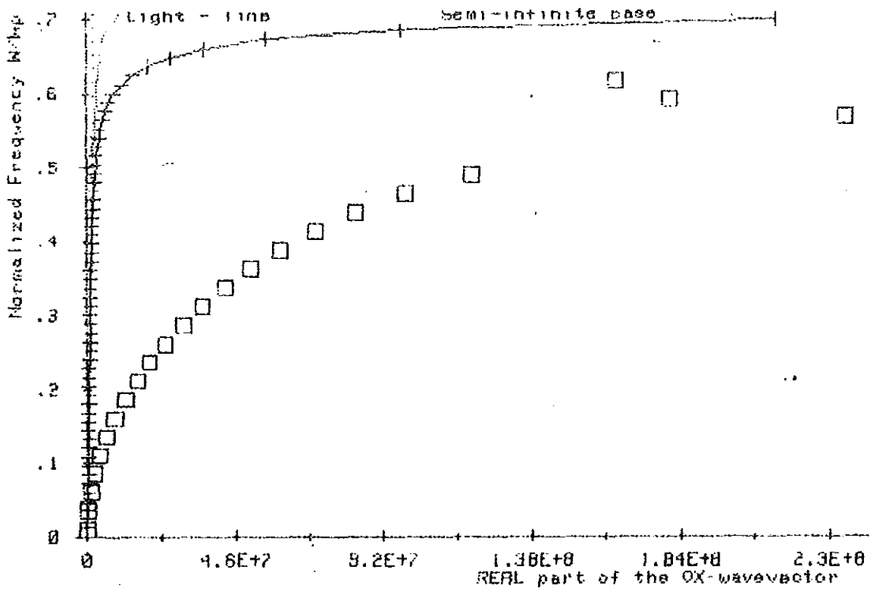

Fig 2.9 .(L31). Graphs for the REAL part of the wavevector versus w/Wp; - solution of the approximate dispersion eq. - (-I-I-I- line type), - solution of the exact dispersion eq. - line with squares in the PMA str E1= 1 , E3= 2.25 , Wp= 1.E+15 Hz, H= 100 'A'. Tau= 1.E-13 sec. *

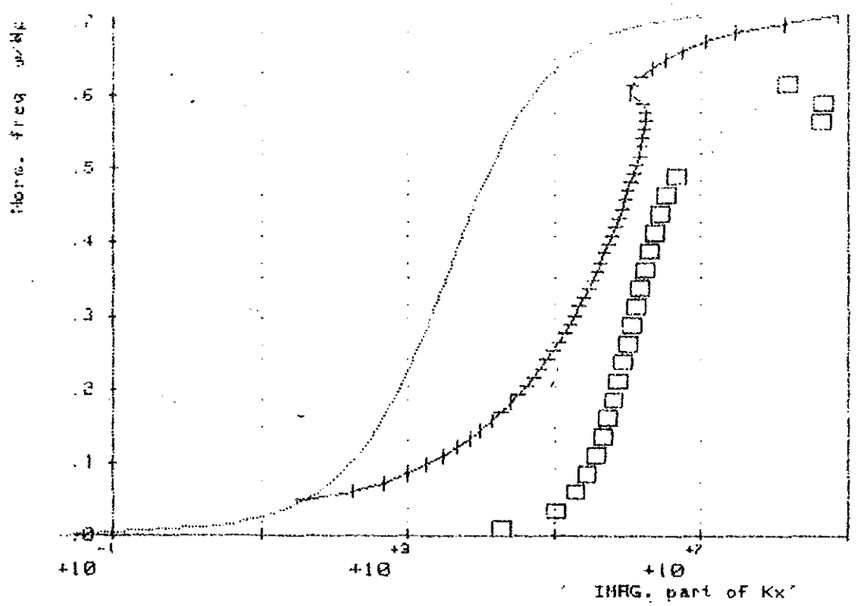

Fig. 2.10 .(L31). Graph for the IMAG. part of the wave vector versus w/Wp- solution of the approximate disp.eq. - (-I-I-I- line type), - solution of the exact disp. eq. - line with squares in the PMA-str. E1 = 1 , E3 = 2.25 , H = 100 A, Wp = 1.E+15 Hz, Tau = 1.E-13 sec*.

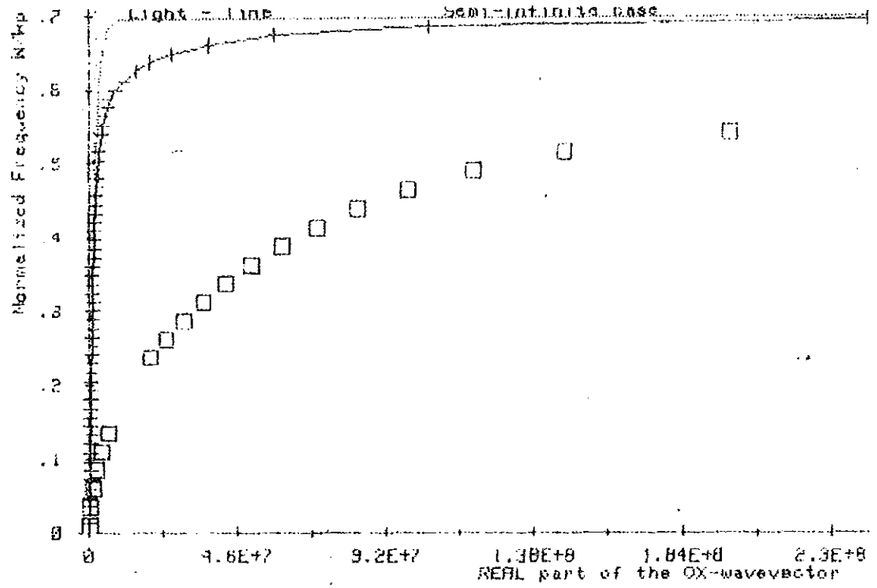

Fig 2.11 .(L28). Graphs for the REAL part of the wavevector versus w/Wp - solution of the approximate dispersion eq. - (-I-I-I- line type), - solution of the exact dispersion eq. - line with squares in the PMA str. E1= 1 , E3= 2.25 , Wp= 1.E+15 Hz, H= 100 'A', Tau= .001 sec. *

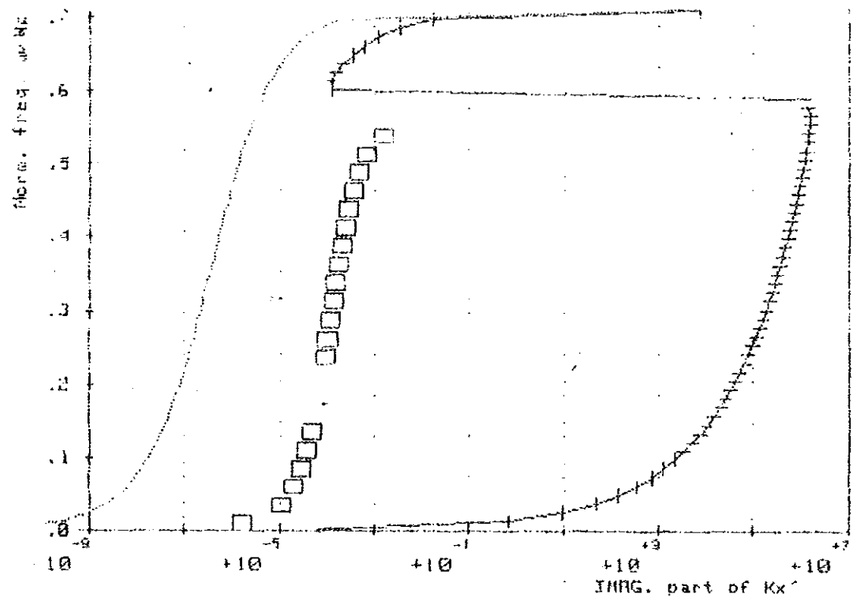

Fig. 2.12 .(L28). Graph for the IMAG. part of the wave vector versus w/Wp= solution of the approximate disp.eq. - (-I-I-I- line type), - solution of the exact disp. eq. - line with squares in the PMA-str. E1 = 1 , E3 = 2.25 , H = 100 A, Wp = 1.E+15 Hz, Tau = .001 sec .*

CHAPTER 3

Analysis of obtained results

3.1 Analysis of the SPLP dispersion at the boundaries of a thin metal film in symmetric environment ($\varepsilon_3 = \varepsilon_1$).

The numerical solution of the exact classical thin film dispersion equation (2.1) for the case of symmetric environment yields, in addition to the two analytical branches given by eqns. (2.22) and 2.23, the mode which we call 'side' and back-bending of the ω^+ mode at about $0.9\omega_p$. The side mode (see Fig.(3.1)) lies to the left of the light line. For this mode no analytical solution is as yet known.

In analysis of these dispersion curves, we take one branch at a time.

1.1. Analysis of the Lower mode ω^- ($k_o < k'_{xo} < k'_x$)

For the thickness and relaxation time under consideration the dispersion curve of ω^- mode shown in Figs (3.1,5,12,16) discloses that at very low k'_x values the surface polaritions are primarily photon-like and the surface polaritions of this mode can be approximated by surface polaritions of semi-infinite metal boundarying dielectric medium since all the light line, semi-infinite, and ω^- mode dispersion curves over lapp in this limit.

In finite k'_x region i.e., near the cross-over of the dispersion curves of uncoupled photons and surface

plasmons, surface polaritions display mixed behavior of both virtual particles namely photons and surface plasmons. In this region (resonance region), as can be seen from the figure, surface polaritions of semi-infinte metal are more closer to the cross-over than surface polaritions of ω^- mode.

The ω^- mode is far removed from the cross-over which implies that the efficiency of coupling of photons to surface plasmons is very low, eventhough weak coupling exists which is responsible for the lower mode curve. Thus the ω^- mode remains non-radiative over the spectral range of interest. The SPLP technique developed in Chapter I is not applicable for this mode since the experimental k_x width (Δk_x) is comparable with the extension of the whole retarded region of the dispersion relation.

In the non-retarded region i.e., $k_x' \to \infty$ the dispersion curve of ω^- mode approaches the dispersion curve of semi-infinite metal. Both curves just mentioned approaches the surface plasmon dispersion curve and hence surface polaritions are primarily surface plasmons. In this region both phase and group velocities go to zero which implies localized surface plasma oscillations.

From fig.(3.2,5,12,16)the curve crresponding to the imaginary part of ω^- mode wave vector shows that k_x'' increases with frequency. In the retarded region the increament

of k_x'' with ω (upto 0.5 ω_p) is slow which means that the dependence of damping on frequency is not a pronounced one. In the non-retared region the dependence of k_x'' on ω (0.5 to .707 ω_p) becomes more pronounced.

The attenuation and propagation properties of SP_s corresponding to ω^- mode can physically be described by considering field distributions and power flows in the symmetric layer system. The magnetic field distribution for this mode is shown in Figs.(3.9,20). The field distribution is anti-symmetric with respect to ox-axis. for this reason this mode is termed as anti-symmetric mode.

The distribution shows that the field is exponentially decaying in the bounding medium and most of the field is concentrated in the film. For frequency range from 0 upto $\frac{\omega_p}{\sqrt{2}}$ this behavior of the field is maintained which means that for a given thickness the SP_s of this mode remains non-radiative. This confirms the conclusion drawn from the observation of ω^- mode dispersion curve. Comparing the field distribution of ω^- mode with that of ω^+ mode (see Figs.(3.10,21)) one can see that the propagation length along the interfaces of SP_s of this mode is shorter and hence it is termed as short-range surface plasmon (SRSP). As the frequency increases the field is more concentrated in the film by decreasing the penetration (skin) depth into the bounding medium.

The partial and net power transmission in ox-direction performed by the ω^- mode is shown in Figs.(3.3,7,14,18). At low frequencies half of the total power flow is flowing in the upper layer (1) and half in the lower layer (3) of the media bounding the metal film. In this case there is practically no power flow in the film. This can also be seen from tables.(3.4,9,14,19). As the frequency increases the flow in the film starts to increase in opposite direction and the equally shared flow in the bounding media starts to decrease. The net flow also starts to decrease. At $\omega = \frac{\omega_p}{\sqrt{2}}$ half of the total flow is in the film in negative ox direction and half of the total flow is equally shared by the bounding media moving in positive ox-direction. Now the net flow is zero which means that surface plasmons are more localized. This describes the part of the dispersion curve where V_g is zero i.e., the non-retarded region.

3.1.2 Analysis of ω^+ mode $(k_o < k_x < k'_{xo})$

For this condition Figs. 3.1,5,12,16) shows that this mode consists of two distinct parts namely the physically unreal part, the physically real part with the back-bending part.

The physically real part of the dispersion curve is slightly to the right of the light line and its real wave vector k_x' is not very much different from the wave vector of the incident light. Thus, this mode can easily be transformed into light by suitable experimental arrangement with a buffer dielectric layer between the prism and the film, the refractive index of the buffer film should be less than that of the prism in order to provide the condition of total internal reflection.

Back-bending of this mode occurs in the range $\frac{\omega_p}{\sqrt{\varepsilon_1 + 1}} < \omega < \omega_p$. For smaller thickness of the film the bending point frequency shifts closer to ω_p and for $h \to \infty$ it tends to $\frac{\omega_p}{\sqrt{\varepsilon_1 + 1}}$ resulting in one degenerated dispersion curve known for the semi-infinite case. The maximum allowed frequency ω^* of SP_s is increased by this mode from $0.707\omega_p$ to about ω_p. At this critical frequency the SP_s of this mode starts to radiate into the bounding media. For frequencies greater than the critical frequency the physically real part of the dispersion curve is bending back and here also this mode is radiating as can be seen from field distribution, see Figs (3.11,22)

From power flow graphs Figs.(3.4,6,13,19) this case of radiation is shown by constant power flow as the frequency increases beyond the critical frequency ω^*.

Thus this mode is radiative for frequencies beyond the critical frequency.

The imaginary part of the ox - wave vector k_x'' of ω^+ mode increases slightly with the frequency (or wavelength of the incident light λ_o) see Figs.(3.2,6,13,17). k_x'' of ω^- mode is about 3 orders of magnitude greater than k''_x of ω^+ mode, this accounts for longer propagation length $L_i = (2k_x'')^{-1}$ of the latter mode. Thus the mode ω^+ is termed as long-range surface plasmon (LRSP). From field distribution of this mode one sees that the distribution is symmetrical with respect to OX-axis and most of the field is in the bounding media due to large penetration (skin) depths given by $\hat{y}_i = \frac{1}{|\hat{k}_{yi}|}$ i.e., the decrease of the amplitude of the field in y-direction is small due to small $|\hat{k}_{yi}|$.

From eqn. (1.6) it can be seen that, since k_x' is close to k_o and k_x'' is very small for this mode, $|\hat{k}_{yi}|$ is small. Thus large portion of the field is in the bounding media with longer propagation length along the interfaces for this SP_s. This makes this mode very sensitive to surface properties (roughness, impurities, etc) and hence suitable for the study of surfaces at relatively long distances compared to ω^- mode. It is also more suitable for non linear interactions where a larger interaction range is desirable.

The strong field intensity (field enhancement) associated with this mode is due to resonance amplification of the electromagnetic field in the interfaces.

As can be seen from Figs.(3.2,6,13) the damping of the high-frequency mode (ω^+) decreases with decreasing thickness h of the metal film which is the reverse of the ω^- mode. This confirms the result obtained by Sarid [6].

The magnitude of k_x'' growing with the decreasing thickness of the film (compare fig. 3.2 and fig. 3.13). However, significant growth of k_x'' is found when a non absorbing film (fig. 3.6) is substituted by a strongly absorbing film of the same thickness (fig. 3.17).

<u>The physically unreal part of ω^+ mode</u> is the part of the dispersion curve with $V_g<0$ and $k_x''<0$, see figs (3.5,3.6). Negative k_x'' implies growing amplitude of the wave in ox-direction which is incompatible with the principle of conservation of energy. Negative group velocity also implies that if the wave is a forward wave then the energy of the wave is transferred in a backward direction which is incompatable with the definition of the group velocity as the velocity of amplitude (and with that energy) displacement in the medium. It is one of the newly obtained results since in the literature [6] the physical validity of this part of ω^+ mode hasn't been checked.

The second new result is the back-bending of the upper part of the physically real branch of the ω^+ mode, see Figs. (3.5, 3.16). This part of the curve correspond to the phenomena of artificial anomaleous dispersion. It is artificially created by PMA structure under consideration since neither of the materials used exhibit property of anomaleous dispersion in the specified frequency range when illuminated separately. This segment of the dispersion curve for k_x' correspond to an abrupt growth of damping (k_x'' grow by 10 orders in the case of non-absorbing film, see Fig. 3.6). The analysis of the power flow in ox-direction indicates that it drops to zero, see table 3.10, Fig 3.8. It means that at the ω and k_x' values corresponding to the back-bending of the ω^+ mode curve all the light energy incident on the PMA structure is either absorbed in it or is totally reflected back in the reverse direction.

Final decision about this point needs additional study of the reflectivity of the PMA structure for the corresponding values of ω, k_x' .

3.13 Analysis of the side mode

The side mode arises from the numerical solution of the thin film dispersion equation. The side mode lies to the left of the light line in Figs.(3.1,3.5,3.12,3.16) with $V_g < 0$. However, the imaginary part of the ox-wave vector corresponding to this mode, k_x'', is positive. The side mode curve looks like an extension of the back-bending

Table 3.1 (L40). Dependance of the REAL and the IMAG. parts of the SPIP OX-wavevector in PMA configuration: E3 = 1.0000001 , E21= E21(ω), E22 = E22(ω), E1 = 1 Plasma frequency Wp = 1.E+15 Hz, Relaxtion time Tau = .001 sec, Thickness of the film H= 5000 'A.'

L O W E R		ω(-)	B R A N C H		
ω/Wp	Ko	Kxr	Kxor	Kxi	No
.03513	+1.171721E+05	+1.1732759E+05	+1.172446E+05	+7.3192E-09	1
.06026	+2.009887E+05	+2.0177607E+05	+2.013559E+05	+2.1647E-08	2
.08538	+2.848053E+05	+2.8705772E+05	+2.858569E+05	+4.3811E-08	3
.11051	+3.686218E+05	+3.7354144E+05	+3.709220E+05	+7.4183E-08	5
.13564	+4.524384E+05	+4.6161940E+05	+4.567390E+05	+1.1329E-07	6
.16077	+5.362549E+05	+5.5171550E+05	+5.435138E+05	+1.6182E-07	7
.18590	+6.200715E+05	+6.4429518E+05	+6.314763E+05	+2.2068E-07	8
.21103	+7.038881E+05	+7.3987733E+05	+7.208878E+05	+2.9103E-07	10
.23615	+7.877046E+05	+8.3904867E+05	+8.120504E+05	+3.7431E-07	11
.26128	+8.715212E+05	+9.4248200E+05	+9.053186E+05	+4.7237E-07	15
.28641	+9.553377E+05	+1.0509593E+06	+1.001115E+06	+5.8757E-07	17
.31154	+1.039154E+06	+1.1654020E+06	+1.099951E+06	+7.2289E-07	19
.33667	+1.122971E+06	+1.2869111E+06	+1.202455E+06	+8.8224E-07	20
.36179	+1.206787E+06	+1.4168216E+06	+1.309414E+06	+1.0707E-06	23
.38692	+1.290604E+06	+1.5567777E+06	+1.421829E+06	+1.2951E-06	25
.41205	+1.374421E+06	+1.7088405E+06	+1.540998E+06	+1.5646E-06	28
.43718	+1.458237E+06	+1.8756444E+06	+1.668641E+06	+1.8921E-06	29
.46231	+1.542054E+06	+2.0606334E+06	+1.807098E+06	+2.2961E-06	32
.48744	+1.625870E+06	+2.2684313E+06	+1.959643E+06	+2.8039E-06	35
.51256	+1.709687E+06	+2.5054482E+06	+2.131024E+06	+3.4577E-06	36
.53769	+1.793503E+06	+2.7809299E+06	+2.328427E+06	+4.3265E-06	39
.56282	+1.877320E+06	+3.1089036E+06	+2.563338E+06	+5.5311E-06	41
.58795	+1.961136E+06	+3.5121238E+06	+2.855491E+06	+7.3005E-06	43
.61308	+2.044953E+06	+4.0311115E+06	+3.242337E+06	+1.0133E-05	45
.63821	+2.128770E+06	+4.7488852E+06	+3.806297E+06	+1.5334E-05	47
.66333	+2.212586E+06	+5.8814388E+06	+4.780128E+06	+2.7684E-05	50
.68846	+2.296403E+06	+8.3931778E+06	+7.300875E+06	+8.6123E-05	52

Table 3.2 .(L40). Dependance of the REAL and IMAG. parts of the SPlP OX-wavevector in PMA configuration : E3 = 1.0000001 , E21= E21(ω), E22 = E22(ω), E1 = 1 Plasma frequency Ωp = 1.E+15 Hz, Relaxtion time Tau = .001 sec, Thickness of the film H= 5000 'A.'

U P P E R	ω(+)	B R A N C H (physically real part)			
ω/Ωp	Ko	Kxr	Kxor	Kxi	No
.23615	+7.877046E+05	+7.9913019E+05	+8.120504E+05	+2.2575E-08	12
.33667	+1.122971E+06	+1.1605385E+06	+1.202455E+06	+6.8685E-08	21
.36179	+1.206787E+06	+1.2553918E+06	+1.309414E+06	+8.9712E-08	24
.38692	+1.290604E+06	+1.3528819E+06	+1.421829E+06	+1.1721E-07	26
.46231	+1.542054E+06	+1.6686066E+06	+1.807098E+06	+2.6790E-07	33
.53769	+1.793503E+06	+2.0499134E+06	+2.328427E+06	+6.7820E-07	38
.63821	+2.128770E+06	+2.9253185E+06	+3.806297E+06	+4.1082E-06	46
.66333	+2.212586E+06	+3.4272986E+06	+4.780128E+06	+9.3983E-06	49
.68846	+2.296403E+06	+4.8637864E+06	+7.300875E+06	+5.9295E-05	51
.71359	+2.380219E+06	+3.4654824E+06	+0.000000E+00	+2.8809E+06	53

Table 3.3 .(L40). Dependance of the REAL and IMAG. parts of the SPlP OX:wavevector in the PMA configuration : E3 = 1.0000001 , E21= E21(ω), E22 = E22(ω), E1 = 1 Plasma frequency Ωp = 1.E+15 Hz, Relaxtion time Tau = .001 sec, Thickness of the film H= 5000 'A.'

U P P E R	ω(+)	B R A N C H (physically unreal part)			
ω/Ωp	Ko	Kxr	Kxor	Kxi	No
.73872	+2.464036E+06	+2.6685507E+06	+0.000000E+00	-2.6900E+06	54

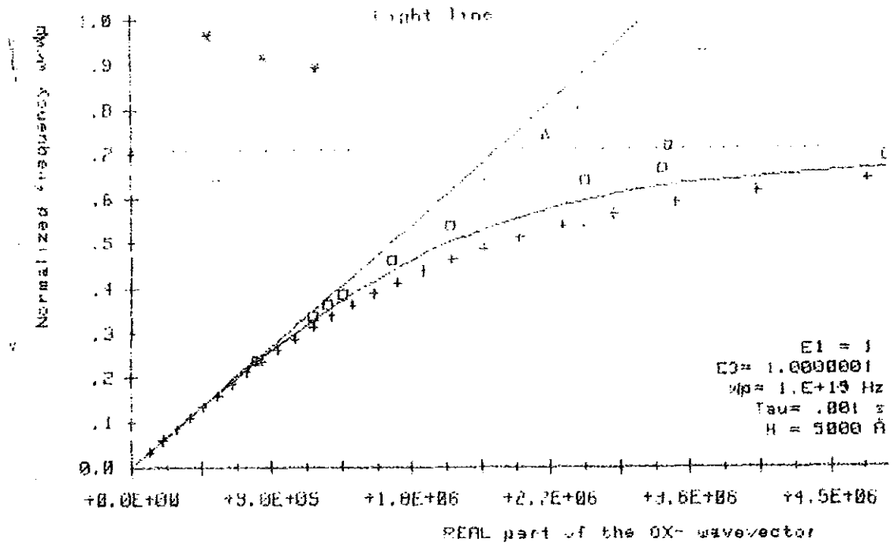

Fig. 3.1 .(L40) REAL part of the OX-wavevector as a function of the normalized frequency: w(-) mode - curve (+ + +), w(+) mode (physically real part)- curve with squares, w(+) mode (physically unreal part) - curve with triangles, semi-infinite case - solid curve, side branch - (* * * curve).

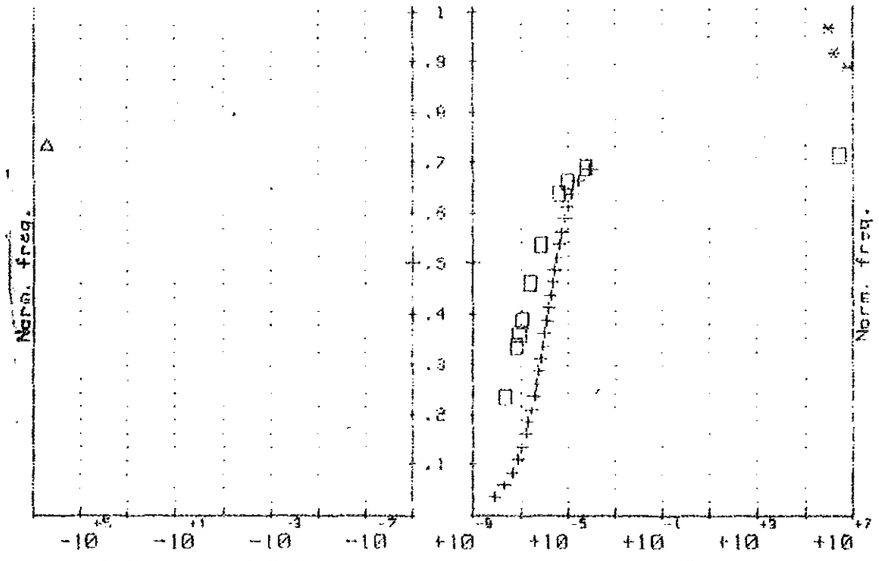

Fig. 3.2 .(L40). IMAG. part of the OX-wavevector as a function of the normalized freq.: w(-) mode - curve (+ + +), w(+) mode (physically real part) - curve with squares, w(+) mode (physically unreal part) - curve with triangles, side branch - (* * *) curve.
E1 = 1 , E3 = 1.0000001 , H = 5000 Å, Wp = 1.E+15 Hz, Tau = .001*sec

Table 3.4 (L40) Calculations for the power flow in Kretschmann PMA configuration with dielectric permittivities: E3 = 1.0000001 E21= E21(ω), E22 = E22(ω) E1 = 1 Plasma frequency Wp = 1 E+15 Hz. Relaxtion time Tau = .001 sec Thickness of the film H= 5000 'A ' Y-coordinate = 0 'A'

L O W E R	ω(-)			B R A N C H			
ω/Wp	Px1	Px2	Px3	Px net	Sy1	Sy2	Sy3	Nc
.02513	+.499977	-.0000011	+.500022	+1.0000	-2.01E-21	-2.01E-21	+2.01E-21	1
.06026	+.499987	-.0000099	+.500003	+1.0000	-2.00E-21	-2.00E-21	+2.00E-21	2
.08538	+.499976	-.0000402	+.499984	+.9999	-1.98E-21	-1.98E-21	+1.98E-21	3
.11051	+.499941	-.0001140	+.499945	+.9998	-1.95E-21	-1.95E-21	+1.95E-21	5
.13564	+.499868	-.0002620	+.499871	+.9995	-1.92E-21	-1.92E-21	+1.92E-21	6
.16077	+.499736	-.0005248	+.499739	+.9990	-1.88E-21	-1.88E-21	+1.88E-21	7
.18590	+.499522	-.0009549	+.499523	+.9981	-1.83E-21	-1.83E-21	+1.83E-21	8
.21103	+.499190	-.0016182	+.499192	+.9968	-1.78E-21	-1.78E-21	+1.78E-21	10
.23615	+.498701	-.0025967	+.498702	+.9948	-1.72E-21	-1.72E-21	+1.72E-21	11
.26128	+.498004	-.0039921	+.498004	+.9920	-1.66E-21	-1.66E-21	+1.66E-21	15
.28641	+.497035	-.0059296	+.497036	+.9881	-1.59E-21	-1.59E-21	+1.59E-21	17
.31154	+.495718	-.0085625	+.495719	+.9829	-1.51E-21	-1.51E-21	+1.51E-21	19
.33667	+.493960	-.0120789	+.493961	+.9758	-1.43E-21	-1.43E-21	+1.43E-21	20
.36179	+.491645	-.0167087	+.491646	+.9666	-1.34E-21	-1.34E-21	+1.34E-21	23
.38692	+.488624	-.0227322	+.488624	+.9545	-1.25E-21	-1.25E-21	+1.25E-21	25
.41205	+.484754	-.0304910	+.484755	+.9390	-1.16E-21	-1.16E-21	+1.16E-21	28
.43718	+.479800	-.0403995	+.479800	+.9192	-1.06E-21	-1.06E-21	+1.06E-21	29
.46231	+.473520	-.0529582	+.473521	+.8941	-9.54E-22	-9.54E-22	+9.54E-22	32
.48744	+.465614	-.0687710	+.465615	+.8625	-8.48E-22	-8.48E-22	+8.48E-22	35
.51256	+.455923	-.0885547	+.455923	+.8229	-7.39E-22	-7.39E-22	+7.39E-22	36
.53769	+.443421	-.1131587	+.443421	+.7737	-6.29E-22	-6.29E-22	+6.29E-22	39
.56282	+.428213	-.1435741	+.428213	+.7129	-5.17E-22	-5.17E-22	+5.17E-22	41
.58795	+.409528	-.1809441	+.409528	+.6381	-4.06E-22	-4.06E-22	+4.06E-22	43
.61308	+.386710	-.2265796	+.386710	+.5468	-2.97E-22	-2.97E-22	+2.97E-22	45
.63821	+.358993	-.2820138	+.358993	+.4360	-1.93E-22	-1.93E-22	+1.93E-22	47
.66333	+.325383	-.3492328	+.325384	+.3015	-9.68E-23	-9.68E-23	+9.68E-23	50
.68846	+.284167	-.4316655	+.284168	+.1367	-2.03E-23	-2.03E-23	+2.03E-23	52

Table 3.5 (L40) Calculations for the power flow in Kretschmann PMA configuration with dielectric permittivities: E3 = 1.0000001 E21= E21(ω), E22 = E22(ω) E1 = 1 Plasma frequency Wp = 1 E+15 Hz. Relaxtion time Tau = .001 sec. Thickness of the film H= 5000 'A ' Y-coordinate = 0 'A'

U P P E R	ω(+)			B R A N C H (physically real part)			
ω/Wp	Px1	Px2	Px3	Px net	Sy1	Sy2	Sy3	No
.23615	+.498660	-.0026808	+.498659	+.9946	-2.48E-22	-2.48E-22	+2.48E-22	12
.33667	+.493764	-.0124716	+.493764	+.9751	-3.02E-22	-3.02E-22	+3.02E-22	21
.36179	+.491373	-.0172534	+.491373	+.9655	-3.18E-22	-3.18E-22	+3.18E-22	24
.38692	+.488262	-.0234761	+.488262	+.9530	-3.37E-22	-3.37E-22	+3.37E-22	26
.41205	+.484263	-.0314367	+.484263	+.8905	-4.01E-22	-4.01E-22	+4.01E-22	33
.53769	+.441444	-.1171127	+.441444	+.7656	-4.93E-22	-4.93E-22	+4.93E-22	38
.63821	+.352990	-.2940207	+.352990	+.4120	-6.31E-22	-6.31E-22	+6.31E-22	46
.66333	+.316880	-.3662406	+.316880	+.2675	-6.77E-22	-6.77E-22	+6.77E-22	49
.68846	+.270601	-.4587985	+.270601	+.0824	-6.71E-22	-6.71E-22	+6.71E-22	51
.71359	+.250000	-.5000000	+.250000	+0.0000	-1.15E-10	-1.15E-10	+1.15E-10	53

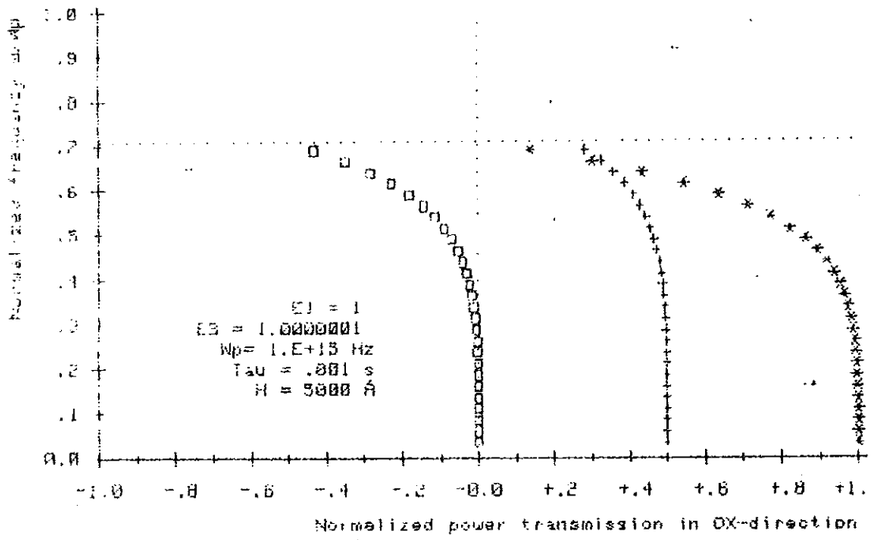

Fig. 3.3 .(L40) Partial and net power transmission in OX-direction performed by the w(-) mode : in media I and III - curve (+ + +), in the film - curve (with squares), the net power - curve (* * *)

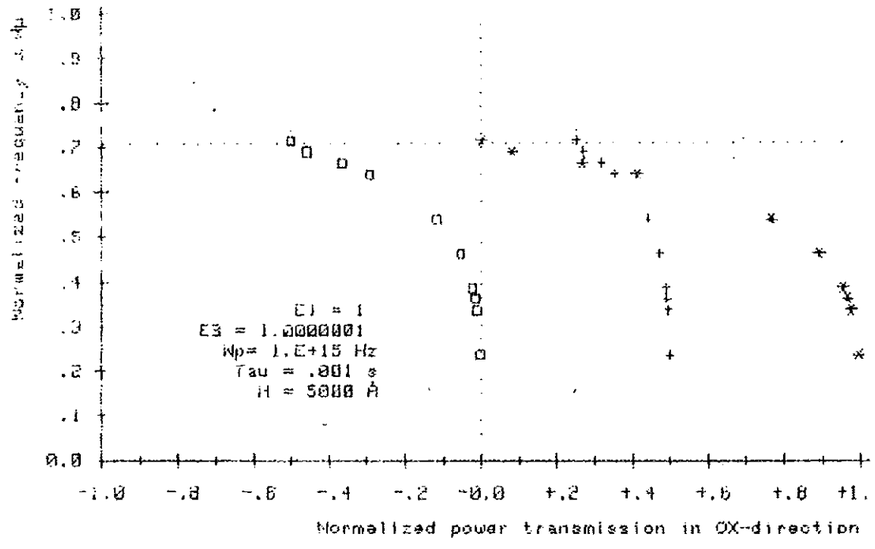

Fig. 3.4 .(L40) Partial and net power transmission in OX-direction performed by the w(+) mode : in media I and III - curve (+ + +), in the film - curve (with squares), the net power - curve (* * *)

Table 3.6 .(L25). Dependance of the PEAL and the IMAG. parts of the SP1P OX-wavevector in PMA configuration: E3 = 1.000000001 , E21= E21(ω), E22 = E22(ω), E1 = 1 Plasma frequency Wp = 1.E+15 Hz, Relaxtion time Tau = .001 sec, Thickness of the film H= 800 'A.'

L O W E R ω(-) B R A N C H

ω/Wp	Ko	Kxr	Kxor	Kxi	No
01000	+3.335557E+04	+3.3450256E+04	+3.335724E+04	+1.8801E-08	1
.02661	+8.875974E+04	+9.0530912E+04	+8.879120E+04	+1.3114E-07	2
.04322	+1.441639E+05	+1.5165196E+05	+1.442990E+05	+3.3660E-07	3
.05983	+1.995681E+05	+2.1906596E+05	+1.999275E+05	+6.2135E-07	4
.07644	+2.549722E+05	+2.9471820E+05	+2.557249E+05	+9.6981E-07	5
.09305	+3.103764E+05	+3.8023735E+05	+3.117408E+05	+1.3676E-06	6
.10966	+3.657806E+05	+4.7697247E+05	+3.680272E+05	+1.8029E-06	7
.12627	+4.211847E+05	+5.8605229E+05	+4.246390E+05	+2.2679E-06	8
.14288	+4.765889E+05	+7.0844848E+05	+4.816341E+05	+2.7561E-06	9
.15949	+5.319931E+05	+8.4503300E+05	+5.390749E+05	+3.2638E-06	10
.17610	+5.873972E+05	+9.9662600E+05	+5.970287E+05	+3.7926E-06	11
.19271	+6.428014E+05	+1.1640347E+06	+6.555685E+05	+4.3410E-06	12
.22593	+7.536098E+05	+1.5496476E+06	+7.747347E+05	+5.4985E-06	14
.25915	+8.644181E+05	+2.0091586E+06	+8.973229E+05	+6.7580E-06	16
.29237	+9.752264E+05	+2.5513030E+06	+1.024271E+06	+8.1514E-06	18
.30898	+1.030631E+06	+2.8566709E+06	+1.089744E+06	+8.9100E-06	20
.32559	+1.086035E+06	+3.1870175E+06	+1.156785E+06	+9.7200E-06	22
.34220	+1.141439E+06	+3.5442061E+06	+1.225609E+06	+1.0583E-05	24
.35881	+1.196843E+06	+3.9303735E+06	+1.296461E+06	+1.1519E-05	26
.37542	+1.252247E+06	+4.3479835E+06	+1.369634E+06	+1.2528E-05	28
.39203	+1.307651E+06	+4.7998949E+06	+1.445471E+06	+1.3630E-05	30
.40864	+1.363056E+06	+5.2894469E+06	+1.524386E+06	+1.4837E-05	32
.42525	+1.418460E+06	+5.8205691E+06	+1.606877E+06	+1.6173E-05	34
.44186	+1.473864E+06	+6.3979253E+06	+1.693552E+06	+1.7663E-05	36
.45847	+1.529268E+06	+7.0271028E+06	+1.785161E+06	+1.9334E-05	38
.47508	+1.584672E+06	+7.7148684E+06	+1.882647E+06	+2.1223E-05	40
.49169	+1.640076E+06	+8.4695188E+06	+1.987206E+06	+2.3400E-05	42
.50831	+1.695481E+06	+9.3013727E+06	+2.100383E+06	+2.5913E-05	44
.52492	+1.750885E+06	+1.0223478E+07	+2.224219E+06	+2.8869E-05	46
.54153	+1.806289E+06	+1.1252660E+07	+2.361469E+06	+3.2406E-05	48
.55814	+1.861693E+06	+1.2411123E+07	+2.515951E+06	+3.6711E-05	50
.57475	+1.917097E+06	+1.3729009E+07	+2.693144E+06	+4.2076E-05	52
.59136	+1.972501E+06	+1.5248683E+07	+2.901227E+06	+4.8968E-05	54
.60797	+2.027906E+06	+1.7032365E+07	+3.153059E+06	+5.8138E-05	56
.62458	+2.083310E+06	+1.9176848E+07	+3.470260E+06	+7.0998E-05	58
.64119	+2.138714E+06	+2.1845017E+07	+3.892684E+06	+9.0312E-05	61
.65780	+2.194118E+06	+2.5344189E+07	+4.504365E+06	+1.2267E-04	64
.67441	+2.249522E+06	+3.0371633E+07	+5.525760E+06	+1.8806E-04	67
.69102	+2.304926E+06	+3.9204138E+07	+7.854794E+06	+3.8988E-04	70

Table 3.7 .(L25). Dependance of the REAL and IMAG. parts of the SP1P OX-wavevector in PMA configuration : E3 = 1.000000001 , E21= E21(ω), E22 = E22(ω), E1 = 1 Plasma frequency Wp = 1.E+15 Hz, Relaxtion time Tau = .001 sec, Thickness of the film H= 800 'A.'

U P P E R ω(+) B R A N C H (physically real part)

ω/Wp	Ko	Kxr	Kxor	Kxi	No
.65780	+2.194118E+06	+2.2204500E+06	+4.504365E+06	+6.3280E-08	63
.67441	+2.249522E+06	+2.2803513E+06	+5.525760E+06	+7.9374E-08	66
.70763	+2.360331E+06	+2.4031844E+06	+0.000000E+00	+1.2784E-07	72
.72424	+2.415735E+06	+2.4667129E+06	+0.000000E+00	+1.6474E-07	74
.74085	+2.471139E+06	+2.5322452E+06	+0.000000E+00	+2.1502E-07	77
.75746	+2.526543E+06	+2.6004710E+06	+0.000000E+00	+2.8515E-07	80
.77407	+2.581947E+06	+2.6724121E+06	+0.000000E+00	+3.8567E-07	83
.79068	+2.637351E+06	+2.7496455E+06	+0.000000E+00	+5.3495E-07	86
.80729	+2.692756E+06	+2.8347324E+06	+0.000000E+00	+7.6673E-07	89
.84051	+2.803564E+06	+3.0504113E+06	+0.000000E+00	+1.8464E-06	95
.85712	+2.858968E+06	+3.2088004E+06	+0.000000E+00	+3.3232E-06	98
.87373	+2.914372E+06	+3.4654978E+06	+0.000000E+00	+7.7043E-06	101
.89034	+2.969776E+06	+4.4644774E+06	+0.000000E+00	+3.2982E+05	104
.90695	+3.025181E+06	+3.8450879E+06	+0.000000E+00	+1.3887E+06	106
.92356	+3.080585E+06	+3.2594951E+06	+0.000000E+00	+1.7025E+06	107

Table 3.8 .(L25). Dependance of the REAL and IMAG. parts of the SP1P OX-wavevector in the PMA configuration : E3 = 1.000000001 , E21= E21(ω), E22 = E22(ω), E1 = 1 Plasma frequency Wp = 1.E+15 Hz, Relaxtion time Tau = .001 sec, Thickness of the film H= 800 'A.'

U P P E R ω(+) B R A N C H (physically unreal part)

ω/Wp	Ko	Kxr	Kxor	Kxi	No
.72424	+2.415735E+06	+3.7114724E+07	+0.000000E+00	-3.6406E-04	75
.74085	+2.471139E+06	+2.8559213E+07	+0.000000E+00	-1.8836E-04	78
.75746	+2.526543E+06	+2.3410168E+07	+0.000000E+00	-1.2819E-04	81
.77407	+2.581947E+06	+1.9679804E+07	+0.000000E+00	-9.7851E-05	84
.79068	+2.637351E+06	+1.6729497E+07	+0.000000E+00	-7.9640E-05	87
.80729	+2.692756E+06	+1.4269587E+07	+0.000000E+00	-6.7603E-05	90
.82390	+2.748160E+06	+1.2141074E+07	+0.000000E+00	-5.9234E-05	93
.84051	+2.803564E+06	+1.0242223E+07	+0.000000E+00	-5.3407E-05	96
.85712	+2.858968E+06	+8.4928570E+06	+0.000000E+00	-4.9849E-05	99
.87373	+2.914372E+06	+6.7921695E+06	+0.000000E+00	-5.0296E-05	102

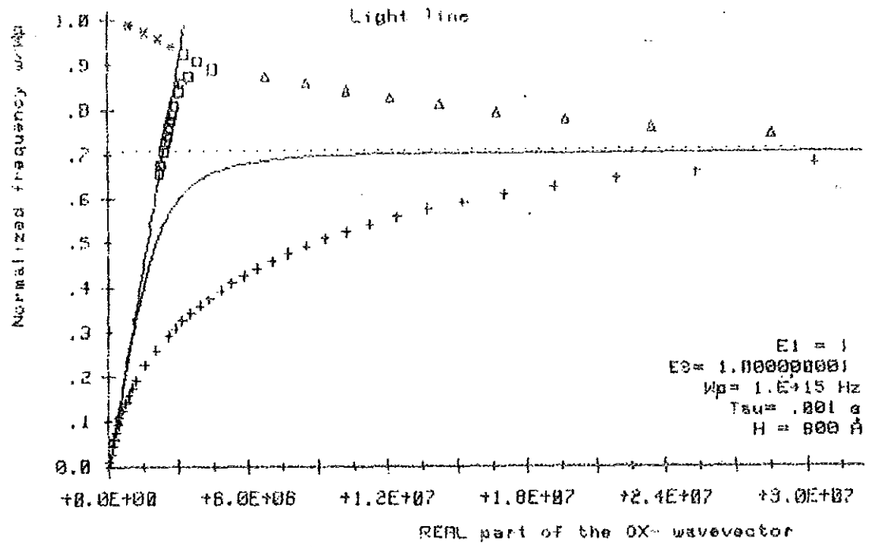

Fig. 3.5 .(L29) REAL part of the OX-wavevector as a function of the normalized frequency: w(-) mode - curve (+ + +), w(+) mode (physically real part)- curve with squares, w(+) mode (physically unreal part) - curve with triangles, semi-infinite case - solid curve, side branch - (x x x curve).

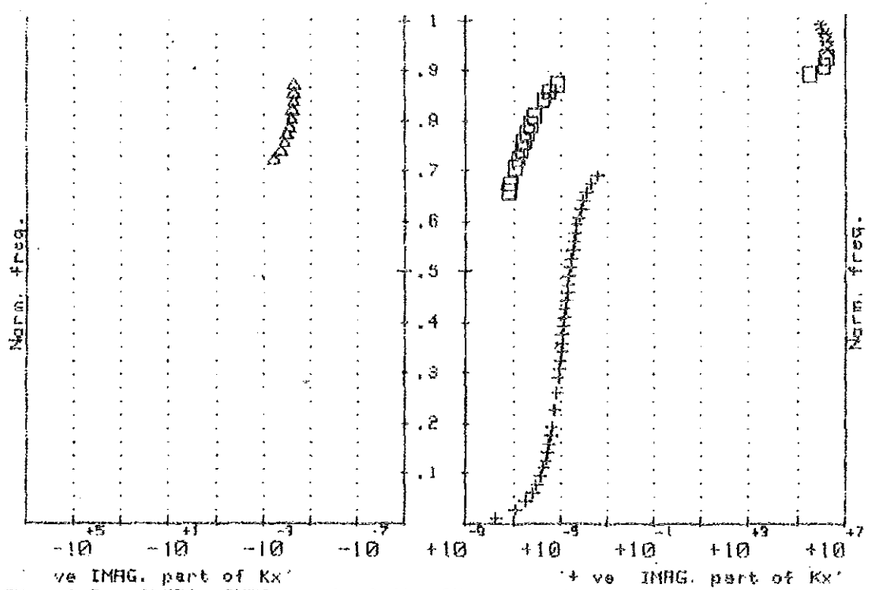

Fig. 3.6 .(L25). IMAG. part of the OX-wavevector as a function of the normalized freq.: w(-) mode - curve (+ + +), w(+) mode (physically real part) - curve with squares, w(+) mode (physically unreal part) - curve with triangles, side branch - (x x x) curve.
E1 = 1 , E3 = 1.000000001 , H = 800 Å, Wp = 1.E+15 Hz, Tau = .00[illegible]

Table 3.9 .(L25). Calculations for the power flow in Kretschmann PMA configuration with dielectric permittivities: E3 = 1.000000001 , E21= E21(ω). E22 = E22(ω), E1 = 1 Plasma frequency Wp = 1.E+15 Hz, Relaxtion time Tau = .001 sec, Thickness of the film H= 800 'A.' Y-coordinate = 0 'A'

L O W E R			ω(-)		B R A N C H			
ω/Wp	Px1	Px2	Px3	Px net	Sy1	Sy2	Sy3	No
.01000	+.500000	-0.0000000	+.500000	+1.0000	-1.25E-20	-1.25E-20	+1.25E-20	1
.02661	+.500000	-.0000003	+.500000	+1.0000	-1.25E-20	-1.25E-20	+1.25E-20	2
.04322	+.499999	-.0000023	+.499999	+1.0000	-1.25E-20	-1.25E-20	+1.25E-20	3
.05983	+.499996	-.0000086	+.499996	+1.0000	-1.24E-20	-1.24E-20	+1.24E-20	4
.07644	+.499988	-.0000231	+.499988	+1.0000	-1.24E-20	-1.24E-20	+1.24E-20	5
.09305	+.499974	-.0000510	+.499974	+.9999	-1.23E-20	-1.23E-20	+1.23E-20	6
.10966	+.499950	-.0000991	+.499950	+.9998	-1.22E-20	-1.22E-20	+1.22E-20	7
.12627	+.499912	-.0001756	+.499912	+.9996	-1.21E-20	-1.21E-20	+1.21E-20	8
.14288	+.499855	-.0002905	+.499855	+.9994	-1.20E-20	-1.20E-20	+1.20E-20	9
.15949	+.499772	-.0004557	+.499772	+.9991	-1.19E-20	-1.19E-20	+1.19E-20	10
.17610	+.499658	-.0006849	+.499658	+.9986	-1.17E-20	-1.17E-20	+1.17E-20	11
.19271	+.499503	-.0009946	+.499503	+.9980	-1.16E-20	-1.16E-20	+1.16E-20	12
.22593	+.499033	-.0019332	+.499033	+.9961	-1.12E-20	-1.12E-20	+1.12E-20	14
.25915	+.498270	-.0034594	+.498270	+.9931	-1.08E-20	-1.08E-20	+1.08E-20	16
.29237	+.497089	-.0058215	+.497089	+.9884	-1.03E-20	-1.03E-20	+1.03E-20	18
.30898	+.496293	-.0074144	+.496293	+.9852	-1.01E-20	-1.01E-20	+1.01E-20	20
.32559	+.495327	-.0093461	+.495327	+.9813	-9.83E-21	-9.83E-21	+9.83E-21	22
.34220	+.494163	-.0116735	+.494163	+.9767	-9.55E-21	-9.55E-21	+9.55E-21	24
.35881	+.492769	-.0144616	+.492769	+.9711	-9.26E-21	-9.26E-21	+9.26E-21	26
.37542	+.491108	-.0177850	+.491108	+.9644	-8.95E-21	-8.95E-21	+8.95E-21	28
.39203	+.489136	-.0217288	+.489136	+.9565	-8.63E-21	-8.63E-21	+8.63E-21	30
.40864	+.486805	-.0263905	+.486805	+.9472	-8.29E-21	-8.30E-21	+8.29E-21	32
.42525	+.484059	-.0318812	+.484059	+.9362	-7.95E-21	-7.95E-21	+7.95E-21	34
.44186	+.480836	-.0383278	+.480836	+.9233	-7.59E-21	-7.59E-21	+7.59E-21	36
.45847	+.477062	-.0458750	+.477062	+.9082	-7.21E-21	-7.21E-21	+7.21E-21	38
.47508	+.472656	-.0546874	+.472656	+.8906	-6.82E-21	-6.82E-21	+6.82E-21	40
.49169	+.467524	-.0649521	+.467524	+.8701	-6.42E-21	-6.42E-21	+6.42E-21	42
.50831	+.461559	-.0768811	+.461559	+.8462	-6.00E-21	-6.00E-21	+6.00E-21	44
.52492	+.454643	-.0907143	+.454643	+.8186	-5.57E-21	-5.57E-21	+5.57E-21	46
.54153	+.446639	-.1067221	+.446639	+.7866	-5.13E-21	-5.13E-21	+5.13E-21	48
.55814	+.437395	-.1252091	+.437395	+.7496	-4.67E-21	-4.67E-21	+4.67E-21	50
.57475	+.426741	-.1465173	+.426741	+.7070	-4.20E-21	-4.20E-21	+4.20E-21	52
.59136	+.414484	-.1710319	+.414484	+.6579	-3.72E-21	-3.71E-21	+3.72E-21	54
.60797	+.400405	-.1991891	+.400405	+.6016	-3.22E-21	-3.22E-21	+3.22E-21	56
.62458	+.384253	-.2314930	+.384253	+.5370	-2.71E-21	-2.71E-21	+2.71E-21	58
.64119	+.365724	-.2685519	+.365724	+.4629	-2.18E-21	-2.18E-21	+2.18E-21	61
.65780	+.344416	-.3111680	+.344416	+.3777	-1.65E-21	-1.65E-21	+1.65E-21	64
.67441	+.319701	-.3605989	+.319701	+.2788	-1.10E-21	-1.10E-21	+1.10E-21	67
.69102	+.290218	-.4195644	+.290218	+.1609	-5.39E-22	-5.39E-22	+5.39E-22	70

Table 3.10 .(L25). Calculations for the power flow in Kretschmann PMA configuration with dielectric permittivities: E3 = 1.000000001 , E21= E21(w), E22 = E22(w), E1 = 1 Plasma frequency Wp = 1.E+15 Hz, Relaxtion time Tau = .001 sec, Thickness of the film H= 800 'A.' Y-coordinate = 0 'A'

U P P E R	w(+)	B R A N C H (physically real part)						
w/Wp	Px1	Px2	Px3	Px net	Sy1	Sy2	Sy3	No
.65780	+.489929	-.0201429	+.489929	+.9597	-2.97E-22	-2.97E-22	+2.97E-22	63
.67441	+.487974	-.0240521	+.487974	+.9519	-3.38E-22	-3.38E-22	+3.38E-22	66
.70763	+.482710	-.0345796	+.482710	+.9308	-4.47E-22	-4.47E-22	+4.47E-22	72
.72424	+.479157	-.0416863	+.479157	+.9166	-5.19E-22	-5.19E-22	+5.19E-22	74
.74085	+.474759	-.0504823	+.474759	+.8990	-6.08E-22	-6.08E-22	+6.08E-22	77
.75746	+.469268	-.0614636	+.469268	+.8771	-7.20E-22	-7.20E-22	+7.20E-22	80
.77407	+.462345	-.0753092	+.462345	+.8494	-8.65E-22	-8.65E-22	+8.65E-22	83
.79068	+.453517	-.0929661	+.453517	+.8141	-1.06E-21	-1.06E-21	+1.06E-21	86
.80729	+.442108	-.1157849	+.442108	+.7684	-1.32E-21	-1.32E-21	+1.32E-21	89
.84051	+.407042	-.1859155	+.407042	+.6282	-2.30E-21	-2.30E-21	+2.30E-21	95
.85712	+.379306	-.2413889	+.379306	+.5172	-3.38E-21	-3.38E-21	+3.38E-21	98
.87373	+.338624	-.3227527	+.338624	+.3545	-6.04E-21	-6.04E-21	+6.04E-21	101
.89034	+.250000	-.5000000	+.250000	+0.0000	-1.45E-10	-1.45E-10	+1.45E-10	104
.90695	+.250000	-.5000000	+.250000	+0.0000	-6.93E-10	-6.93E-10	+6.93E-10	106
.92356	+.250000	-.5000000	+.250000	+0.0000	-9.74E-10	-9.74E-10	+9.74E-10	107

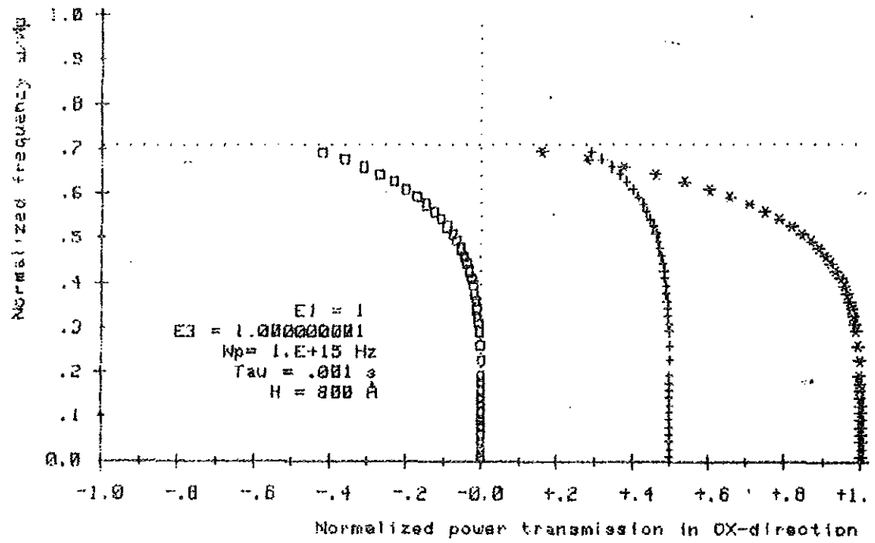

Fig. 3.7 .(L25) Partial and net power transmission in OX-direction performed by the w(-) mode : in media I and III - curve (+ + +), in the film - curve (with squares), the net power - curve (* * *)

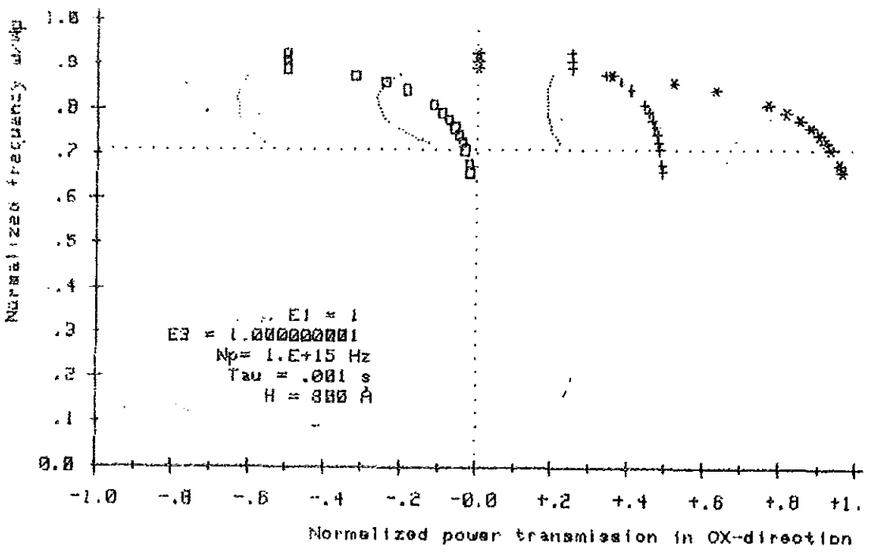

Fig. 3.8 .(L25) Partial and net power transmission in OX-direction performed by the w(+) mode : in media I and III - curve (+ + +), in the film - curve (with squares), the net power - curve (* * *)

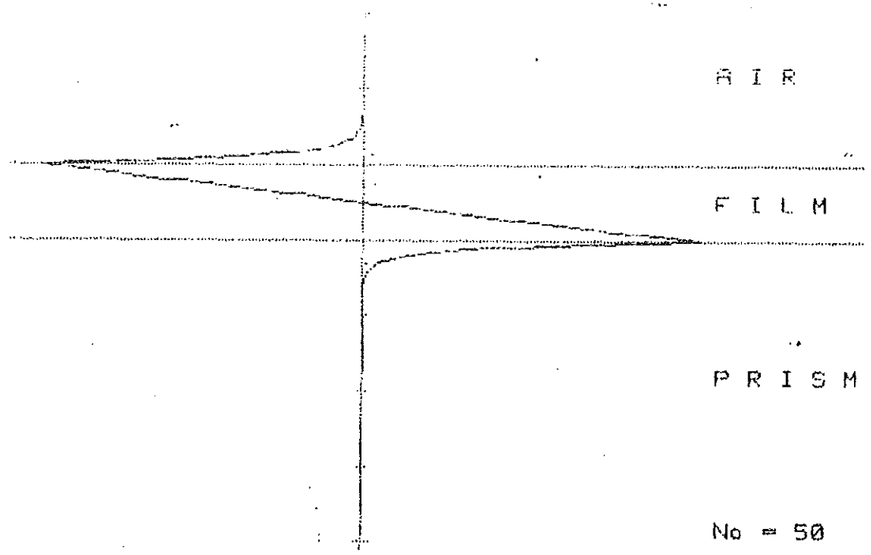

Fig. 3.9 .(L25) Magnetic field distribution in the w(-) mode
E1 = 1 , E3 = 1.000000001 , Wp = 1.E+15 Hz, Tau = .001 s, Wn = .5581355
H = 800 A, Ko = 1.0616931061 4E+6 Kxr = 1.24111230692E+7
Kxor = 2.51595125004E+6 , Kxi = 9.67105700356E-5 Data file name:L25

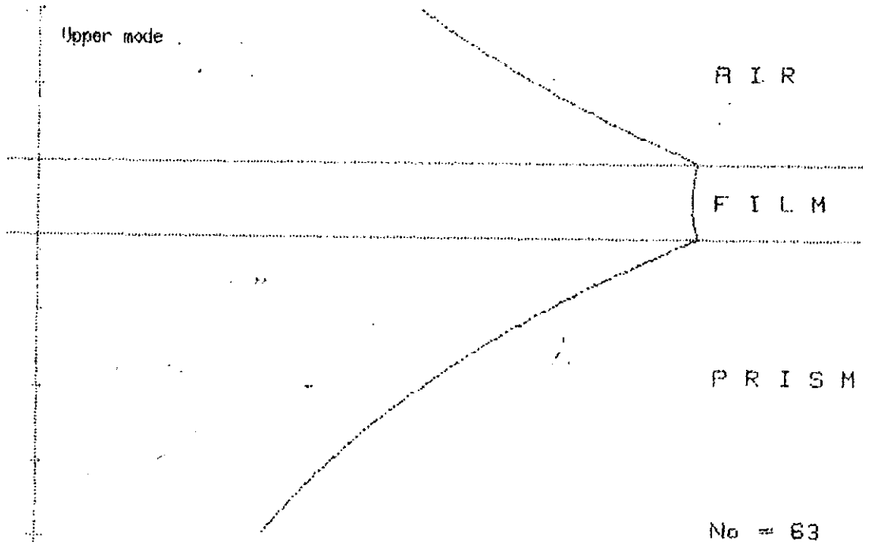

Fig. 3.10 .(L25) Magnetic field distribution in the w(+) mode
E1 = 1 , E3 = 1.000000001 , Wp = 1.E+15 Hz, Tau = .001 s, Wn = .6577966
H = 800 A, Ko = 2.1941101126 4E+6 Kxr = 2.22045082037E+6
Kxor= 4.50436495046E+6 , Kxi = 6.3279606697E-9 Data file name:L25

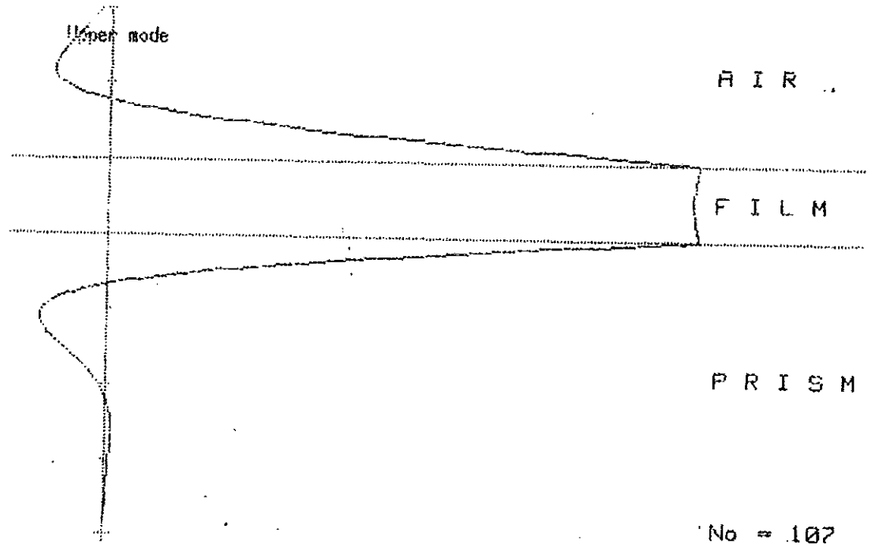

Fig. 3.11 ,(L25) Magnetic field distribution in the w(+) mode
E1 = 1 , E3 = 1.000000001 , Wp = 1.E+15 Hz, Tau = .001 s, Wn = .9235583;
H = 800 A, Ko = 3.000504796G4E+6 Kxr = 3.259495100033E+6
Kxor= 0 , Kxi = 1.702593249IE+6 Data file name:L25

Table 3.11 .(L18) Dependance of the REAL and the IMAG. parts of the SP1P OX-wavevector in PMA configuration: E3 = 1.000000001 , E21= E21(ω), E22 = E22(ω), E1 = 1 Plasma frequency Wp = 1.E+15 Hz, Relaxtion time Tau = .001 sec. Thickness of the film H= 100 'A.'

L O W E R ω(-) B R A N C H

ω/Wp	Ko	Kxr	Kxor	Kxi	No
.01000	+3.335557E+04	+3.8894065E+04	+3.335724E+04	+1.0287E-06	1
.02241	+7.473337E+04	+1.2520666E+05	+7.475214E+04	+3.5989E-06	2
.07203	+2.402446E+05	+1.0703560E+06	+2.408734E+05	+1.4182E-05	6
.15886	+5.298891E+05	+5.2066961E+06	+5.368847E+05	+3.3287E-05	13
.17127	+5.712669E+05	+6.0729987E+06	+5.800990E+05	+3.6227E-05	14
.24570	+8.195337E+05	+1.2893960E+07	+8.471995E+05	+5.5762E-05	20
.25810	+8.609115E+05	+1.4325673E+07	+8.933822E+05	+5.9436E-05	21
.29532	+9.850449E+05	+1.9194422E+07	+1.035768E+06	+7.1448E-05	24
.32013	+1.067800E+06	+2.2963516E+07	+1.134535E+06	+8.0457E-05	28
.33253	+1.109178E+06	+2.5021191E+07	+1.185304E+06	+8.5298E-05	29
.36975	+1.233312E+06	+3.1960193E+07	+1.344344E+06	+1.0172E-04	32
.39456	+1.316067E+06	+3.7328958E+07	+1.457249E+06	+1.1454E-04	36
.40696	+1.357445E+06	+4.0259084E+07	+1.516241E+06	+1.2163E-04	38
.41937	+1.398823E+06	+4.3372578E+07	+1.577195E+06	+1.2935E-04	40
.43177	+1.440201E+06	+4.6684245E+07	+1.640352E+06	+1.3762E-04	42
.44418	+1.481578E+06	+5.0210982E+07	+1.705993E+06	+1.4667E-04	44
.45658	+1.522956E+06	+5.3972185E+07	+1.774448E+06	+1.5657E-04	46
.46899	+1.564334E+06	+5.7990251E+07	+1.846110E+06	+1.6739E-04	48
.48139	+1.605712E+06	+6.2291225E+07	+1.921445E+06	+1.7936E-04	50
.49380	+1.647090E+06	+6.6905618E+07	+2.001019E+06	+1.9274E-04	52
.50620	+1.688467E+06	+7.1869480E+07	+2.085516E+06	+2.0758E-04	54
.51861	+1.729845E+06	+7.7225807E+07	+2.175781E+06	+2.2442E-04	56
.53101	+1.771223E+06	+8.3026441E+07	+2.272869E+06	+2.4352E-04	58
.54342	+1.812601E+06	+8.9334646E+07	+2.378113E+06	+2.6545E-04	60
.55582	+1.853979E+06	+9.6228721E+07	+2.493227E+06	+2.9088E-04	62
.56823	+1.895356E+06	+1.0380715E+08	+2.620460E+06	+3.2079E-04	64
.58063	+1.936734E+06	+1.1219610E+08	+2.762824E+06	+3.5649E-04	66
.59304	+1.978112E+06	+1.2156129E+08	+2.924466E+06	+3.9981E-04	68

Table 3.12 .(L18). Dependance of the PEAL and IMAG. parts of the SPIP OX-wavevector in PMA configuration : E3 = 1.000000001 , E21= E21(ω), E22 = E22(ω), E1 = 1 Plasma frequency Ωp = 1.E+15 Hz, Relaxtion time Tau = .001 sec, Thickness of the film H= 100 'A.' .

U P P E R	ω(+)	B R A N C H (physically real part)			
ω/Ωp	Ko	Kxr	Kxor	Kxi	No
.65506	+2.185001E+06	+2.1854011E+06	+4.384446E+06	+9.1870E-10	77
.67987	+2.267757E+06	+2.2682607E+06	+6.050549E+06	+1.2755E-09	81
.69228	+2.309134E+06	+2.3097020E+06	+8.179650E+06	+1.5102E-09	83
.71709	+2.391890E+06	+2.3926150E+06	+0.000000E+00	+2.1424E-09	87
.72949	+2.433268E+06	+2.4340908E+06	+0.000000E+00	+2.5693E-09	90
.75430	+2.516023E+06	+2.5170956E+06	+0.000000E+00	+3.7582E-09	94
.77911	+2.598779E+06	+2.6002008E+06	+0.000000E+00	+5.6465E-09	99
.79152	+2.640157E+06	+2.6418075E+06	+0.000000E+00	+7.0091E-09	102
.80392	+2.681535E+06	+2.6834636E+06	+0.000000E+00	+8.7870E-09	105
.81633	+2.722912E+06	+2.7251835E+06	+0.000000E+00	+1.1142E-08	108
.82873	+2.764290E+06	+2.7669872E+06	+0.000000E+00	+1.4314E-08	111
.87835	+2.929801E+06	+2.9358535E+06	+0.000000E+00	+4.6826E-08	120
.89076	+2.971179E+06	+2.9789165E+06	+0.000000E+00	+6.7279E-08	122
.91557	+3.053935E+06	+3.0677194E+06	+0.000000E+00	+1.5831E-07	126
.92797	+3.095312E+06	+3.1148937E+06	+0.000000E+00	+2.6712E-07	128
.97759	+3.260824E+06	+3.5549840E+06	+0.000000E+00	+1.8043E-05	136

Table 3.13 .(L18). Dependance of the REAL and IMAG. parts of the SPIP OX:wavevector in the PMA configuration : E3 = 1.000000001 , E21= E21(ω), E22 = E22(ω), E1 = 1 Plasma frequency Ωp = 1.E+15 Hz, Relaxtion time Tau = .001 sec, Thickness of the film H= 100 'A.'

U P P E R	ω(+)	B R A N C H (physically unreal part)			
ω/Ωp	Ko	Kxr	Kxor	Kxi	No
.77911	+2.598779E+06	+1.5409424E+08	+0.000000E+00	-7.2806E-04	100
.79152	+2.640157E+06	+1.3736511E+08	+0.000000E+00	-6.2575E-04	103
.80392	+2.681535E+06	+1.2282544E+08	+0.000000E+00	-5.4962E-04	106
.81633	+2.722912E+06	+1.0994708E+08	+0.000000E+00	-4.9067E-04	109
.82873	+2.764290E+06	+9.8372886E+07	+0.000000E+00	-4.4375E-04	112
.84114	+2.805668E+06	+8.7849955E+07	+0.000000E+00	-4.0553E-04	115
.85354	+2.847046E+06	+7.8192580E+07	+0.000000E+00	-3.7368E-04	117
.86595	+2.888424E+06	+6.9260282E+07	+0.000000E+00	-3.4685E-04	119
.87835	+2.929801E+06	+6.0944107E+07	+0.000000E+00	-3.2386E-04	121
.89076	+2.971179E+06	+5.3157680E+07	+0.000000E+00	-3.0400E-04	123
.90316	+3.012557E+06	+4.5831101E+07	+0.000000E+00	-2.8670E-04	125
.91557	+3.053935E+06	+3.8906556E+07	+0.000000E+00	-2.7150E-04	127
.92797	+3.095312E+06	+3.2334823E+07	+0.000000E+00	-2.5812E-04	129
.94038	+3.136690E+06	+2.6071821E+07	+0.000000E+00	-2.4649E-04	131
.95278	+3.178068E+06	+2.0073279E+07	+0.000000E+00	-2.3676E-04	133
.96519	+3.219446E+06	+1.4279322E+07	+0.000000E+00	-2.3029E-04	135
.97759	+3.260824E+06	+8.5124826E+06	+0.000000E+00	-2.4001E-04	137

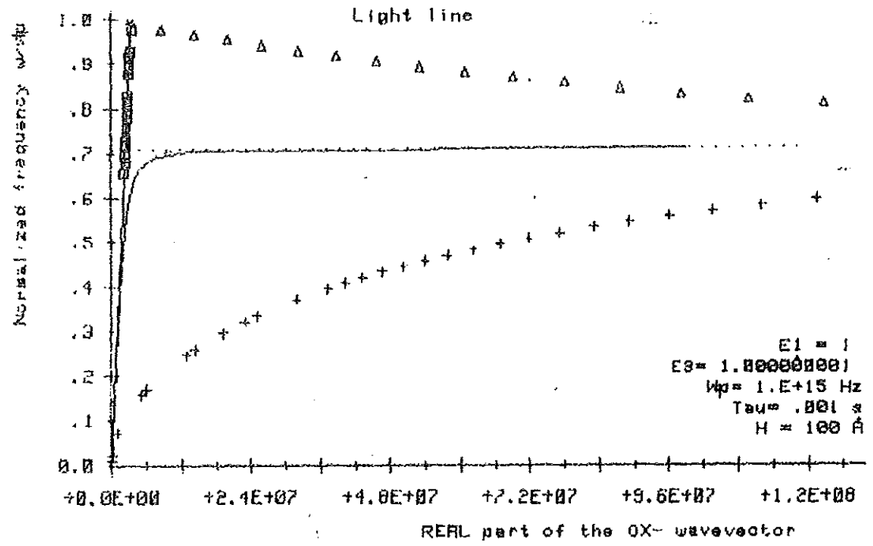

Fig. 3.12 .(L18) REAL part of the OX-wavevector as a function of the normalized frequency: w(-) mode - curve (+ + +), w(+) mode (physically real part)- curve with squares, w(+) mode (physically unreal part) - curve with triangles, semi-infinite case - solid curve, side branch - (* * * curve).

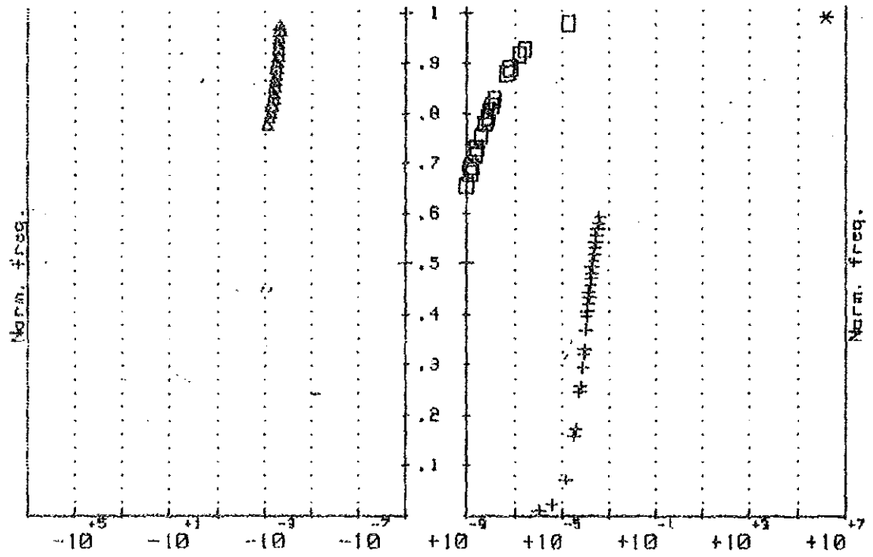

Fig. 3.13 .(L18). IMAG. part of the OX-wavevector as a function of the normalized freq.: w(-) mode - curve (+ + +), w(+) mode (physically real part) - curve with squares, w(+) mode (physically unreal part) - curve with triangles, side branch - (* * *) curve.
E1 = 1 , E3 = 1.000000001 , H = 100 Å, Wp = 1.E+15 Hz, Tau = .00* s.

Table 3.14 .(L18). Calculations for the power flow in Kretschmann PMA configuration with dielectric permittivities: E3 = 1.000000001 , E21= E21(ω), E22 = E22(ω), E1 = 1 Plasma frequency Ωp = 1.E+15 Hz, Relaxtion time Tau = .001 sec, Thickness of the film H= 100 'A.' Y-coordinate = 0 'A'

L O W E R	ω(-)			B R A N C H				
w/Ωp	Px1	Px2	Px3	Px net	Sy1	Sy2	Sy3	No
.01000	+.500000	-0.0000000	+.500000	+1.0000	-1.00E-19	-1.00E-19	+1.00E-19	1
.02241	+.500000	-.0000002	+.500000	+1.0000	-9.99E-20	-9.99E-20	+9.99E-20	2
.07203	+.499991	-.0000181	+.499991	+1.0000	-9.89E-20	-9.90E-20	+9.89E-20	6
.15886	+.499777	-.0004468	+.499777	+.9991	-9.50E-20	-9.50E-20	+9.50E-20	13
.17127	+.499696	-.0006085	+.499696	+.9988	-9.41E-20	-9.41E-20	+9.41E-20	14
.24570	+.498627	-.0027465	+.498627	+.9945	-8.79E-20	-8.79E-20	+8.79E-20	20
.25810	+.498306	-.0033880	+.498306	+.9932	-8.67E-20	-8.67E-20	+8.67E-20	21
.29532	+.496970	-.0060604	+.496970	+.9879	-8.26E-20	-8.26E-20	+8.26E-20	24
.32013	+.495680	-.0086398	+.495680	+.9827	-7.95E-20	-7.95E-20	+7.95E-20	28
.33253	+.494884	-.0102313	+.494884	+.9795	-7.79E-20	-7.79E-20	+7.79E-20	29
.36975	+.491736	-.0165272	+.491736	+.9669	-7.27E-20	-7.26E-20	+7.27E-20	32
.39456	+.488844	-.0223120	+.488844	+.9554	-6.89E-20	-6.88E-20	+6.89E-20	36
.40696	+.487102	-.0257950	+.487102	+.9484	-6.69E-20	-6.69E-20	+6.69E-20	38
.41937	+.485134	-.0297321	+.485134	+.9405	-6.48E-20	-6.48E-20	+6.48E-20	40
.43177	+.482913	-.0341742	+.482913	+.9317	-6.27E-20	-6.27E-20	+6.27E-20	42
.44418	+.480411	-.0391780	+.480411	+.9216	-6.05E-20	-6.05E-20	+6.05E-20	44
.45658	+.477597	-.0448054	+.477597	+.9104	-5.83E-20	-5.83E-20	+5.83E-20	46
.46899	+.474437	-.0511251	+.474437	+.8977	-5.60E-20	-5.60E-20	+5.60E-20	48
.48139	+.470894	-.0582124	+.470894	+.8836	-5.36E-20	-5.37E-20	+5.36E-20	50
.49380	+.466925	-.0661502	+.466925	+.8677	-5.12E-20	-5.12E-20	+5.12E-20	52
.50620	+.462485	-.0750294	+.462485	+.8499	-4.87E-20	-4.88E-20	+4.87E-20	54
.51861	+.457525	-.0849497	+.457525	+.8301	-4.62E-20	-4.62E-20	+4.62E-20	56
.53101	+.451990	-.0960204	+.451990	+.8080	-4.36E-20	-4.36E-20	+4.36E-20	58
.54342	+.445820	-.1083608	+.445820	+.7833	-4.09E-20	-4.09E-20	+4.09E-20	60
.55582	+.438949	-.1221012	+.438949	+.7558	-3.82E-20	-3.82E-20	+3.82E-20	62
.56823	+.431308	-.1373839	+.431308	+.7252	-3.54E-20	-3.54E-20	+3.54E-20	64
.58063	+.422818	-.1543642	+.422818	+.6913	-3.26E-20	-3.26E-20	+3.26E-20	66
.59304	+.413394	-.1732123	+.413394	+.6536	-2.97E-20	-2.97E-20	+2.97E-20	68

Table 3.15 .(L18). Calculations for the power flow in Kretschmann PMA configuration with dielectric permittivities: E3 = 1.000000001 , E21= E21(ω), E22 = E22(ω), E1 = 1 Plasma frequency Ωp = 1.E+15 Hz, Relaxtion time Tau = .001 sec, Thickness of the film H= 100 'A.' Y-coordinate = 0 'A'

U P P E R	ω(+)		B R A N C H (physically real part)					
ω/Ωp	Px1	Px2	Px3	Px net	Sy1	Sy2	Sy3	Nc
.65506	+.499843	-.0003142	+.499843	+.9994	-3.66E-23	-3.66E-23	+3.66E-23	77
.67987	+.499794	-.0004108	+.499795	+.9992	-4.45E-23	-4.45E-23	+4.45E-23	81
.69228	+.499764	-.0004709	+.499765	+.9991	-4.92E-23	-4.92E-23	+4.92E-23	83
.71709	+.499688	-.0006230	+.499689	+.9988	-6.06E-23	-6.06E-23	+6.06E-23	87
.72949	+.499640	-.0007193	+.499641	+.9986	-6.76E-23	-6.76E-23	+6.76E-23	90
.75430	+.499516	-.0009686	+.499516	+.9981	-8.52E-23	-8.52E-23	+8.52E-23	94
.77911	+.499337	-.0013260	+.499337	+.9973	-1.09E-22	-1.09E-22	+1.09E-22	99
.79152	+.499218	-.0015636	+.499218	+.9969	-1.25E-22	-1.25E-22	+1.25E-22	102
.80392	+.499072	-.0018551	+.499073	+.9963	-1.44E-22	-1.44E-22	+1.44E-22	105
.81633	+.498892	-.0022166	+.498892	+.9956	-1.67E-22	-1.67E-22	+1.67E-22	108
.82873	+.498665	-.0026707	+.498665	+.9947	-1.95E-22	-1.95E-22	+1.95E-22	111
.87835	+.496840	-.0063204	+.496840	+.9874	-4.14E-22	-4.14E-22	+4.14E-22	120
.89076	+.495913	-.0081737	+.495913	+.9837	-5.22E-22	-5.22E-22	+5.22E-22	122
.91557	+.492585	-.0148303	+.492585	+.9703	-9.08E-22	-9.08E-22	+9.08E-22	126
.92797	+.489418	-.0211635	+.489418	+.9577	-1.28E-21	-1.28E-21	+1.28E-21	128
.97759	+.383041	-.2339187	+.383041	+.5322	-2.25E-20	-2.25E-20	+2.25E-20	136

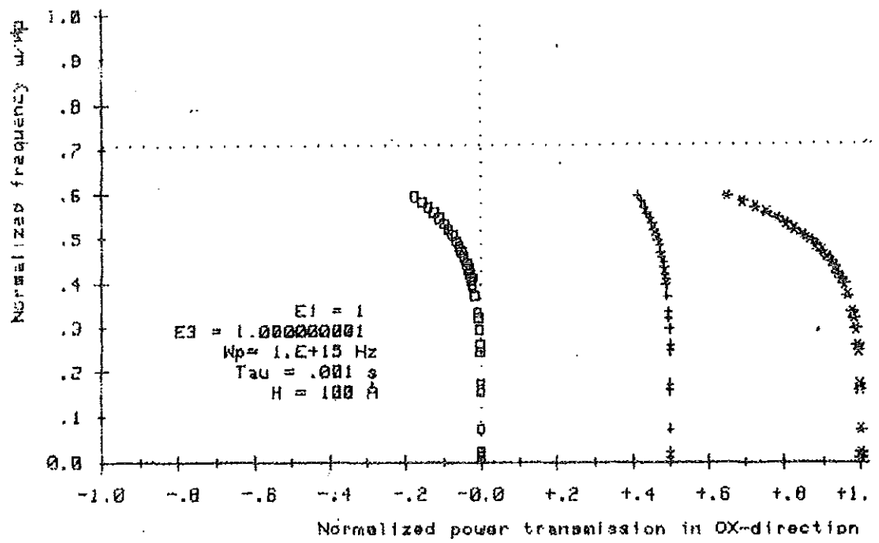

Fig. 3.14 .(L18) Partial and net power transmission in OX-direction performed by the w(-) mode : in media I and III - curve (+ + +), in the film - curve (with squares), the net power - curve (* * *)

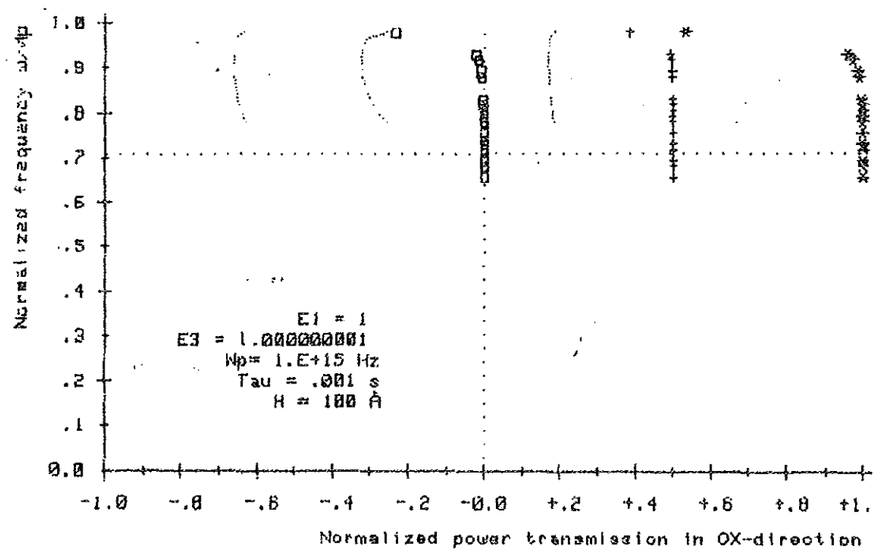

Fig. 3.15 .(L18) Partial and net power transmission in OX-direction performed by the w(+) mode : in media I and III - curve (+ + +), in the film - curve (with squares), the net power - curve (* * *)

Table 3.16 .(L19). Dependance of the REAL and the IMAG. parts of the SP1P OX-wavevector in PMA configuration: E3 = 1.000000001 , E21= E21(ω), E22 = E22(ω), E1 = 1 Plasma frequency Wp = 1.E+15 Hz, Relaxtion time Tau = 1.E-13 sec, Thickness of the film H= 800 'A.'

L O W E R ω(-) B R A N C H

ω/Wp	Ko	Kxr	Kxor	Kxi	No
.03513	+1.171721E+05	+1.2092200E+05	+1.172446E+05	+2.2619E+03	2
.06026	+2.009887E+05	+2.2045983E+05	+2.013558E+05	+6.3073E+03	3
.08538	+2.848053E+05	+3.3895246E+05	+2.858567E+05	+1.1803E+04	4
.11051	+3.686218E+05	+4.8175099E+05	+3.709216E+05	+1.8279E+04	5
.13564	+4.524384E+05	+6.5291137E+05	+4.567382E+05	+2.5420E+04	6
.16077	+5.362549E+05	+8.5568359E+05	+5.435124E+05	+3.3059E+04	7
.18590	+6.200715E+05	+1.0929403E+06	+6.314740E+05	+4.1141E+04	8
.21103	+7.038881E+05	+1.3674972E+06	+7.208843E+05	+4.9683E+04	9
.23615	+7.877046E+05	+1.6823506E+06	+8.120452E+05	+5.8750E+04	10
.26128	+8.715212E+05	+2.0408667E+06	+9.053108E+05	+6.8445E+04	11
.28641	+9.553377E+05	+2.4469578E+06	+1.001104E+06	+7.8908E+04	12
.31154	+1.039154E+06	+2.9052689E+06	+1.099935E+06	+9.0315E+04	14
.33667	+1.122971E+06	+3.4214003E+06	+1.202433E+06	+1.0289E+05	16
.36179	+1.206787E+06	+4.0021927E+06	+1.309383E+06	+1.1693E+05	18
.38692	+1.290604E+06	+4.6561104E+06	+1.421786E+06	+1.3280E+05	20
.41205	+1.374421E+06	+5.3937756E+06	+1.540936E+06	+1.5102E+05	22
.43718	+1.458237E+06	+6.2287376E+06	+1.668554E+06	+1.7225E+05	24
.46231	+1.542054E+06	+7.1786161E+06	+1.806972E+06	+1.9748E+05	26
.48744	+1.625870E+06	+8.2668646E+06	+1.959458E+06	+2.2809E+05	28
.51256	+1.709687E+06	+9.5256077E+06	+2.130745E+06	+2.6622E+05	30
.53769	+1.793503E+06	+1.1000448E+07	+2.327988E+06	+3.1524E+05	32
.56282	+1.877320E+06	+1.2759150E+07	+2.562615E+06	+3.8089E+05	34
.58795	+1.961136E+06	+1.4908677E+07	+2.854211E+06	+4.7373E+05	36
.61308	+2.044953E+06	+1.7632554E+07	+3.239808E+06	+6.1562E+05	38
.63821	+2.128770E+06	+2.1286871E+07	+3.800313E+06	+8.6022E+05	41
.66333	+2.212586E+06	+2.6716754E+07	+4.760040E+06	+1.3836E+06	44
.68846	+2.296403E+06	+3.6921851E+07	+7.124678E+06	+3.2757E+06	47

Table 3.17 .(L19). Dependance of the PEAL and IMAG. parts of the SPIP OX-wavevector in PMA configuration : E3 = 1.000000001 , E21= E21(ω), E22 = E22(ω), E1 = 1 Plasma frequency Wp = 1.E+15 Hz, Relaxtion time Tau = 1.E-13 sec, Thickness of the film H= 800 'A.'

U P P E R	ω(+)	B R A N C H (physically real part)			
ω/Wp	Ko	Kxr	Kxor	Kxi	No
.01000	+3.335557E+04	+3.3357179E+04	+3.335724E+04	+1.8852E+02	1
.63821	+2.128770E+06	+2.1507255E+06	+3.800313E+06	+4.8837E+02	40
.66333	+2.212586E+06	+2.2403143E+06	+4.760040E+06	+6.8183E+02	43
.68846	+2.296403E+06	+2.3317311E+06	+7.124678E+06	+9.6652E+02	46
.71359	+2.380219E+06	+2.4257601E+06	+0.000000E+00	+1.3976E+03	49
.73872	+2.464036E+06	+2.5236548E+06	+0.000000E+00	+2.0749E+03	52
.76385	+2.547852E+06	+2.6275312E+06	+0.000000E+00	+3.1916E+03	55
.78897	+2.631669E+06	+2.7412260E+06	+0.000000E+00	+5.1588E+03	58
.81410	+2.715486E+06	+2.8724330E+06	+0.000000E+00	+8.9784E+03	61
.83923	+2.799302E+06	+3.0391549E+06	+0.000000E+00	+1.7678E+04	64
.86436	+2.883119E+06	+3.2971405E+06	+0.000000E+00	+4.5196E+04	67
.88949	+2.966935E+06	+3.9453517E+06	+0.000000E+00	+3.8207E+05	70
.91462	+3.050752E+06	+3.4920293E+06	+0.000000E+00	+1.4032E+06	72

Table 3.18 .(L19). Dependance of the REAL and IMAG. parts of the SPIP OX:wavevector in the PMA configuration : E3 = 1.000000001 , E21= E21(ω), E22 = E22(ω), E1 = 1 Plasma frequency Wp = 1.E+15 Hz, Relaxtion time Tau = 1.E-13 sec, Thickness of the film H= 800 'A.'

U P P E R	ω(+)	B R A N C H (physically unreal part)			
ω/Wp	Ko	Kxr	Kxor	Kxi	No
.71359	+2.380219E+06	+4.6307678E+07	+0.000000E+00	-8.0398E+06	50
.73872	+2.464036E+06	+2.9231727E+07	+0.000000E+00	-1.9893E+06	53
.76385	+2.547852E+06	+2.1803386E+07	+0.000000E+00	-1.1410E+06	56
.78897	+2.631669E+06	+1.6980653E+07	+0.000000E+00	-8.1049E+05	59
.81410	+2.715486E+06	+1.3347896E+07	+0.000000E+00	-6.3760E+05	62
.83923	+2.799302E+06	+1.0372771E+07	+0.000000E+00	-5.3736E+05	65
.86436	+2.883119E+06	+7.7517390E+06	+0.000000E+00	-4.9198E+05	68
.88949	+2.966935E+06	+5.0440096E+06	+0.000000E+00	-7.7819E+05	71
.91462	+3.050752E+06	+3.6467674E+06	+0.000000E+00	-1.7649E+06	73

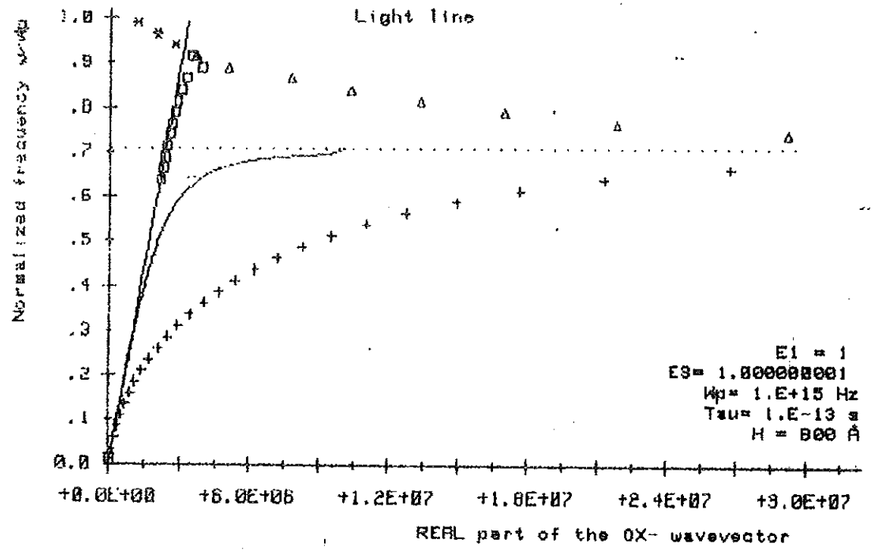

Fig. 3.16 .(L18) REAL part of the OX-wavevector as a function of the normalized frequency: w(-) mode - curve (+ + +), w(+) mode (physically real part)- curve with squares, w(+) mode (physically unreal part) - curve with triangles, semi-infinite case - solid curve, side branch - (* * * curve).

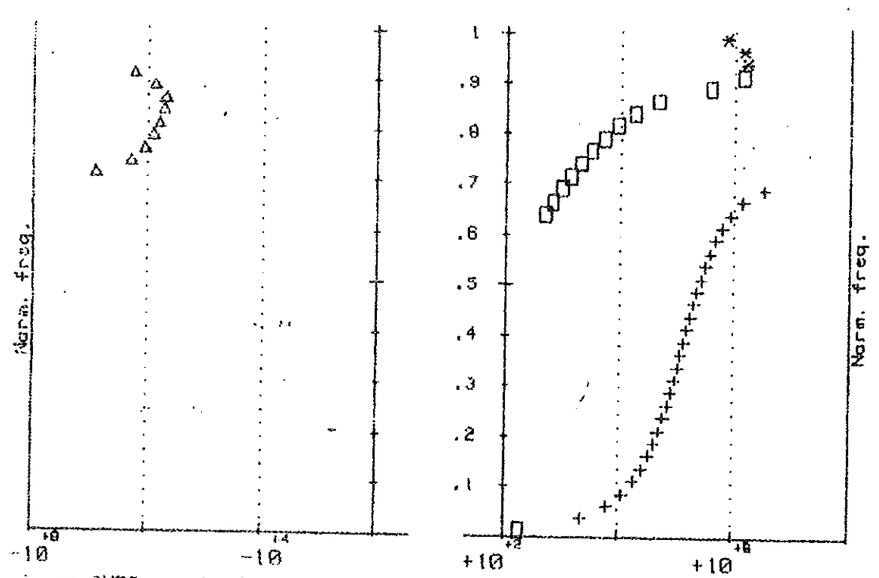

Fig. 3.17 .(L18). IMAG. part of the OX-wavevector as a funption of the normalized freq.: w(-) mode - curve (+ + +), w(+) mode (physically real part) - curve with squares, w(+) mode (physically unreal part) - curve with triangles, side branch - (* * *) curve.
E1 = 1 , E9 = 1.000000001 , H = 800 Å, Wp = 1.E+15 Hz, Tau = 1.E-13

Table 3.19 .(L19). Calculations for the power flow in Kretschmann PMA configuration with dielectric permittivities: E3 = 1.000000001 , E21= E21(ω), E22 = E22(ω), E1 = 1 Plasma frequency Wp = 1.E+15 Hz, Relaxtion time Tau = 1.E-13 sec, Thickness of the film H= 800 'A.' Y-coordinate = 0 'A'

L O W E R			ω(-)		B R A N C H			
w/Wp	Px1	Px2	Px3	Px net	Sy1	Sy2	Sy3	No
.03513	+.499999	-.0000010	+.499999	+1.0000	-1.25E-10	-1.25E-10	+1.25E-10	2
.06026	+.499996	-.0000088	+.499996	+1.0000	-1.24E-10	-1.24E-10	+1.24E-10	3
.08538	+.499982	-.0000359	+.499982	+.9999	-1.23E-10	-1.23E-10	+1.23E-10	4
.11051	+.499949	-.0001019	+.499949	+.9998	-1.22E-10	-1.22E-10	+1.22E-10	5
.13564	+.499883	-.0002343	+.499883	+.9995	-1.20E-10	-1.20E-10	+1.20E-10	6
.16077	+.499765	-.0004696	+.499765	+.9991	-1.18E-10	-1.18E-10	+1.18E-10	7
.18590	+.499573	-.0008547	+.499573	+.9983	-1.16E-10	-1.16E-10	+1.16E-10	8
.21103	+.499276	-.0014489	+.499276	+.9971	-1.14E-10	-1.14E-10	+1.14E-10	9
.23615	+.498837	-.0023259	+.498837	+.9953	-1.11E-10	-1.11E-10	+1.11E-10	10
.26128	+.498212	-.0035769	+.498212	+.9928	-1.08E-10	-1.08E-10	+1.08E-10	11
.28641	+.497343	-.0053148	+.497343	+.9894	-1.04E-10	-1.04E-10	+1.04E-10	12
.31154	+.496161	-.0076778	+.496161	+.9846	-1.01E-10	-1.01E-10	+1.01E-10	14
.33667	+.494582	-.0108362	+.494582	+.9783	-9.64E-11	-9.64E-11	+9.64E-11	16
.36179	+.492501	-.0149984	+.492501	+.9700	-9.20E-11	-9.20E-11	+9.20E-11	18
.38692	+.489790	-.0204203	+.489790	+.9592	-8.73E-11	-8.73E-11	+8.73E-11	20
.41205	+.486293	-.0274148	+.486293	+.9452	-8.23E-11	-8.23E-11	+8.23E-11	22
.43718	+.481817	-.0363650	+.481817	+.9273	-7.69E-11	-7.69E-11	+7.69E-11	24
.46231	+.476131	-.0477382	+.476131	+.9045	-7.12E-11	-7.12E-11	+7.12E-11	26
.48744	+.468949	-.0621027	+.468949	+.8758	-6.52E-11	-6.52E-11	+6.52E-11	28
.51256	+.459926	-.0801472	+.459926	+.8397	-5.89E-11	-5.89E-11	+5.89E-11	30
.53769	+.448649	-.1027012	+.448649	+.7946	-5.23E-11	-5.23E-11	+5.23E-11	32
.56282	+.434621	-.1307585	+.434621	+.7385	-4.54E-11	-4.54E-11	+4.54E-11	34
.58795	+.417248	-.1655033	+.417248	+.6690	-3.82E-11	-3.82E-11	+3.82E-11	36
.61308	+.395824	-.2083530	+.395824	+.5833	-3.07E-11	-3.07E-11	+3.07E-11	38
.63821	+.369472	-.2610559	+.369472	+.4779	-2.29E-11	-2.29E-11	+2.29E-11	41
.66333	+.336993	-.3260149	+.336993	+.3480	-1.48E-11	-1.48E-11	+1.48E-11	44
.68846	+.296184	-.4076322	+.296184	+.1847	-6.55E-12	-6.55E-12	+6.55E-12	47

Table 3.20 .(L19). Calculations for the power flow in Kretschmann PMA configuration with dielectric permittivities: E3 = 1.000000001 , E21= E21(ω), E22 = E22(ω), E1 = 1 Plasma frequency Wp = 1.E+15 Hz, Relaxtion time Tau = 1.E-13 sec, Thickness of the film H= 800 'A.' Y-coordinate = 0 'A'

U P P E R			ω(+)		B R A N C H (physically real part)			
w/Wp	Px1	Px2	Px3	Px net	Sy1	Sy2	Sy3	No
.01000	+.500000	-0.0000000	+.500000	+1.0000	-1.25E-10	-1.25E-10	+1.25E-10	1
.63821	+.491812	-.0163760	+.491812	+.9672	-2.56E-12	-2.56E-12	+2.56E-12	40
.66333	+.489323	-.0213544	+.489323	+.9573	-3.10E-12	-3.10E-12	+3.10E-12	43
.68846	+.486006	-.0279871	+.486006	+.9440	-3.79E-12	-3.79E-12	+3.79E-12	46
.71359	+.481531	-.0369378	+.481531	+.9261	-4.71E-12	-4.71E-12	+4.71E-12	49
.73872	+.475397	-.0492057	+.475397	+.9016	-5.96E-12	-5.96E-12	+5.96E-12	52
.76385	+.466830	-.0663402	+.466830	+.8673	-7.71E-12	-7.71E-12	+7.71E-12	55
.78897	+.454585	-.0908302	+.454585	+.8183	-1.03E-11	-1.03E-11	+1.03E-11	58
.81410	+.436573	-.1268548	+.436573	+.7463	-1.46E-11	-1.46E-11	+1.46E-11	61
.83923	+.409048	-.1819034	+.409048	+.6362	-2.24E-11	-2.24E-11	+2.24E-11	64
.86436	+.364355	-.2712908	+.364355	+.4574	-4.17E-11	-4.17E-11	+4.17E-11	67
.88949	+.281208	-.4375835	+.281208	+.1248	-2.11E-10	-2.11E-10	+2.11E-10	70
.91462	+.261936	-.4761273	+.261936	+.0477	-7.97E-10	-7.97E-10	+7.97E-10	72

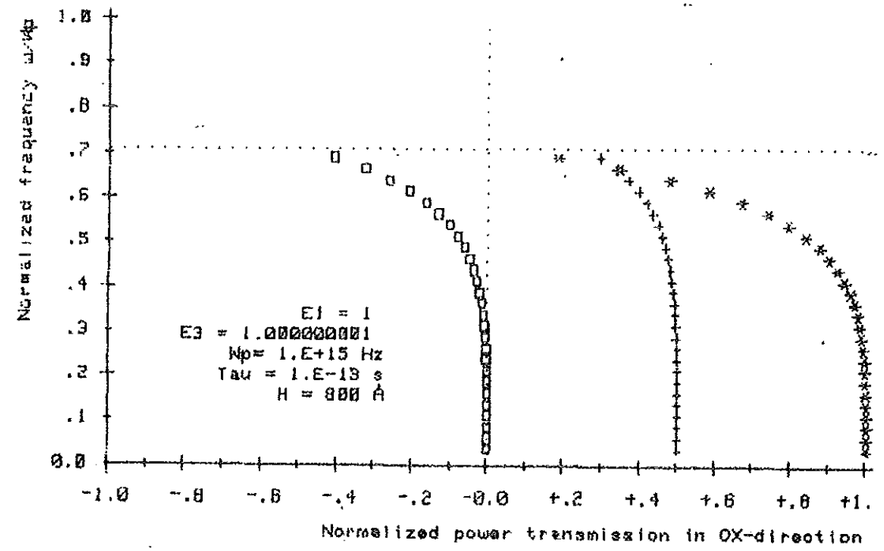

Fig. 3.18 .(L19) Partial and net power transmission in OX-direction performed by the w(-) mode : in media I and III - curve (+ + +), in the film - curve (with squares), the net power - curve (* * *)

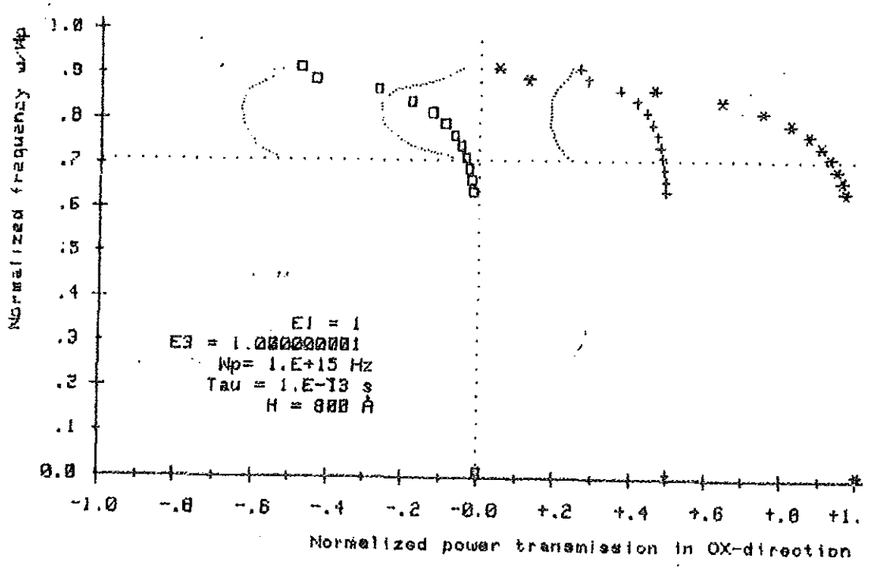

Fig. 3.19 .(L18) Partial and net power transmission in OX-direction performed by the w(+) mode : in media I and III - curve (+ + +), in the film - curve (with squares), the net power - curve (* * *)

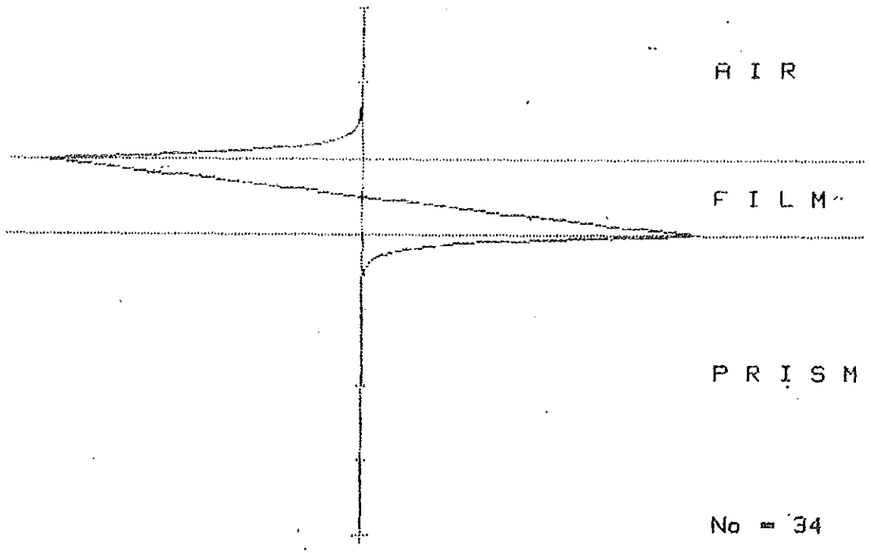

Fig. 3.20 .(L18) Magnetic Field distribution in the w(-) mode
E1 = 1 , E3 = 1.000000001 , Wp = 1.E+15 Hz, Tau = 1.E-13 s, Wn = .562023
H = 800 A, Ko = 1.87731992268E+6 Kxr = 1.27591499054E+7
Kxor = 2.56261505036E+6 , Kxi = 900089.030935 Data file name:L19 «

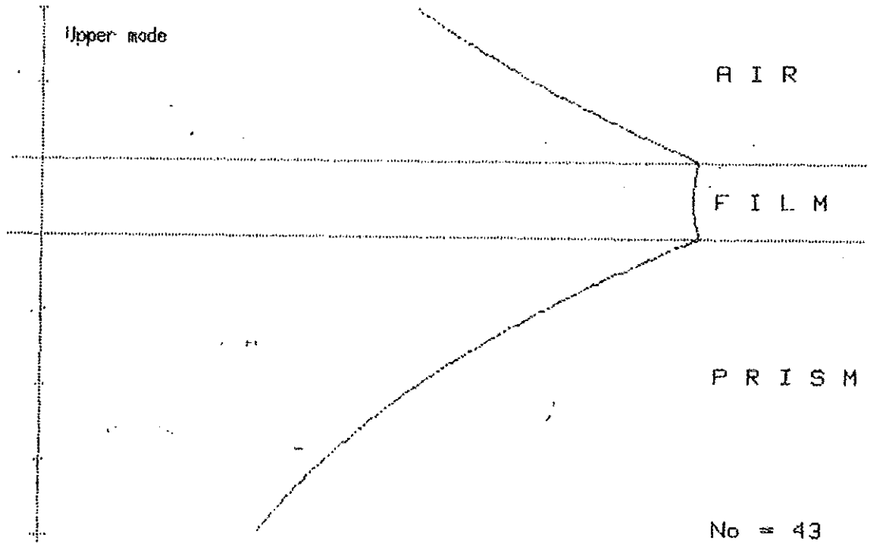

Fig. 3.21 .(L18) Magnetic Field distribution in the w(+) mode
E1 = 1 , E3 = 1.000000001 , Wp = 1.E+15 Hz, Tau = 1.E-13 s, Wn = .663339
H = 800 A, Ko = 2.21250616056E+6 Kxr = 2.24031432761E+6
Kxor= 4.76004035000E+6 , Kxi = 601.032561607 Data file name:L19 «

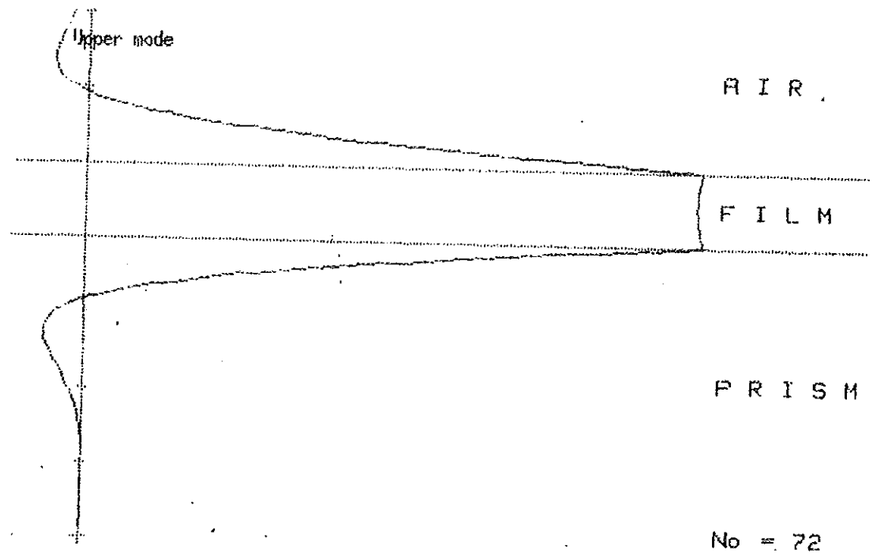

Fig. 3.22 .(L19) Magnetic field distribution in the H(+) mode
E1 = 1 , E3 = 1.000000001 , Wp = 1.E+15 Hz, Tau = 1.E-13 s, Wn = .91461!
H = 800 A, Ko = 9.050751780924E+6 Kxr = 3.48202929954E+6
Kxor= 0 , Kxi = 1.403231243917E+6 Data file name:L19

segment of the ω^+ mode to the region left of the light line, thus corresponding to phase velocities greater than c and with group velocity negative. This mode is physically unreal. The field distribution corresponding to this mode is oscillatory with decreasing amplitude of oscillation away from the film in the media bounding the film and remains constant in the film. This behavior maintains for all frequencies upto ω_p. Thus this mode is strongly radiative eventhough it is unphysical.

3.2 Analysis of the SPLP dispersion at the boundaries of a thin metal film in asymmetric environment ($\varepsilon_3 \neq \varepsilon_1$)

The numerical solution of the exact thin film dispersion eqn. (2.1) for the case of asymmetric environment yields also the three modes we encountered in the case of symmetric environment namely the ω^+, the ω^-, and the 'side' modes.

In the analysis of these dispersion curves, we take one branch at a time as usual. Data presented at the figures can be found in the subsequent relevant tables.

3.21 Analysis of the lower mode ω^- ($k_o < k'_{xo} < k'_x$).

For the thickness of 800A^o, the dispersion curve of ω^- mode is analyzed for two cases: (a) case of weak absorption (relaxation time, tau, large) and (b) case of strong absorption (relaxation time, tau, small). We analyze them separately and try to see their common features and differences.

a) Case of weak absorption

The dispersion curve of ω^- mode for this case is shown in Fig. (3.23) which discloses that at very low k_x' and ω values the surface polaritions are primarily photon-like. In the finite k_x' region i.e., near the cross-over of the dispersion curves of uncoupled photons and surface plasmons, surface polaritions display mixed behavior of both virtual particles namely photons and surface plasmons. In this region surface polaritions of semi-infinite metal are more closer to the cross-over than surface polaritons of ω^- mode which implies that the efficiency of coupling of photons to surface plasmons is very low eventhough weak coupling exists which is responsible for the lower mode curve. As in the case of symmetric environment the ω^- mode of this case remains non-radiative over the spectral range of interest.

Unlike the symmetric environment, the asymmetric environment shows upper cutoff $k_x'^*$ which implies that surface polaritions cannot be localized more than the value given by $k_x'^*$. For the case under consideration the ω^- mode curve upon reaching $k_x'^*$ bends back with somewhat steep slope. The back-bending segment is described, as already mentioned in section 3.12, as a phenomenon of artificial anomalous dispersion.

From Fig. (3.24) the curve corresponding to k_x'' of this segement shows an abrupt growth of damping (k_x'' grow by 11 orders in this case of weakly absorbing film), see also table 3.21. The analysis of the power flow in ox-direction indicates the net power flow drops to zero for this segment of ω^- mode, see Fig.(3.25) and table 3.23. The field distributions of this mode are shown in Figs. (3.27, 3.28). From observation of these distributions the field intensity switches from Prism/metal interface to metal/air interface as the frequency increases without showing any symmetry with respect to ox-axis and with a reversal of intensity amplitude with respect to oy-axis.

b) Case of strong obsorption

The dispersion curve of ω^- mode for this case is shown in Fig. (3.31) . The behavior of the curve is in general not very different from that of case (a), except for the increase of $k_x'^*$ and low value of the slope of back-bending segment which means that strong absorption causes more localized surface polartions than the previous case. From Fig. (3.32) one observes that k_x'' is increased compared to that of case (a) and there is no significant growth of damping due to back-bending, see also table 3.25. The power flow in ox-direction shows that for this segment the net flow is close to zero, see table 3.27 and Fig. (3.33).

The fact that the net flow never vanish indicates that at the ω and k_x' values corresponding to the back-bending of the ω^- mode curve very small portion of the light energy incident on the PMA structure appears as radiation in the structure whereas large portion of the light energy incident on the PMA structure is either absorbed in it or is reflected.

As has been mentioned in the last part of section 3.12 the final decision about this point needs additional study of the reflectivity of the PMA structure for the corresponding values of ω and k_x' . Most probably the observed back-bending is due to absorption of light incident on the PMA structure at angles $\theta \geq \theta_c$ as mentioned by Koverner and his co-workers [8]. This can also be checked by observing the continuity of the transverse power flow at y = -h for these cases.

The field distributions for this case of strong absorption are shown in Figs. 3.35 through 3.45 for different cases. Common to all these figures is that most of the field is concentrated in the film. The amount of field in the bounding media decreases with increasing frequency and the field distributions at higher frequencies, wave vectors, and damping show complicated patterns at the interfaces of the film and within the film, see Figs. 3.42 through 3.45. Notice that the field distributions shown in Figs. 3.35 through 3.42, except Fig. 3.40,

behaves in the same manner which seems like the anti-symmetric distribution of the symmetric environment, see Fig. (3.20). This part corresponds to ω and k_x' just below the upper cut off wave vector $k_x'^*$, see table 3.25. The field distribution changes its behavior totally at the upper cut off wave vector $k_x'^*$, see Figs. 3.43 through 3.45 the distribution show some common features and seems like the symmetric distribution of the symmetric environment, see Fig.(3.21)

Therefore for ω and k_x' corresponding to back-bending segment of ω^- mode the field distributions are different from the distribution corresponding to ω and k_x' less than ω^* and $k_x'^*$. This change of field behavior from anti-symmetric to symmetric like distribution is related to the phenomena of artificial anomalous dispersion and with maximum field intensity in the film/air interface, which reminds us about transformation of incident light into surface plasmons i.e.,) the incident light is almost totally absorbed. This lifts our suspicion that the back-bending is due to reflection. Fig. 3.40 shows the existence of slight modulation (bending-back and return) near ω and k_x' corresponding to the figure , for the ω^- mode curve, the reason for this needs further study, see table 3.25. At the frequency under consideration the net power flow drops close to zero and again abruptly increase at the same frequency which means that this frequency is an eigen frequency in some unknown material

in the Prism/metal interface i.e., absorbing and instantly radiating it back with the same frequency and different wave vector. This does not appear for weak absorption.

3.22 Analysis of the Upper mode ω^+ ($k_o < k'_x < k'_{xo}$).

For the same thickness of 800A^o, the physically real part of ω^+ mode and its physically unreal part appears as discrete points only, see Fig. 3.23. Here we consider the physically real part of ω^+ mode for the cases of weak and strong absorptions in the asymmetric environment.

i) Case of weak absorption

The dispersion curve which is a small segment with three discrete points between $0.8\omega_p$ and $0.9\omega_p$ is shown in Fig. (3.23). This segment also shows back-bending behavior, see also table 3.22. The net power flow in ox-direction drops to zero at the last frequency point which is described, as usual, as a phenomenon of artificial anomalous dispersion i.e., absorption of incident light, see Fig (3.26) and table 3.24. From Fig.(3.24) the k''_x corresponding to back-bending segment of ω^+ mode shows abrupt growth of damping (k''_x increases by 10 orders) see also table 3.22. k''_x of ω^+ mode and ω^- mode for this case shows similar behavior whereas the k''_x of ω^+ mode and ω^- mode for symmetric environment differs by about 3 orders of magnitude, see Fig. (3.6). The corresponding field distributions are shown in Figs. (3.29) and (3.30).

At the frequency point $0.81\omega_p$ the field is exponentially decaying in all of the three media, the decaying in all of the three media, the decay of the field is fast in air, slow in prism, and medium in the film. Most of the field is in the bounding media, mainly in the prism. at $\omega \cong 0.89\omega_p$ the field remains constant in the film and shows damped oscillations of different nature in air and prism, here the field is pushed into the film. This frequency corresponds to back-bending i.e., the corresponding k_x' is clsoder to k_o (wave vector in air) which means that surface polaritions of this mode are almost transformed into light (photons) which is responsible for the observed radiation (leaky plasmons), absorbing the incident light at $\omega \cong 0.89\omega_p$ and corresponding k_x' and radiating it back instantly at same ω and k_x' .

ii) Case of strong absorption

In this case physically real part of the ω^+ mode is represented by five discrete points with one point far removed from the rest at very large k_x' at $\omega \cong 0.714\omega_p$, figure the separate point of the ω^+ mode at the right has about the same k_x' value with $k_x'^*$ corresponding to ω^- mode, see table 3.25 for comparison. to table 3.26 .

The net power flow in ox-direction shows that the net flow corresponding to this separate point is close to zero which implies the existence of artificial anomalous dispersion at the corresponding eigen frequency which is also true of the last two points in back-bending segment.

The only frequency almost non-absorbing is $\simeq 0.814\omega_p$, see table 3.28. The corresponding field distributions are shown in Figs. (3.46) and (3.47). At the frequency point $0.814\omega_p$, the field behavior is almost the same as the weak absorption case except that the decay in the bounding media and film is slightly increased. The behavior at $\simeq 0.89\omega_p$ is practically the same.

The physically unreal part of ω^+ mode corresponding to both weak and strong absorptions is also shown in Figs. (3.23) and (3.31) with similar behavior. This part also appears in asymmetric environment. It is characterized by $v_g<0$ and $k_x''<0$. These makes this segment of ω^+ mode unphysical.

.23 Analysis of the Side Mode ($k_x'<k_o<k_{xo}'$)

As in the symmetric environment the side mode appears as an extension of ω^+ mode, extending upto ω_p. It is shown in Figs. (3.23) and (3.31) with similar behavior in both cases of weak and strong absorptions. As usual this mode is characterized by $v_g<0$, $k_x''>0$, and discontinuity in the transverse power flow at the interfaces. Two of these makes this mode unphysical. Note that the existence of ω^+, ω^-, and side modes in the strongly asymmetric ($\varepsilon_3 \neq \varepsilon_1$) environment is also new result not found in literature. The difference in the general properties of

the dispersion curves for the two environments is that the existence of back-bending segment and upper cut off k'* in the ω^- mode of the asymmetric environment which is also a new result.

Table 3.21 .(L30). Dependance of the PEAL and the IMAG. parts of the SPlP OX-wavevector in PMA configuration: E3 = 2.25 , E21= E21(ω), E22 = E22(ω) E1 = 1 Plasma frequency Wp = 1.E+15 Hz, Relaxtion time Tau = .001 sec. Thickness of the film H= 800 'A.'

L O W E R ω(-) B R A N C H

ω/Wp	Ko	Kxr	Kxor	Kxi	No
.03513	+1.171721E+05	+1.8022975E+05	+1.172446E+05	+2.7515E-07	2
.08538	+2.848053E+05	+5.0477088E+05	+2.858569E+05	+1.9118E-06	4
.13564	+4.524384E+05	+9.9456500E+05	+4.567390E+05	+4.3248E-06	6
.16077	+5.362549E+05	+1.3186961E+06	+5.435138E+05	+5.6271E-06	7
.21103	+7.038881E+05	+2.1482176E+06	+7.208878E+05	+8.4150E-06	10
.28641	+9.553377E+05	+3.9293456E+06	+1.001115E+06	+1.3435E-05	14
.31154	+1.039154E+06	+4.6989329E+06	+1.099951E+06	+1.5507E-05	18
.38692	+1.290604E+06	+7.7491607E+06	+1.421829E+06	+2.4222E-05	30
.41205	+1.374421E+06	+9.1099615E+06	+1.540998E+06	+2.8682E-05	34
.43718	+1.458237E+06	+1.0730875E+07	+1.668641E+06	+3.4729E-05	38
.46231	+1.542054E+06	+1.2719292E+07	+1.807098E+06	+4.3597E-05	42
.48744	+1.625870E+06	+1.5282941E+07	+1.959643E+06	+5.8367E-05	47
.51256	+1.709687E+06	+1.8923755E+07	+2.131024E+06	+8.9497E-05	52
.53769	+1.793503E+06	+2.5633514E+07	+2.328427E+06	+2.1168E-04	57
.66333	+2.212586E+06	+2.1188852E+07	+4.780128E+06	+1.9644E+07	82

Table 3.22 .(L20). Dependance of the PEAL and IMAG. parts of the SPlP OX-wavevector in PMA configuration : E3 = 2.25 , E21= E21(ω), E22 = E22(ω), E1 = 1 Plasma frequency Wp = 1.E+15 Hz, Relaxtion time Tau = .001 sec, Thickness of the film H= 800 'A.'

U P P E R ω(+) B R A N C H (physically real part)

ω/Wp	Ko	Kxr	Kxor	Kxi	No
.81410	+2.715486E+06	+4 0739645E+06	+0.000000E+00	+4.4207E-07	110
.83923	+2.799302E+06	+4.6722417E+06	+0.000000E+00	+3.1689E-05	114
.88949	+2.966935E+06	+3.6587223E+06	+0.000000E+00	+1.9551E+06	122

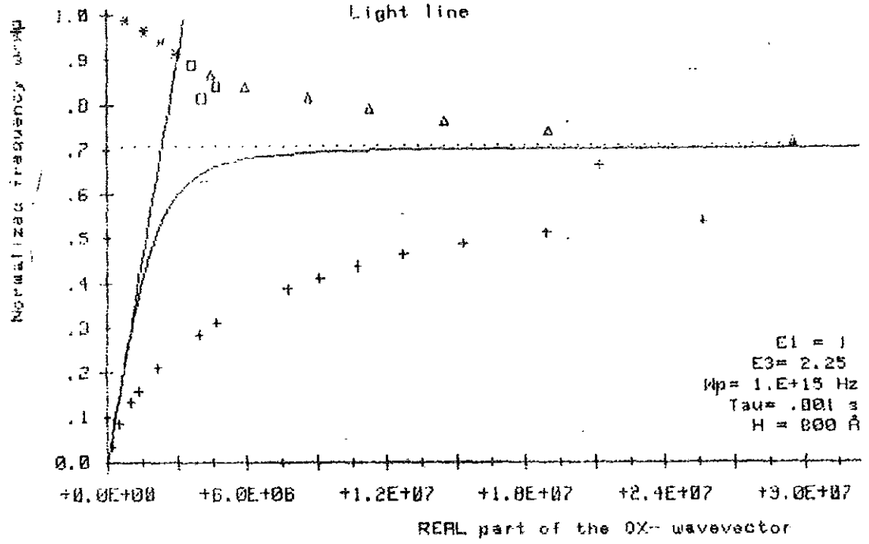

Fig. 3.23 .(L30) REAL part of the OX-wavevector as a function of the normalized frequency: w(-) mode - curve (+ + +), w(+) mode (physically real part)- curve with squares, w(+) mode (physically unreal part) - curve with triangles, semi-infinite case - solid curve, side branch - (* * * curve).

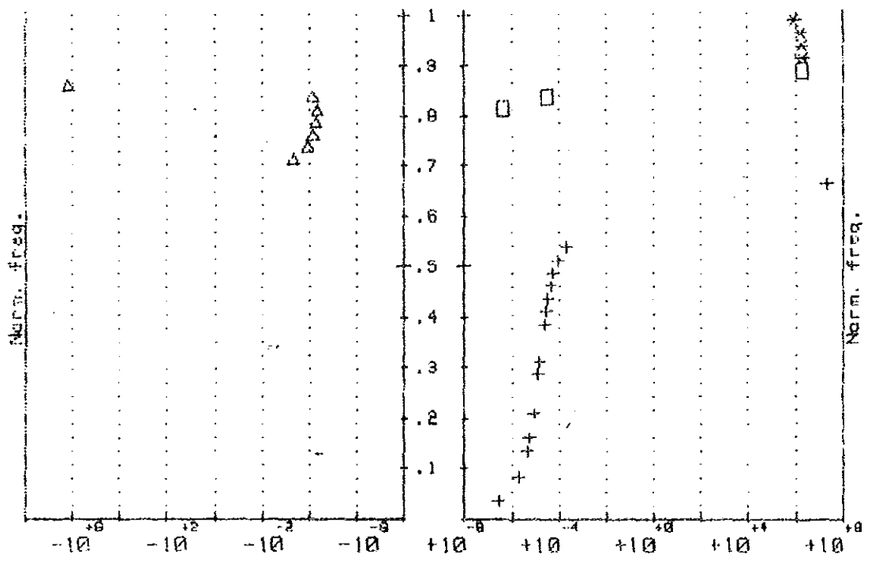

Fig. 3.24 .(L30). IMAG. part of the OX-wavevector as a function of the normalized freq.: w(-) mode - curve (+ + +), w(+) mode (physically real part) - curve with squares, w(+) mode (physically unreal part) - curve with triangles, side branch - (* * *) curve.
Ei = 1 , E3 = 2.25 , H = 800 Å, Wp = 1.E+15 Hz, Tau = .001 sec .*

Table 3.23 (L30). Calculations for the power flow in Kretschmann PMA configuration with dielectric permittivities: E3 = 2.25 , E21= E21(ω), E22 = E22(ω), E1 = 1 Plasma frequency Ωp = 1 E+15 Hz, Relaxtion time Tau = .001 sec, Thickness of the film H= 800 'A.' Y-coordinate = 0 'A'

L O W E R ω(-) B R A N C H								
ω/Ωp	Px1	Px2	Px3	Px net	Sy1	Sy2	Sy3	No
.03513	+.010299	-.0000052	+.989696	+1.0000	-8.13E-23	-8.13E-23	+7.81E-21	2
.08538	+.102839	-.0001684	+.896993	+.9997	-1.03E-21	-1.03E-21	+8.95E-21	4
.13564	+.191557	-.0010101	+.807433	+.9980	-2.05E-21	-2.05E-21	+8.63E-21	6
.16077	+.218212	-.0019708	+.779817	+.9961	-2.32E-21	-2.32E-21	+8.30E-21	7
.21103	+.248956	-.0058776	+.745166	+.9882	-2.52E-21	-2.52E-21	+7.54E-21	10
.28641	+.263284	-.0210039	+.715712	+.9580	-2.29E-21	-2.29E-21	+6.23E-21	14
.31154	+.262113	-.0301734	+.707713	+.9397	-2.14E-21	-2.14E-21	+5.77E-21	18
.38692	+.239093	-.0792481	+.680859	+.8415	-1.52E-21	-1.52E-21	+4.32E-21	30
.41205	+.224672	-.1060617	+.669266	+.7879	-1.29E-21	-1.29E-21	+3.84E-21	34
.43718	+.204235	-.1403578	+.655407	+.7193	-1.05E-21	-1.05E-21	+3.36E-21	38
.46231	+.177410	-.1840703	+.638520	+.6319	-8.00E-22	-8.00E-22	+2.88E-21	42
.48744	+.142677	-.2398413	+.617482	+.5203	-5.57E-22	-5.57E-22	+2.41E-21	47
.51256	+.098114	-.3116988	+.590187	+.3766	-3.24E-22	-3.24E-22	+1.95E-21	52
.53769	+.041736	-.4075299	+.550734	+.1849	-1.13E-22	-1.13E-22	+1.49E-21	57
.66333	+.355821	-.5000000	+.144179	+0.0000	-5.63E-10	-5.63E-10	+2.28E-10	82

Table 3.24 (L30). Calculations for the power flow in Kretschmann PMA configuration with dielectric permittivities: E3 = 2.25 , E21= E21(ω), E22 = E22(ω), E1 = 1 Plasma frequency Ωp = 1.E+15 Hz, Relaxtion time Tau = .001 sec, Thickness of the film H= 800 'A.' Y-coordinate = 0 'A'

U P P E R ω(+) B R A N C H (physically real part)								
ω/Ωp	Px1	Px2	Px3	Px net	Sy1	Sy2	Sy3	No
.81410	+.057928	-.0509323	+.891140	+.8981	-4.08E-22	-4.08E-22	+6.27E-21	110
.83923	+.326968	-.4334324	+.239600	+.1331	-1.87E-20	-1.87E-20	+1.37E-20	114
.88949	+.310254	-.5000000	+.189746	+0.0000	-1.12E-09	-1.12E-09	+6.86E-10	122

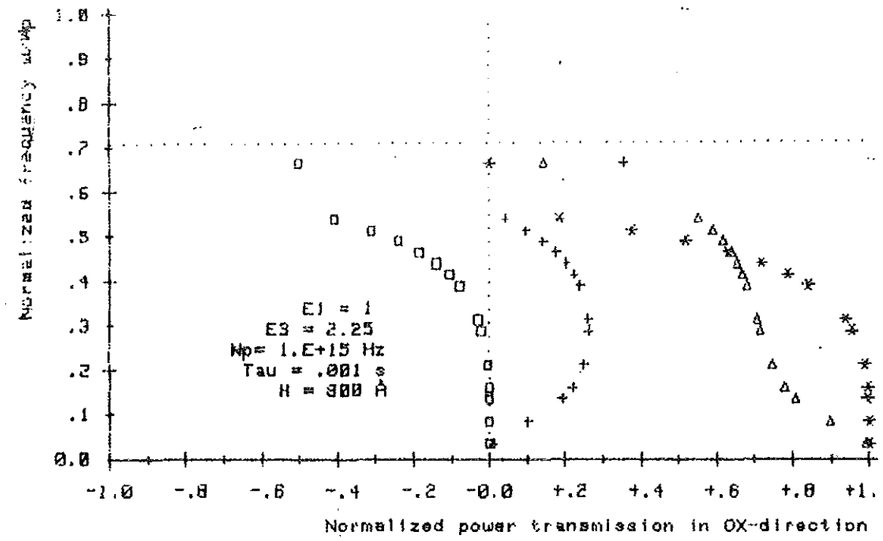

Fig. 3.25 .(L30) Partial and net power transmission in OX-direction performed by the w(-) mode : in media I - curve (+ + +), in media III - curve (with triangles), in the film - curve (with squares), the net power transmission - curve (* * *)

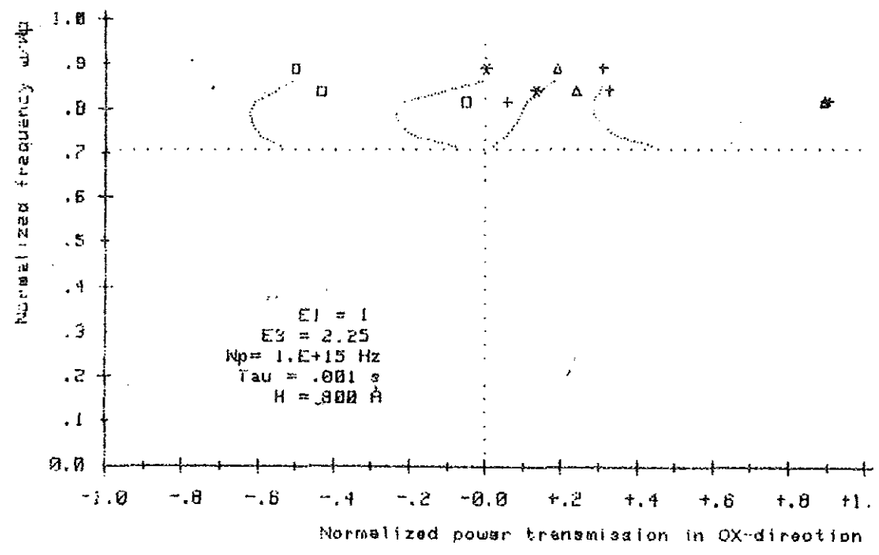

Fig. 3.26 .(L30) Partial and net power transmission in OX-direction performed by the w(+) mode : in media I - curve (+ + +), in media III - curve (with triangles), in the film - curve (with squares), the net power transmission - curve (* * *)

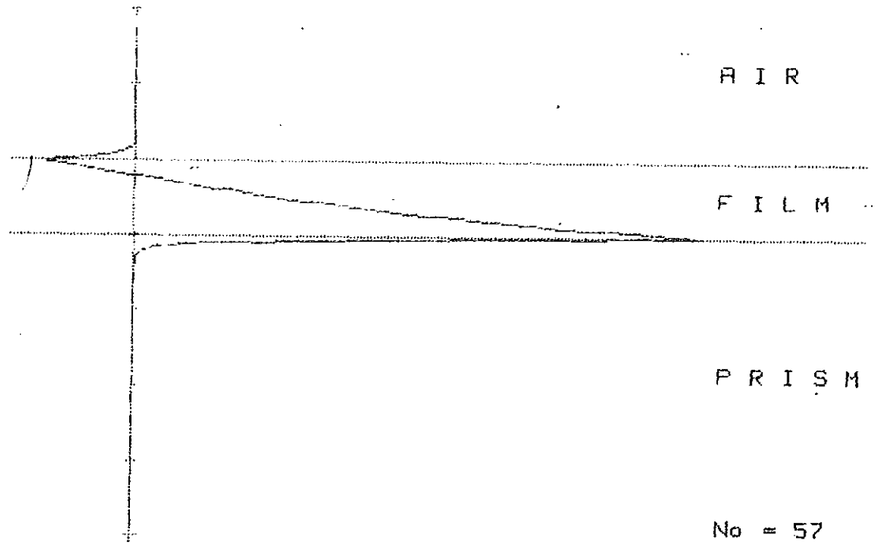

Fig. 3.27 .(L30) Magnetic field distribution in the w(-) mode
E1 = 1 , E3 = 2.25 , Wp = 1.E+15 Hz, Tau = .001 s, Wn = .5376923076923
H = 800 A, Ko = 1.79350336122E+6 Kxr = 2.56335136672E+7
Kxor = 2.32042681296E+6 , Kxi = .000211678067265 Data file name:L30*

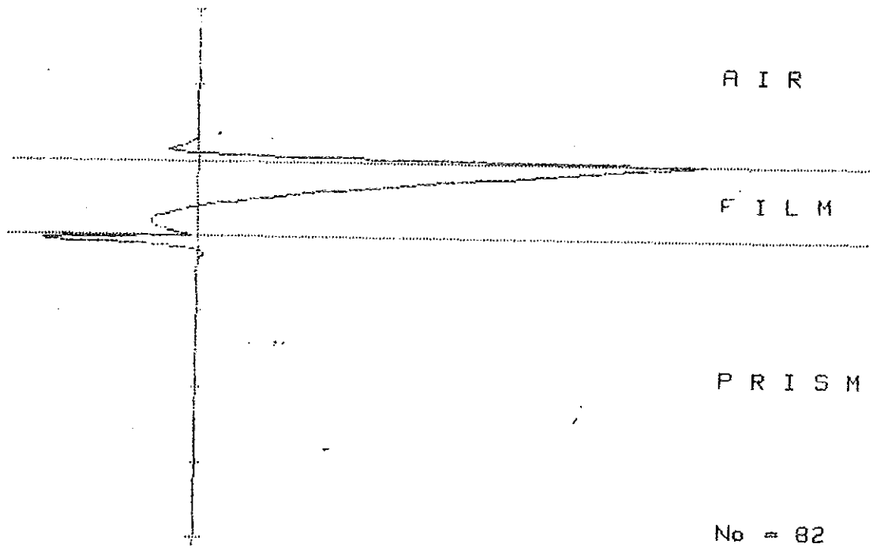

Fig. 3.28 .(L30) Magnetic field distribution in the w(-) mode
E1 = 1 , E3 = 2.25 , Wp = 1.E+15 Hz, Tau = .001 s, Wn = .6693333333333
H = 800 A, Ko = 2.21250616856E+6 Kxr = 2.11800516864E+7
Kxor = 4.78012761712E+6 , Kxi = 1.96441729621E+7 Data file name:L30*

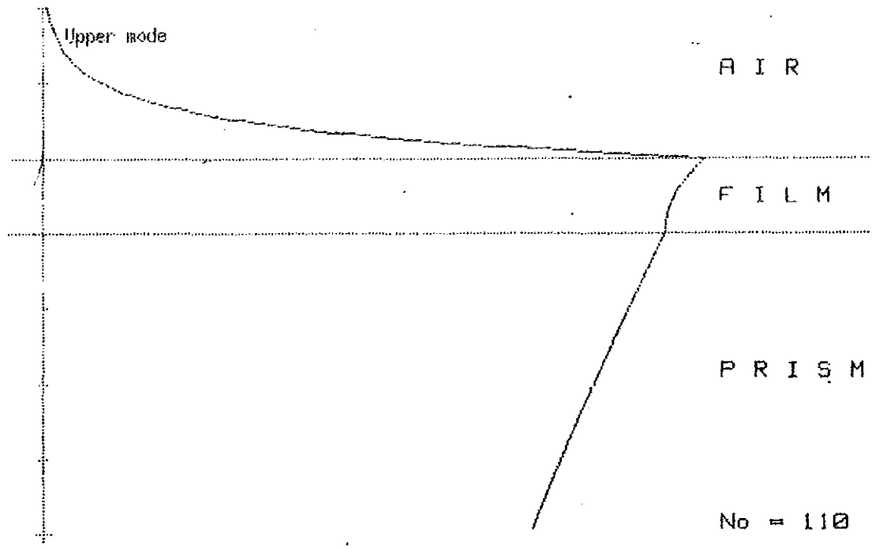

Fig. 3.29 .(L30) Magnetic field distribution in the w(+) mode
E1 = 1 , E3 = 2.25 , Wp = 1.E+15 Hz, Tau = .001 s, Wn = .814102564103
H = 800 A, Ko = 2.71540553737E+6 Kxr = 4.07396449536E+6
Kxor= 0 , Kxi = 4.42070402274E-7 Data file name:L30 *

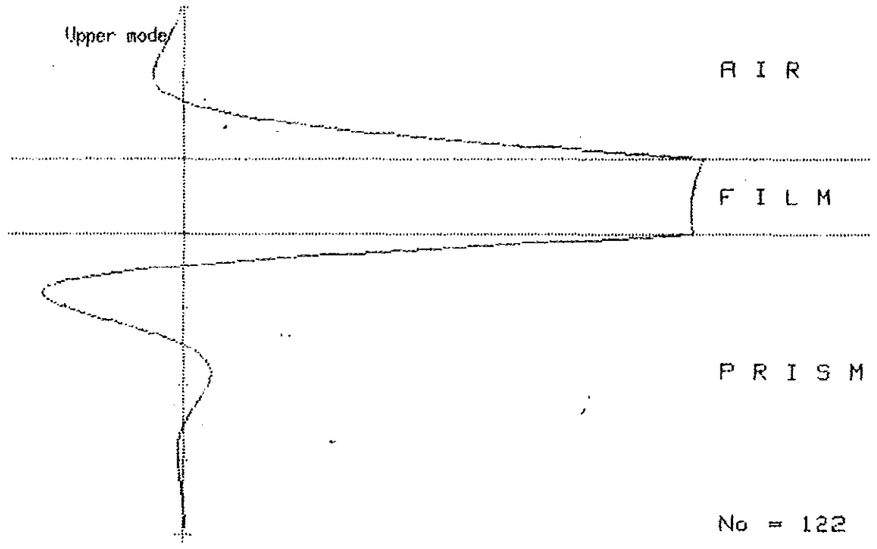

Fig. 3.30 .(L30) Magnetic field distribution in the w(+) mode
E1 = 1 , E3 = 2.25 , Wp = 1.E+15 Hz, Tau = .001 s, Wn = .808487179487
H = 800 A, Ko = 2.96693522177E+6 Kxr = 3.650722269l0E+6
Kxor= 0 , Kxi = 1.95509520994E+6 Data file name:L30 *

Table 3.25 .(L37). Dependance of the PEAL and the IMAG. parts of the SPIP OX-wavevector in PMA configuration: E3 = 2.25 , E21= E21(ω), E22 = E22(ω), E1 = 1 Plasma frequency Wp = 1.E+15 Hz, Relaxtion time Tau = 1.E-13 sec, Thickness of the film H= 800 'A.'

L O W E R ω(-) B R A N C H

ω/Wp	Ko	Kxr	Kxor	Kxi	No
.01000	+3.335557E+04	+5.0025741E+04	+3.335724E+04	+1.7254E+02	1
.01000	+3.335557E+04	+3.3365539E+04	+3.335724E+04	+5.4840E+01	2
.03513	+1.171721E+05	+1.7974114E+05	+1.172446E+05	+2.7364E+03	3
.03513	+1.171721E+05	+1.1840356E+05	+1.172446E+05	+5.1233E+00	4
.06026	+2.009887E+05	+3.2605087E+05	+2.013558E+05	+9.2696E+03	5
.08538	+2.848053E+05	+5.0373537E+05	+2.858567E+05	+1.9159E+04	6
.11051	+3.686218E+05	+7.2395346E+05	+3.709216E+05	+3.0812E+04	7
.13564	+4.524384E+05	+9.9370591E+05	+4.567382E+05	+4.3286E+04	8
.16077	+5.362549E+05	+1.3179308E+06	+5.435124E+05	+5.6299E+04	9
.18590	+6.200715E+05	+1.7009994E+06	+6.314740E+05	+6.9874E+04	10
.21103	+7.038881E+05	+2.1475293E+06	+7.208843E+05	+8.4175E+04	11
.23615	+7.877046E+05	+2.6629089E+06	+8.120452E+05	+9.9451E+04	12
.26128	+8.715212E+05	+3.2537579E+06	+9.053108E+05	+1.1604E+05	13
.28641	+9.553377E+05	+3.9284578E+06	+1.001104E+06	+1.3437E+05	14
.31154	+1.039154E+06	+4.6978641E+06	+1.099935E+06	+1.5506E+05	16
.33667	+1.122971E+06	+5.5763579E+06	+1.202433E+06	+1.7897E+05	19
.36179	+1.206787E+06	+6.5834977E+06	+1.309383E+06	+2.0735E+05	21
.38692	+1.290604E+06	+7.7467775E+06	+1.421786E+06	+2.4219E+05	23
.41205	+1.374421E+06	+9.1065602E+06	+1.540936E+06	+2.8679E+05	25
.43718	+1.458237E+06	+1.0725706E+07	+1.668554E+06	+3.4716E+05	27
.46231	+1.542054E+06	+1.2710679E+07	+1.806972E+06	+4.3569E+05	29
.48744	+1.625870E+06	+1.5266216E+07	+1.959458E+06	+5.8292E+05	32
.51256	+1.709687E+06	+1.8304444E+07	+2.130745E+06	+4.0133E+07	37
.51256	+1.709687E+06	+1.8879715E+07	+2.130745E+06	+8.9168E+05	38
.53769	+1.793503E+06	+2.5351088E+07	+2.327988E+06	+2.0609E+06	45
.53769	+1.793503E+06	+2.5351088E+07	+2.327988E+06	+2.0609E+06	49
.56282	+1.877320E+06	+2.9276670E+07	+2.562615E+06	+1.7262E+07	51
.58795	+1.961136E+06	+2.2501014E+07	+2.854211E+06	+1.9293E+07	57

Table 3.26 .(L37). Dependance of the PEAL and IMAG. parts of the SPIP OX-wavevector in PMA configuration : E3 = 2.25 , E21= E21(ω), E22 = E22(ω), E1 = 1 Plasma frequency Wp = 1.E+15 Hz, Relaxtion time Tau = 1.E-13 sec, Thickness of the film H= 800 'A.'

U P P E R ω(+) B R A N C H (physically real part)

ω/Wp	Ko	Kxr	Kxor	Kxi	No
.71359	+2.380219E+06	+2.9451654E+07	+0.000000E+00	+3.5280E+07	83
.71359	+2.380219E+06	+2.9451654E+07	+0.000000E+00	+3.5280E+07	87
.81410	+2.715486E+06	+4.0673356E+06	+0.000000E+00	+4.2794E+03	96
.83923	+2.799302E+06	+4.5646083E+06	+0.000000E+00	+2.4126E+05	101
.86436	+2.883119E+06	+4.3258662E+06	+0.000000E+00	+1.4054E+06	103
.88949	+2.966935E+06	+3.6323615E+06	+0.000000E+00	+1.8095E+06	105

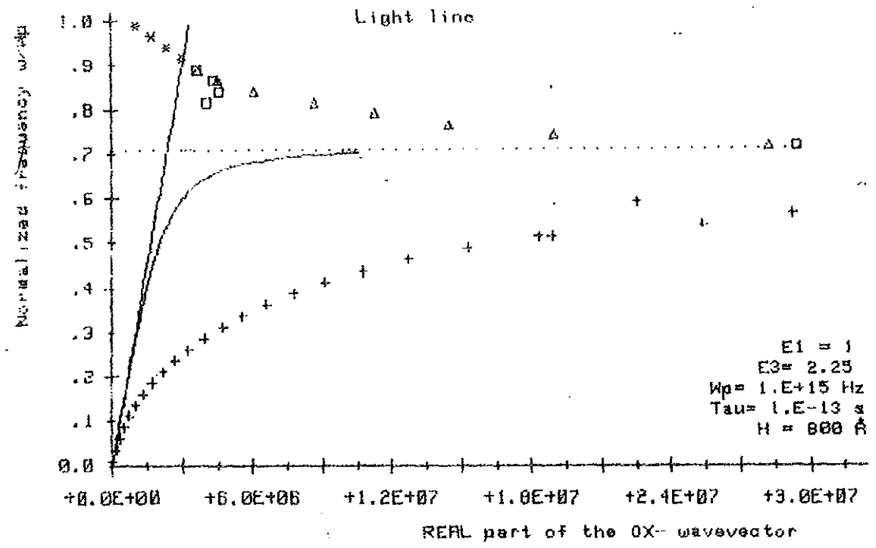

Fig. 3.31 .(L37) REAL part of the OX-wavevector as a function of the normalized frequency: w(-) mode - curve (+ + +), w(+) mode (physically real part)- curve with squares, w(+) mode (physically unreal part) - curve with triangles, semi-infinite case - solid curve, side branch - (* * * curve).

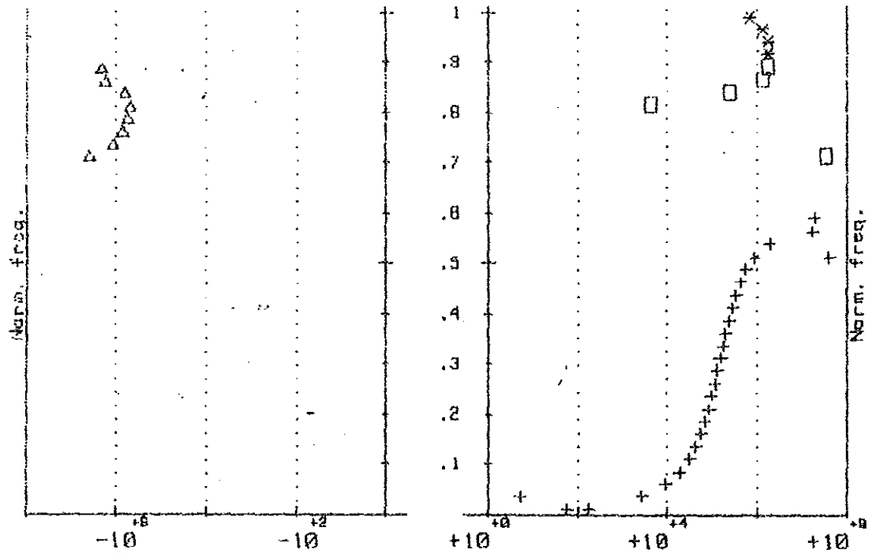

Fig. 3.32 .(L37). IMAG. part of the OX-wavevector as a function of the normalized freq.: w(-) mode - curve (+ + +), w(+) mode (physically real part) - curve with squares, w(+) mode (physically unreal part) - curve with triangles, side branch - (* * *) curve.
E1 = 1 , E3 = 2.25 , H = 800 Å, Wp = 1.E+15 Hz, Tau = 1.E-13 sec*.

Table 3.27 .(L37). Calculations for the power flow in Kretschmann PMA configuration with dielectric permittivities: E3 = 2.25 , E21= E21(w), E22 = E22(w), E1 = 1 Plasma frequency Wp = 1.E+15 Hz; Relaxtion time Tau = 1.E-13 sec, Thickness of the film H= 800 'A.' Y-coordinate = 0 'A'

L O W E R			w(-)	B R A N C H				
w/Wp	Px1	Px2	Px3	Px net	Sy1	Sy2	Sy3	No
.01000	+.000412	-0.0000000	+.999588	+1.0000	-2.75E-14	-2.75E-14	+6.68E-11	1
.01000	+.850915	-0.0000000	+.149085	+1.0000	-4.73E-09	-4.73E-09	+8.29E-10	2
.03513	+.011207	-.0000051	+.988788	+1.0000	-8.86E-13	-8.86E-13	+7.82E-11	3
.03513	+.007509	-0.0000000	+.992491	+1.0000	-6.22E-12	-6.22E-12	+8.22E-10	4
.06026	+.049487	-.0000431	+.950470	+.9999	-4.51E-12	-4.51E-12	+8.66E-11	5
.08538	+.104754	-.0001671	+.895079	+.9997	-1.05E-11	-1.05E-11	+8.96E-11	6
.11051	+.154963	-.0004530	+.844584	+.9991	-1.63E-11	-1.63E-11	+8.88E-11	7
.13564	+.192489	-.0010053	+.806505	+.9980	-2.06E-11	-2.06E-11	+8.63E-11	8
.16077	+.218800	-.0019635	+.779237	+.9961	-2.33E-11	-2.33E-11	+8.30E-11	9
.18590	+.236918	-.0035072	+.759575	+.9930	-2.48E-11	-2.48E-11	+7.94E-11	10
.21103	+.249207	-.0058630	+.744930	+.9883	-2.52E-11	-2.52E-11	+7.54E-11	11
.23615	+.257192	-.0093129	+.733496	+.9814	-2.50E-11	-2.50E-11	+7.13E-11	12
.26128	+.261765	-.0142056	+.724030	+.9716	-2.42E-11	-2.42E-11	+6.69E-11	13
.28641	+.263384	-.0209689	+.715647	+.9581	-2.29E-11	-2.29E-11	+6.24E-11	14
.31154	+.262199	-.0301275	+.707674	+.9397	-2.14E-11	-2.14E-11	+5.77E-11	16
.33667	+.258124	-.0423229	+.699553	+.9154	-1.95E-11	-1.95E-11	+5.29E-11	19
.36179	+.250877	-.0583402	+.690783	+.8833	-1.75E-11	-1.75E-11	+4.81E-11	21
.38692	+.239987	-.0791427	+.680870	+.8417	-1.52E-11	-1.52E-11	+4.33E-11	23
.41205	+.224788	-.1059200	+.669292	+.7882	-1.29E-11	-1.29E-11	+3.84E-11	25
.43718	+.204391	-.1401625	+.655447	+.7197	-1.05E-11	-1.05E-11	+3.36E-11	27
.46231	+.177635	-.1837896	+.638575	+.6324	-8.02E-12	-8.02E-12	+2.88E-11	29
.48744	+.143036	-.2394052	+.617559	+.5212	-5.59E-12	-5.59E-12	+2.41E-11	32
.51256	+.080629	-.4818988	+.437472	+.0362	-1.73E-10	-1.73E-10	+9.36E-10	37
.51256	+.098787	-.3108996	+.590313	+.3782	-3.27E-12	-3.27E-12	+1.96E-11	38
.53769	+.043675	-.4051242	+.551201	+.1898	-1.20E-12	-1.20E-12	+1.52E-11	45
.53769	+.043675	-.4051242	+.551201	+.1898	-1.20E-12	-1.20E-12	+1.52E-11	49
.56282	+.028637	-.4848189	+.486544	+.0304	-3.78E-12	-3.78E-12	+6.42E-11	51
.58795	+.105099	-.4866233	+.408278	+.0268	-5.25E-11	-5.25E-11	+2.04E-10	57

Table 3.28 .(L37). Calculations for the power flow in Kretschmann PMA configuration with dielectric permittivities: E3 = 2.25 , E21= E21(w), E22 = E22(w), E1 = 1 Plasma frequency Wp = 1.E+15 Hz, Relaxtion time Tau = 1.E-13 sec, Thickness of the film H= 800 'A.' Y-coordinate = 0 'A'

U P P E R			w(+)	B R A N C H (physically real part)				
w/Wp	Px1	Px2	Px3	Px net	Sy1	Sy2	Sy3	N
.71359	+.491800	-.4851018	+.023098	+.0298	-2.14E-09	-2.14E-09	+1.00E-10	8
.71359	+.491800	-.4851018	+.023098	+.0298	-2.14E-09	-2.14E-09	+1.00E-10	8
.81410	+.056528	-.0495256	+.893947	+.9009	-3.95E-12	-3.95E-12	+6.25E-11	9
.83923	+.327270	-.4174241	+.255305	+.1652	-1.48E-10	-1.48E-10	+1.16E-10	1(
.86436	+.320113	-.4805780	+.199309	+.0388	-7.67E-10	-7.67E-10	+4.77E-10	1(
.88949	+.317149	-.4830035	+.199847	+.0340	-1.08E-09	-1.08E-09	+6.78E-10	1(

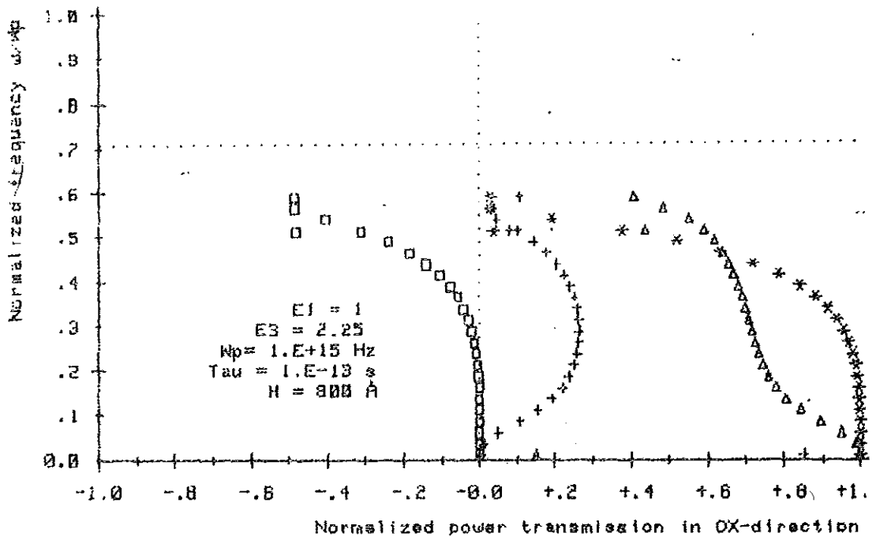

Fig. 3.33 .(L37) Partial and net power transmission in OX-direction performed by the w(-) mode : in media I - curve (+ + +), in media III - curve (with triangles), in the film - curve (with squares), the net power transmission - curve (* * *)

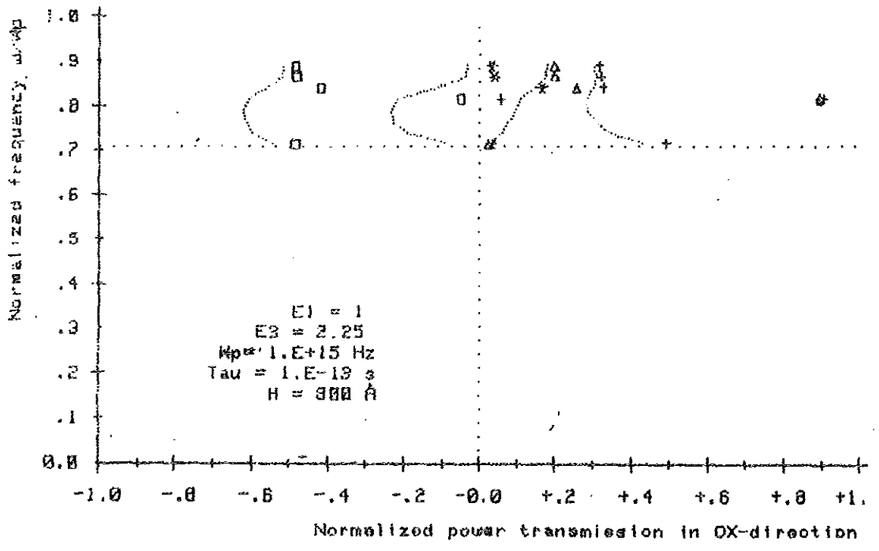

Fig. 3.34 .(L37) Partial and net power transmission in OX-direction performed by the w(+) mode : in media I - curve (+ + +), in media III - curve (with triangles), in the film - curve (with squares), the net power transmission - curve (* * *)

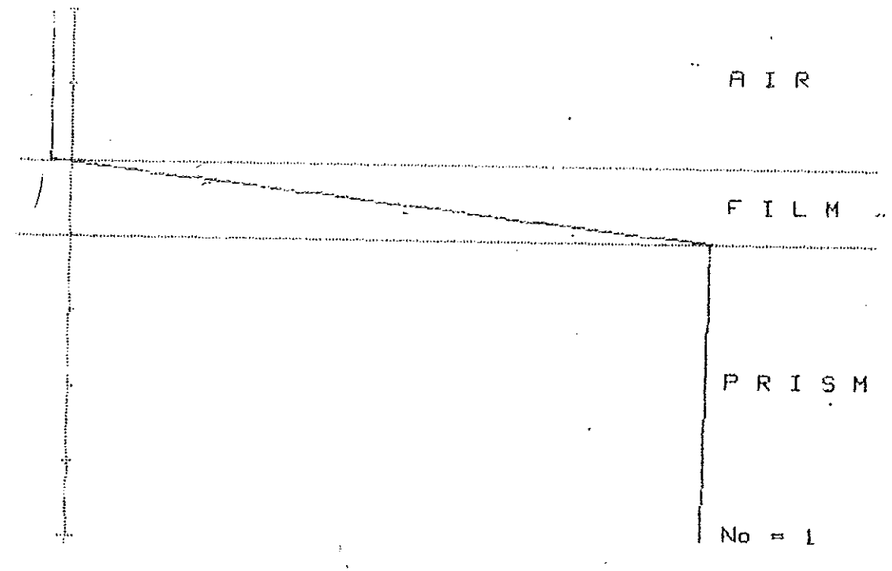

Fig. 3.35 .(L37) Magnetic field distribution in the w(-) mode
E1 = 1 , E3 = 2.25 , Wp = 1.E+15 Hz, Tau = 1.E-13 s, Wn = .01
H = 800 A, Ko = 33355.5703803 Kxr = 50025.7410708
Kxor = 33357.2381507 , Kxi = 172.537412026 Data file name:L37

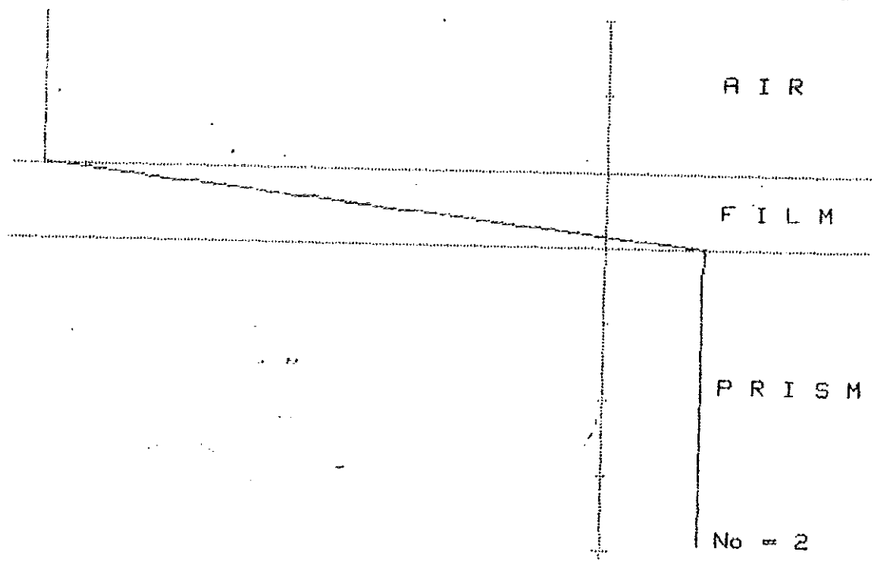

Fig. 3.36 .(L37) Magnetic Field distribution in the w(-) mode
E1 = 1 , E3 = 2.25 , Wp = 1.E+15 Hz, Tau = 1.E-13 s, Wn = .01
H = 800 A, Ko = 33355.5703803 Kxr = 33365.5381249
Kxor = 33357.2381507 , Kxi = 54.840211653 Data file name:L37

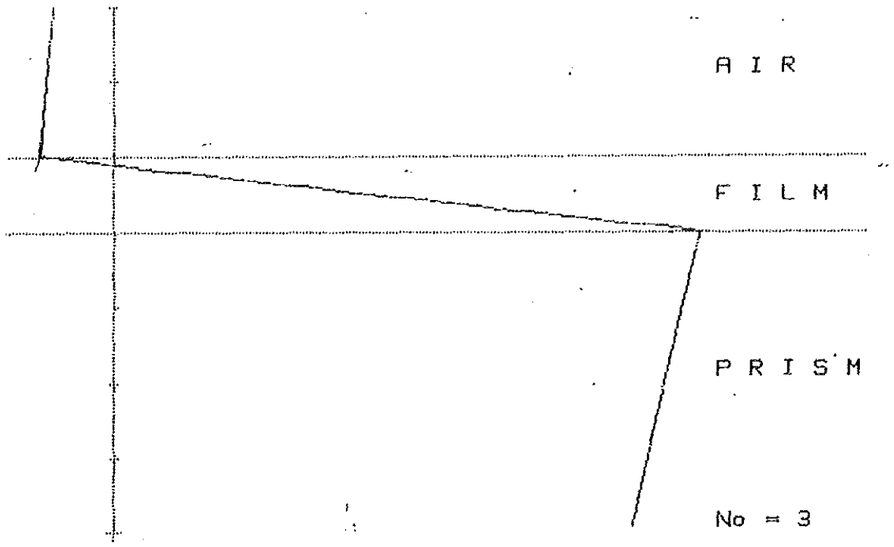

Fig. 3.37 .(L37) Magnetic field distribution in the w(-) mode
El = 1 , E3 = 2.25 , Wp = 1.E+15 Hz, Tau = 1.E-13 s, Wn = .035128205128;
H = 800 A, Ko = 117172.131849 Kxr = 179741.140347
Kxor = 117244.570243 , Kxi = 2736.4441392 Data file name:L37 *

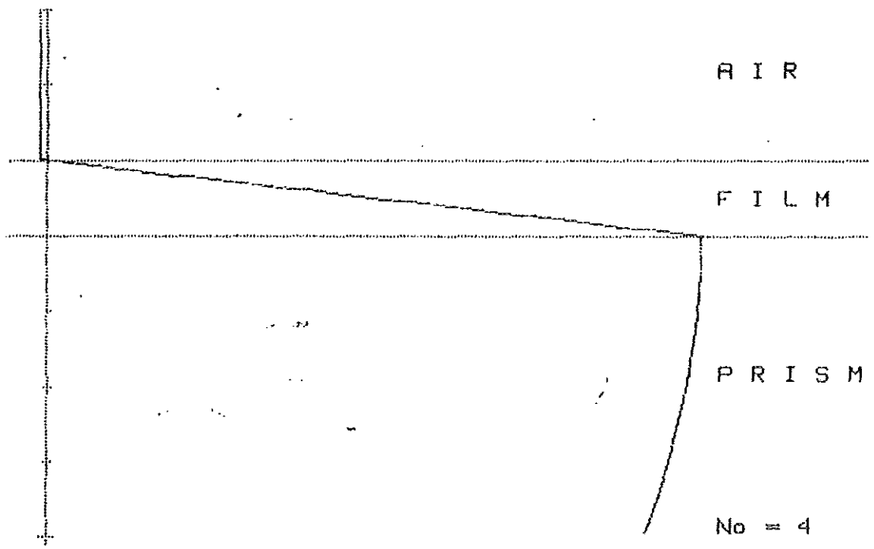

Fig. 3.38 .(L37) Magnetic field distribution in the w(-) mode
El = 1 , E3 = 2.25 , Wp = 1.E+15 Hz, Tau = 1.E-13 s, Wn = .035128205128;
H = 800 A, Ko = 117172.131849 Kxr = 118403.561407
Kxor = 117244.570243 , Kxi = 5.12330415411 Data file name:L37 *

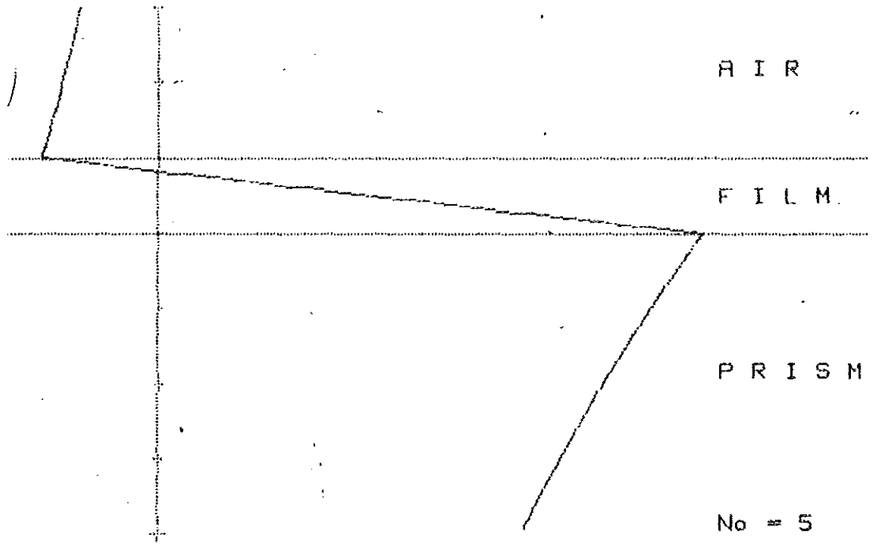

Fig. 3.39 .(L37) Magnetic field distribution in the w(-) mode
E1 = 1 , E3 = 2.25 , Wp = 1.E+15 Hz, Tau = 1.E-13 s, Wn = .060256410256
H = 800 A, Ko = 200988.693317 Kxr = 326050.869298
Kxor = 201355.840140 , Kxi = 9268.57558844 Data file name:L37

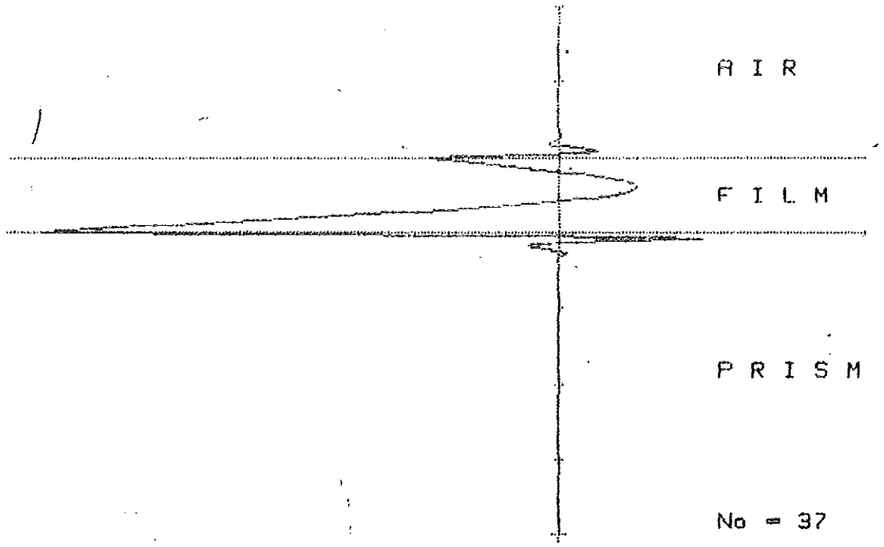

Fig. 3.40 .(L37) Magnetic Field distribution in the ω(-) mode
E1 = 1 , E3 = 2.25 , Wp = 1.E+15 Hz, Tau = 1.E-13 s, Wn = .512564102564
H = 800 Å, Ko = 1.709868679875E+6 Kxr = 1.83044442929E+7
Kxor = 2.13074454509E+6 , Kxi = 4.01327391477E+7 Data file name:L37«

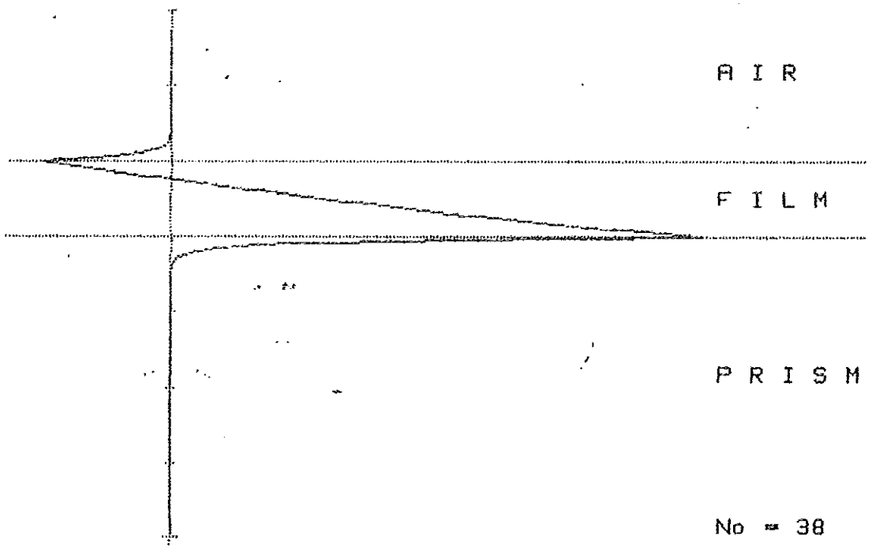

Fig. 3.41 .(L37) Magnetic Field distribution in the ω(-) mode
E1 = 1 , E3 = 2.25 , Wp = 1.E+15 Hz, Tau = 1.E-13 s, Wn = .512564102564
H = 800 Å, Ko = 1.709868679875E+6 Kxr = 1.80797154147E+7
Kxor = 2.13074454509E+6 , Kxi = 881678.621787 Data file name:L37 «

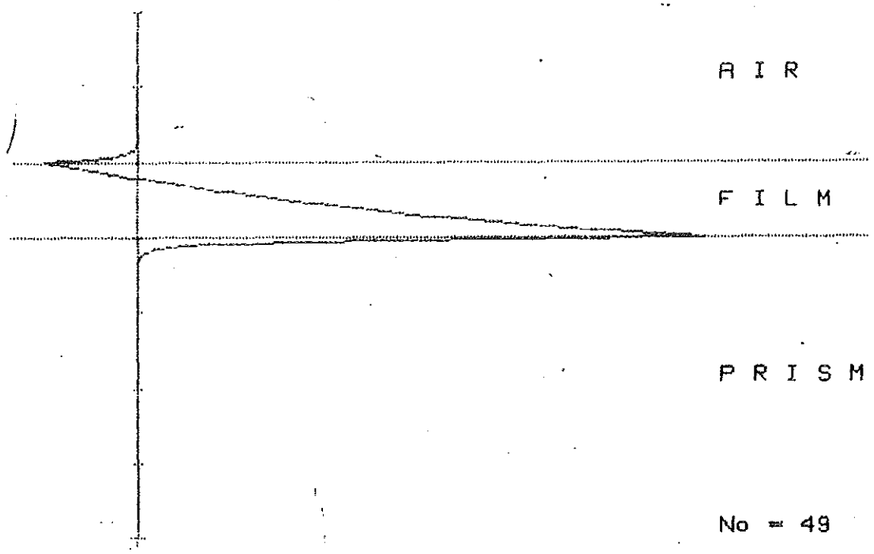

Fig. 3.42 .(L37) Magnetic field distribution in the w(-) mode
E1 = 1 , E3 = 2.25 , Wp = 1.E+15 Hz, Tau = 1.E-13 s, Wn = .597692307692
H = 800 A, Ko = 1.79350336122E+6 Kxr = 2.53510875053E+7
Kxor = 2.32790831510E+6 , Kxi = 2.06097459922E+6 Data file name:L37*

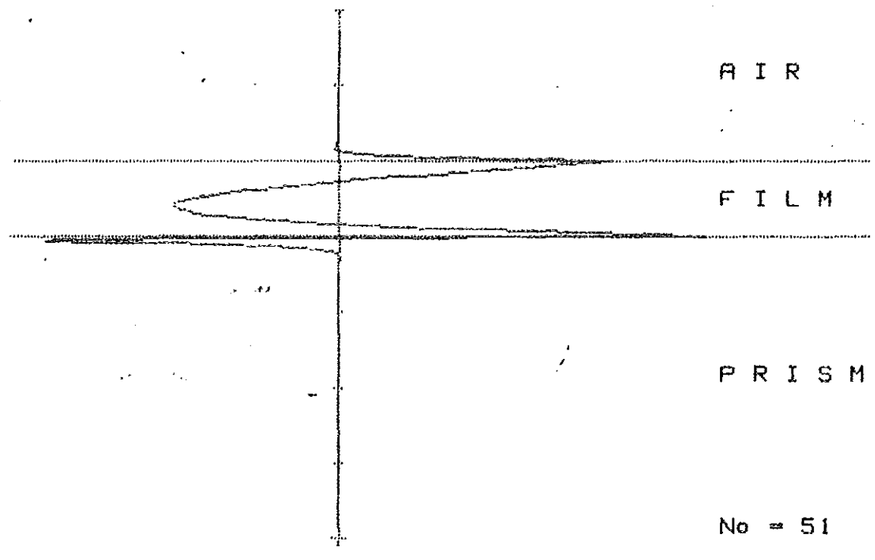

Fig. 3.43 .(L37) Magnetic field distribution in the w(-) mode
E1 = 1 , E3 = 2.25 , Wp = 1.E+15 Hz, Tau = 1.E-13 s, Wn = .562820512821
H = 800 A, Ko = 1.87731992268E+6 Kxr = 2.92766800503E+7
Kxor = 2.56261585036E+6 , Kxi = 1.72610661301E+7 Data file name:L37*

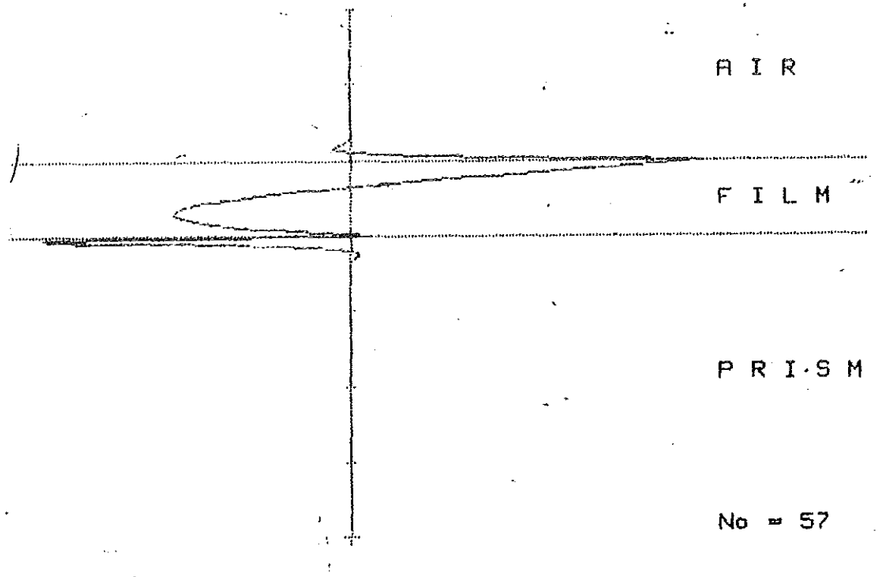

Fig. 3.44 .(L37) Magnetic field distribution in the w(-) mode
E1 = 1 , E3 = 2.25 , Wp = 1.E+15 Hz, Tau = 1.E-13 s, Wn = .597948717948
H = 800 A, Ko = 1.96113648415E+6 Kxr = 2.25010137368E+7
Kxor = 2.05421113996E+6 , Kxi = 1.92927555016E+7 Data file name:L37*

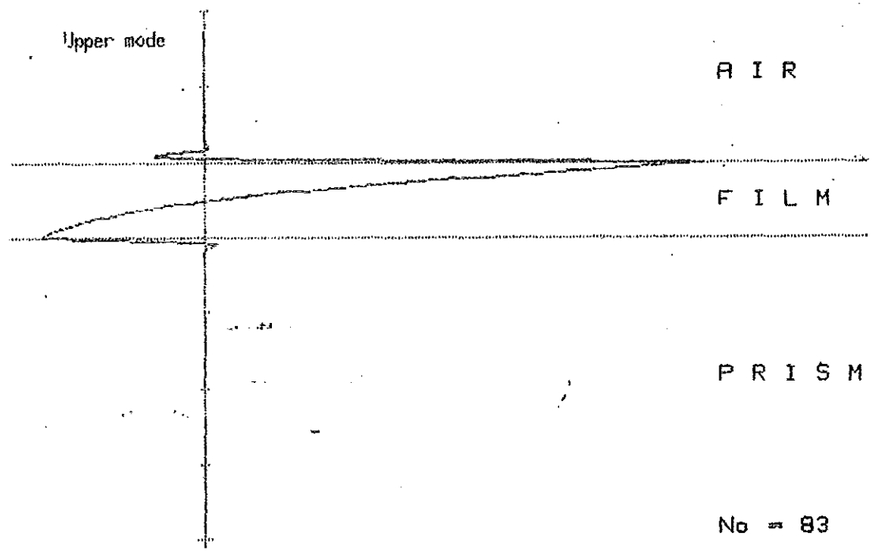

Fig. 3.45 .(L37) Magnetic field distribution in the w(+) mode
E1 = 1 , E3 = 2.25 , Wp = 1.E+15 Hz, Tau = 1.E-13 s, Wn = .71358974358
H = 800 A, Ko = 2.30021928148E+6 Kxr = 2.94516537045E+7
Kxor= 0 , Kxi = 3.52785351829E+7 Data file name:L37 *

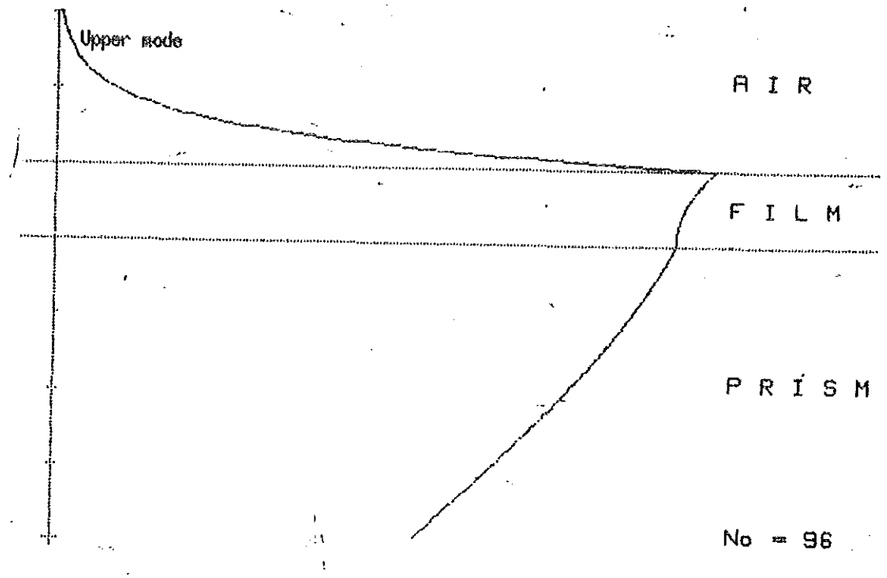

Fig. 3.46 .(L37) Magnetic field distribution in the w(+) mode
El = 1 , E3 = 2.25 , Wp = 1.E+15 Hz, Tau = 1.E-13 s, Wn = .814102564103
H = 800 A, Ko = 2.71548553797E+6 Kxr = 4.067335B0410E+6
Kxor= 0 , Kxi = 4279.42668852 Data file name:L37

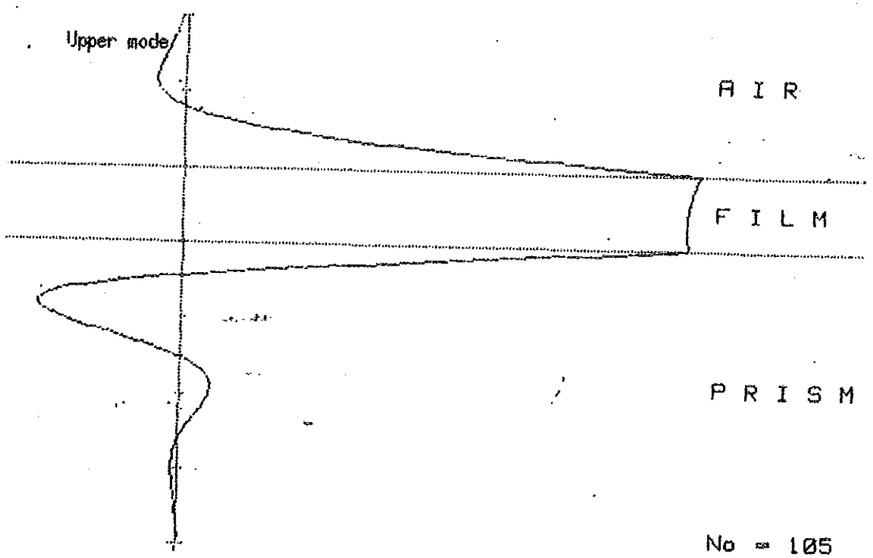

Fig. 3.47 .(L37) Magnetic field distribution in the w(+) mode
El = 1 , E3 = 2.25 , Wp = 1.E+15 Hz, Tau = 1.E-13 s, Wn = .809407179487
H = 800 A, Ko = 2.96693522177E+6 Kxr = 3.692361529333E+6
Kxor= 0 , Kxi = 1.009529459021E+6 Data file name:L37

3.3 A suggested Modification of the Existing SPLP Method.

The existing SPLP method found in literature is reviewed in section 1.2. The reasons which initiated the modification of the method are

i) The previous study by Mr. Abdurahman Ahmed and Dr. D.A. Letov [13] revealed that the existing SPLP method fails:

a) at small h, thicknesses less than $\sim 250\mathring{A}$

b) near $h \equiv h_{opt}$, where $R_{min} \to 0$

c) for $\omega > 0.4\omega_p''$.

ii) As mentioned earlier the method cannot be applied to the symmetric environment ($\varepsilon_3 = \varepsilon_1$).

iii) Upon solving the exact thin film dispersion equation (2.1) numerically by the computer using the 'Downhill' method for the asymmetric environment we observed that there exist several new results which are not shown by the approximate analytical solution of the existing method.

We avoided the following asumptions used in the existing SPLP method.

1) $\mathrm{Re}\tilde{k}_x \approx \mathrm{Re}\tilde{k}_{xo}$

2) Approximate solution for k_x'' .

By avoiding the first assumption one increases the accuracy in the determination of ε_2' , which particularly improves with growing frequency. The elimination of the former also allows the determination of small h value physically possible for both environments and avoids the over estimation of radiation damping in the case of weak absorption, see fig. (2.12) and also the under estimation of radiation damping in the case of strong absorption, see fig. (2.10)

For the modification we borrow the following expressions from the existing method:

I) $$\varepsilon_2''(\theta_{res}, R_{min}, \omega_\theta) = \frac{\omega_\theta}{2}(1 \pm \sqrt{R_{min}}) \frac{\varepsilon_1^2 \varepsilon_3 \tan\theta_{res}}{(\varepsilon_1 - \varepsilon_3 \sin^2\theta_{res})^2} \quad (3.1)$$

II) $$k_x' = k_3 \sin\theta_{res} \quad (3.2)$$

III) $$k_x'' = \frac{k_3 \omega_\theta}{2 \cos\theta_{res}} \quad (3.3)$$

Where $k_3 = k_o n_3$ is the wave vector of light in Prism. From section 2.1 we have the following equations satisfying the thin film dispersion eqn. (2.1).

$$F_1(\varepsilon_2', \varepsilon_2'', h, k_x', k_x'') = 0 \quad (3.4)$$

$$F_2(\varepsilon_2', \varepsilon_2'' \; h, k_x', k'') = 0 \quad (3.5)$$

From eqns. (2.13) and (2.20) the expressions for F_1 and F_2 are

$$F_1 = B e^{-2k''_{2y}h} + \sin C \qquad (3.6)$$

$$F_2 = (A^2+B^2) e^{-4k''_{2y}h} - 1 \qquad (3.7)$$

Where

$$A = r'_{21}r'_{23} - r''_{21}r''_{23} \qquad (3.8)$$

$$B = r'_{21}r''_{23} + r''_{21}r'_{23} \qquad (3.9)$$

$$C = 2k'_{2y}h \qquad (3.10)$$

With

$$r'_{21} = \frac{|\dot{\varepsilon}_1\dot{k}_{2y}|^2 - |\dot{\varepsilon}_2\dot{k}_{1y}|^2}{D} \; ; \; r''_{21} = \frac{2\mathrm{Im}(\dot{\varepsilon}_1\dot{k}_{2y}(\dot{\varepsilon}_2\dot{k}_{1y})^*)}{D} \qquad (3.11)$$

$$r'_{23} = \frac{|\dot{\varepsilon}_3\dot{k}_{2y}|^2 - |\dot{\varepsilon}_2\dot{k}_{3y}|^2}{E} \; ; \; r''_{23} = \frac{2\mathrm{Im}(\dot{\varepsilon}_3\dot{k}_{2y}(\dot{\varepsilon}_2\dot{k}_{3y})^*)}{E} \qquad (3.12)$$

Where

$$D = |\dot{\varepsilon}_1\dot{k}_{2y}|^2 + |\dot{\varepsilon}_2\dot{k}_{1y}|^2 + 2\mathrm{Re}(\dot{\varepsilon}_1\dot{k}_{2y}(\dot{\varepsilon}_2\dot{k}_{1y})^*)$$

$$E = |\dot{\varepsilon}_3\dot{k}_{2y}|^2 + |\dot{\varepsilon}_2\dot{k}_{3y}|^2 + 2\mathrm{Re}(\dot{\varepsilon}_3\dot{k}_{2y}(\dot{\varepsilon}_2\dot{k}_{3y})^*)$$

and

$$\dot{k}_{iy} = \sqrt{k_o^2\,\dot{\varepsilon}_i - \dot{k}_x^2} \quad ; \; i = 1,2,3. \qquad (3.13)$$

$$\dot{k}_{iy} = k'_{iy} + ik''_{iy}$$

ε_2'' , k_x', and k_x'' are determined experimentally using the ATR device by eqns. (3.1) through (3.3). After fixing their values and putting in eqns. (3.6) and (3.7) we have two equations with two unknowns ε_2' and h. Therefore eqns. (3.4) and (3.5) can be written as

$$F_1 (\varepsilon_2' , h) = 0 \qquad (3.14)$$

$$F_2 (\varepsilon_2' , h) = 0 \qquad (3.15)$$

Which can be solved simultaneously for ε_2' and h numerically by the computer using the 'Downhill' method.

3.4 Summary and Conclusions

In trying to improve the existing SPLP method we assessed both symmetric and asymmetric environments of the film. The restriction upon the type of the environment i.e., the requirement that the environment must be strongly asymmetric ($\varepsilon_3 \neq \varepsilon_1$) is lifted. The modified method suggested in the thesis can be applied to any type of environment in which the film is placed. It is also important to note that the modified method does not require any preset model for the $\dot{\varepsilon}_2 \equiv \dot{\varepsilon}_2(\omega)$ function. Therefore the applicability of the method can be very large covering not only different metal films but also various semiconductor films. The studies of the dielectric function are very useful in the determination of the overall band structure of a crystal since $\dot{\varepsilon}_2(\omega)$ depends sensitively on the electronic band structure of a crystal.

Several new results have also been obtained upon solving the thin film dispersion eqn. (2.1) numerically by the computer using the 'Downhill' method. These are

i) the existence of back-bending segements for both environments in the ω^- and ω^+ modes.

ii) the existence of ω^- and ω^+ modes for the asymmetric environment. However, the ω^+ mode appears only as discrete points.

iii) the existence of upper cut off wave vector $k_x'^*$ for the ω^- mode of the asymmetric environment.

iv) the existence of 'side' mode which appears as an extension of ω^+ mode. The 'side' mode is labelled unphysical.

iv) the existence of modulation in the ω^- mode of the asymmetric environment ($\varepsilon_3 \neq \varepsilon_1$) at about $0.51\omega_p$. However, this latter point requires additional studying since the type of field distributions obtained at the corresponding points of the dispersion curve does not fit any of the standards known so far.

The derivation of the experesions for the components of cycle-average power flows in the PMA structure is also our achievement. We have not come across these experessions in literature. These expressions for the power flows can be applied without any restriction on the type of the environment, see appendix B. We have also shown, starting with the thin film dispersion eqn. (2.1), the splitting of the dispersion eqn. into ω^- and ω^+ modes

in the symmetric environment, eqns. (2.22) and (2.23), for very thin metal films, see appendix A.

The back-bending and modulation segments are checked for Physicall validity and we described them as a consequence of artificial anomalous dispersion which is most probably due to absorption of the incident light on PMA structure since the net power flow drops very close to zero for τ small or is zero for τ big. It was found out that the magnetic field distributions change their symmetry properties at ω and k_x' corresponding to these segments.

It is also established that part of the ω^+ mode dispersion curve is physically unreal. The physical validity of this part of this part of ω^+ mode has not been checked in literature [9].

Appendix A

Derivation of the Splitting of the dispersion equation of thin metal film in the symmetric environment ($\varepsilon_3 = \varepsilon_1$) into two branches.

The classical thin metal film dispersion equation in the asymmetric environment is

$$\dot{r}_{32}\dot{r}_{21}\, e^{2i\dot{k}_{2y}h} + 1 = 0 \qquad (A.1)$$

For the case of symmetric environment, $\varepsilon_3 = \varepsilon_1$

$$\dot{r}_{32} = \dot{r}_{12}$$

This implies

$$\dot{r}_{12}\dot{r}_{21}\, e^{2i\dot{k}_{2y}h} + 1 = 0 \qquad (A.2)$$

but $\dot{r}_{12} = -\dot{r}_{21}$

Thus eqn. (A.2) can be written as

$$1 - (\dot{r}_{21}\, e^{i\dot{k}_{2y}h})^2 = 0 \qquad (A.3)$$

Equation (A.3) can be interpreted as a difference of two squares, i.e., like $a^2 - b^2 = (a+b)(a-b)$ and hence

$$(1+\dot{r}_{21}\, e^{i\dot{k}_{2y}h}) \cdot (1-\dot{r}_{21}\, e^{i\dot{k}_{2y}h}) = 0 \qquad (A.4)$$

By putting each bracket in eqn. (A.4) equal to zero, we have

$$1 + \dot{r}_{21}\, e^{i\dot{k}_{2y}h} = 0 \qquad (A.5)$$

and

$$1 - \dot{r}_{21}\, e^{i\dot{k}_{2y}h} = 0 \qquad (A.6)$$

Where $\dot{r}_{21}$ is Fresnel's reflection coefficient for P-polarized light, see eqn. (1.13), given by

$$\dot{r}_{21} = \left(\frac{\dot{k}_{2y}}{\dot{\varepsilon}_2} - \frac{\dot{k}_{1y}}{\varepsilon_1}\right) \Big/ \left(\frac{\dot{k}_{2y}}{\dot{\varepsilon}_2} + \frac{\dot{k}_{1y}}{\varepsilon_1}\right) \qquad (A.7)$$

Putting eqn. (A.7) into eqn. (A.5), we have

$$\left(\frac{\dot{k}_{2y}}{\dot{\varepsilon}_2} + \frac{\dot{k}_{2y}}{\varepsilon_1}\right) + \left(\frac{\dot{k}_{2y}}{\dot{\varepsilon}_2} - \frac{\dot{k}_{1y}}{\varepsilon_1}\right) e^{i\dot{k}_{2y}h} = 0$$

This implies

$$\frac{\dot{k}_{2y}}{\dot{\varepsilon}_2}\left(1 + e^{i\dot{k}_{2y}h}\right) + \frac{\dot{k}_{1y}}{\varepsilon_1}\left(1 - e^{i\dot{k}_{2y}h}\right) = 0 \qquad (A.8)$$

Dividing throughout, eqn. (A.8), by $(1-e^{i\dot{k}_{2y}h})$ we get

$$\frac{\dot{k}_{1y}}{\varepsilon_1} + \frac{\dot{k}_{2y}}{\dot{\varepsilon}_2}\left(\frac{e^{i\dot{k}_{2y}h} + 1}{1 - e^{i\dot{k}_{2y}h}}\right) = 0$$

This goes to

$$\frac{\dot{k}_{1y}}{\dot{\varepsilon}_1} - \frac{\dot{k}_{2y}}{\dot{\varepsilon}_2}\left(\frac{e^{i\dot{k}_{2y}h} + 1}{e^{i\dot{k}_{2y}h} - 1}\right) = 0 \qquad (A.9)$$

but

$$\frac{e^{i\dot{k}_{2y}h} + 1}{e^{i\dot{k}_{2y}h} - 1} = \operatorname{ctgh}\left(\frac{i\dot{k}_{2y}h}{2}\right)$$

Now eqn. (A.9) becomes

$$\frac{\dot{k}_{1y}}{\dot{\varepsilon}_1} - \frac{\dot{k}_{2y}}{\dot{\varepsilon}_2} \operatorname{ctgh}\left(\frac{i\dot{k}_{2y}h}{2}\right) = 0 \qquad \text{(A.10)}$$

since $$-\operatorname{ctgh}\left(\frac{i\dot{k}_{2y}h}{2}\right) = \operatorname{ctgh}\left(\frac{-i\dot{k}_{2y}h}{2}\right), \text{ eqn(A.10)}$$

can be written as

$$\frac{\dot{k}_{1y}}{\dot{\varepsilon}_1} + \frac{\dot{k}_{2y}}{\dot{\varepsilon}_2} \operatorname{ctgh}\left(\frac{-i\dot{k}_{2y}h}{2}\right) = 0 \qquad \text{(A.11)}$$

Multiplying eqn. (A.11) throughtout by $\dot{\varepsilon}_1\dot{\varepsilon}_2$ we have

$$\dot{\varepsilon}_2\dot{k}_{1y} + \dot{\varepsilon}_1\dot{k}_{2y} \operatorname{ctgh}\left(\frac{-i\dot{k}_{2y}h}{2}\right) = 0 \qquad \text{(A.12)}$$

but in eqn. (A.12) the argument can be simplified as

$$\frac{-i\dot{k}_{2y}h}{2} \cdot \frac{i}{i} = \frac{\dot{k}_{2y}h}{2i} \qquad \text{(A.13)}$$

Hence eqn. (A.12) takes the following form

$$\dot{\varepsilon}_2\dot{k}_{1y} + \dot{\varepsilon}_1\dot{k}_{2y} \operatorname{ctgh}\left(\frac{\dot{k}_{2y}h}{2i}\right) = 0 \qquad \text{(A.14)}$$

Similarly, putting eqn. (A.7) into eqn. (A.6). we have

$$\left(\frac{\dot{k}_{2y}}{\dot{\varepsilon}_2} + \frac{\dot{k}_{1y}}{\dot{\varepsilon}_1}\right) - \left(\frac{\dot{k}_{2y}}{\dot{\varepsilon}_2} - \frac{\dot{k}_{1y}}{\dot{\varepsilon}_1}\right) e^{i\dot{k}_{2y}h} = 0$$

This implies

$$\frac{\dot{k}_{2y}}{\dot{\varepsilon}_2}\left(1 - e^{i\dot{k}_{2y}h}\right) + \frac{\dot{k}_{1y}}{\varepsilon_1}\left(1 + e^{i\dot{k}_{2y}h}\right) = 0 \qquad \text{(A.15)}$$

Dividing eqn. (A.15) throughout by $(1+e^{i\dot{k}_{2y}h})$ we get

$$\frac{\dot{k}_{1y}}{\varepsilon_1} + \frac{\dot{k}_{2y}}{\dot{\varepsilon}_2}\left(\frac{1-e^{i\dot{k}_{2y}h}}{e^{i\dot{k}_{2y}h}+1}\right) = 0$$

This goes to

$$\frac{\dot{k}_{1y}}{\varepsilon_1} - \frac{\dot{k}_{2y}}{\dot{\varepsilon}_2}\left(\frac{e^{i\dot{k}_{2y}h}-1}{e^{i\dot{k}_{2y}h}+1}\right) = 0 \qquad \text{(A.16)}$$

but

$$\frac{e^{i\dot{k}_{2y}h}-1}{e^{i\dot{k}_{2y}h}+1} = \tanh\left(\frac{i\dot{k}_{2y}h}{2}\right)$$

Now eqn. (A.16) becomes

$$\frac{\dot{k}_{1y}}{\varepsilon_1} - \frac{\dot{k}_{2y}}{\dot{\varepsilon}_2}\tanh\left(\frac{i\dot{k}_{2y}h}{2}\right) = 0 \qquad \text{(A.17)}$$

since $-\tanh\left(\frac{i\dot{k}_{2y}h}{2}\right) = \tanh\left(\frac{-i\dot{k}_{2y}h}{2}\right)$, eqn. (A.17) can be written as

$$\frac{\dot{k}_{1y}}{\varepsilon_1} + \frac{\dot{k}_{2y}}{\dot{\varepsilon}_2} \tanh\left(\frac{-i\dot{k}_{2y}h}{2}\right) = 0 \qquad \text{(A.18)}$$

Multiplying eqn. (A18) throughout by $\varepsilon_1 \dot{\varepsilon}_2$ and using eqn. (A.13) we get

$$\dot{\varepsilon}_2 \dot{k}_{1y} + \varepsilon_1 \dot{k}_{2y} \tanh\left(\frac{\dot{k}_{2y}h}{2i}\right) = 0 \qquad \text{(A.19)}$$

So eqn.s (A.14) and (A.19) are the final forms of the splitting of the dispersion eqn. (A.2) into two branches. So the eqns. corresponding to the upper mode ($\omega+$) and lower mode ($\omega-$) are

$$\omega^+ : L^+ = \dot{\varepsilon}_2 \dot{k}_{1y} + \varepsilon_1 \dot{k}_{2y} \tanh\left(\frac{\dot{k}_{2y}h}{2i}\right) = 0 \qquad \text{(A.20)}$$

$$\omega^- : L^- = \dot{\varepsilon}_2 \dot{k}_{1y} + \varepsilon_1 \dot{k}_{2y} \operatorname{ctgh}\left(\frac{\dot{k}_{2y}h}{2i}\right) = 0 \qquad \text{(A.21)}$$

APPENDIX B

Derivation of Cycle-Average Power Flow in Kretschmann PMA Configuration.

The cycle-average power flow is given by

$$\langle \vec{s} \rangle = \frac{1}{2} R_e \, (\vec{E} \times \vec{H}^*) \tag{B.1}$$

Suppose a TM polarization, $\vec{H} = \vec{H}_z$, wave incident on the film. From Maxwell's eqn.

$$\text{rot } \vec{H}_i = \epsilon_i \frac{\partial \vec{E}_i}{\partial t} \tag{B.2}$$

We see that

$$\vec{E} = E_{xi}\hat{i} + E_y\hat{j} \tag{B.3}$$

Now eqn. (B.1) becomes

$$\langle s_x\hat{i} + s_y\hat{j} \rangle = \frac{1}{2} R_e \, (E_y H_z^*)\, \hat{i} - \frac{1}{2} R_e (E_x H_z^*)\, \hat{j}$$

Resolving gives

$$\langle s_x \rangle = \frac{1}{2} R_e \, (E_y H_z^*) \tag{B.4}$$

$$\langle s_y \rangle = -\frac{1}{2} R_e (E_x H_z^*)$$

The magnetic field distributions for the three media are

$$H_{z1} = A_1 \, e^{ik_{1y}y + i(k_x x - \omega t)}$$

$$H_{z2} = (A_2 \, e^{ik_{2y}y} + B_2 \, e^{-ik_{2y}y}) \, e^{i(k_x x - \omega t)}$$

$$H_{z3} = A_3 \, e^{-ik_{3y}y + i(k_x x - \omega t)} \tag{B.5}$$

From eqn. (B.2), we have

$$E_{xi} = \frac{1}{-i\omega\varepsilon_i} \frac{H_{zi}}{\partial y} \qquad (B.6)$$

$$E_{yi} = \frac{1}{i\omega\varepsilon_i} \frac{H_{zi}}{\partial x}$$

where i = 1,2,3.

For our layered system, using eqn (B.6) we get

$$\dot{E}_{x1} = -\frac{\dot{k}_{1y}}{\omega\varepsilon_1} \dot{H}_{z1}$$

$$\dot{E}_{x2} = \frac{\dot{k}_{2y}}{\omega\dot{\varepsilon}_2} \left[-\dot{A}_2 e^{ik_{2y}y} + B_2 e^{-ik_{2y}y} \right] e^{i(k_x x - \omega t)}$$

$$\dot{E}_{x3} = \frac{\dot{k}_{3y}}{\omega\varepsilon_3} \dot{H}_{z3} \qquad (B.7)$$

and

$$E_{y1} = \frac{\dot{k}_x}{\omega\varepsilon_1} \dot{H}_{z1}$$

$$E_{y2} = \frac{\dot{k}_x}{\omega\dot{\varepsilon}_2} \dot{H}_{z2} \qquad (B.8)$$

$$\dot{E}_{y3} = \frac{\dot{k}_x}{\omega\varepsilon_3} \dot{H}_{z3}$$

Using eqns. (B.7) and (B.8) in eqn. (B.4) we have

$$\langle s_{xi} \rangle = \frac{1}{2} R_e \frac{\dot{k}_x}{\omega\varepsilon_i} |\dot{H}_{zi}|^2 \quad \text{where } i = 1,2,3. \qquad (B.9)$$

and

$$\langle S_{y1} \rangle = \frac{1}{2} R_e \frac{\dot{k}_{1y}}{\omega \varepsilon_1} | H_{z1} |^2 \qquad (B.10)$$

$$\langle S_{y2} \rangle = -\frac{1}{2} R_e \frac{\dot{k}_{2y}}{\omega \varepsilon_2} \left[-| A_2 |^2 e^{-2k''_{2y}Y} + \right.$$

$$\left. | \dot{B}_2 |^2 e^{2k''_{2y}Y} + B_2 A_2^* e^{-2ik'_{2y}Y} - A_2 B_2^* e^{-2ik'_{2y}Y} e^{-2k''_x x} \right] \qquad (B.11)$$

$$\langle S_{y3} \rangle = -\frac{1}{2} R_e \frac{\dot{k}_{3y}}{\omega \varepsilon_3} | H_{z3} |^2 \qquad (B.12)$$

Now we need to express the amplitudes $\dot{A}_1$ $\dot{A}_2$, and $\dot{B}_2$ interms of $\dot{A}_3$. This is accomplished using boundary conditions at the two interfaces i.e., continuity of the field vectors $\vec{E}$ and $\vec{H}$.

At y = 0, (metal/air) interface

$$E_{x1} = E_{x2} \text{ and } H_{z1} = H_{z2} \qquad (B.13)$$

At y = -h, (prism/metal) interface

$$E_{x2} = E_{x3} \text{ and } H_{z2} = H_{z3} \qquad (B.14)$$

From Eqn. (B.13) we obtain

$$\dot{A}_1 = \frac{\varepsilon_1 \dot{k}_{2y}}{\varepsilon_2 \dot{k}_{1y}} (\dot{A}_2 - \dot{B}_2) \text{ and } \dot{A}_1 = \dot{A}_2 + \dot{B}_2, \text{ respectively.}$$

(B.15)

From eqn. (B.14) we obtain

$$\frac{\dot{k}_{2y}}{\dot{\varepsilon}_2}(-A_2\, e^{-i\dot{k}_{2y}h} + B_2\, e^{i\dot{k}_{2y}h}) = \frac{\dot{k}_{3y}}{\varepsilon_3}\, \dot{A}_3\, e^{i\dot{k}_{3y}h} \qquad (B.16)$$

and

$$(A_2\, e^{-ik_{2y}h} + B_2\, e^{ik_{2y}h}) = A_3\, e^{ik_{3y}h}$$

respectively.

Where k_{iy} are determined by solving the wave eqn. for each mdium

$$\nabla^2 H_{zi} = \frac{\varepsilon_i}{c^2}\, \frac{\partial^2 H_{zi}}{\partial t^2} \quad , \text{ where } i = 1,2,3. \qquad (B.17)$$

and is given by

$$\dot{k}_{iy} = [\, k_o^2\, \varepsilon_i - \dot{k}_x^{\,2}\,]^{\frac{1}{2}} \qquad (B.18)$$

From eqns. (B.15) we have

$$\dot{B}_2 = \dot{A}_2\, \left(\frac{\dot{k}_{2y}}{\dot{\varepsilon}_2} - \frac{k_{1y}}{\varepsilon_2}\right) / \left(\frac{\dot{k}_{2y}}{\dot{\varepsilon}_2} + \frac{\dot{k}_{1y}}{\varepsilon_1}\right) \qquad (B.19)$$

From eqn. (1.13) we see that

$$\dot{r}_{21} = \frac{\dot{B}_2}{A_2} = \left(\frac{\dot{k}_{2y}}{\dot{\varepsilon}_2} - \frac{\dot{k}_{1y}}{\varepsilon_1}\right) / \left(\frac{\dot{k}_{2y}}{\dot{\varepsilon}_2} + \frac{\dot{k}_{1y}}{\varepsilon_1}\right) \qquad (B.20)$$

is the Fresnel reflection coefficient at metal/air interface.

From eqn. (16) we get

$$\dot{A}_2 = \dot{B}_2 \, \dot{r}_{23} \, e^{2ik_{2y}h} \tag{B.21}$$

where

$$\dot{r}_{23} = \left(\frac{\dot{k}_{2y}}{\dot{\varepsilon}_2} - \frac{\dot{k}_{3y}}{\varepsilon_3}\right) \Big/ \left(\frac{\dot{k}_{2y}}{\dot{\varepsilon}_2} + \frac{\dot{k}_{3y}}{\varepsilon_3}\right) \tag{B.22}$$

is the Fresnel reflection coefficient given by eqn. (1.13)

Using eqn. (B.20) in eqn. (B.21), we arrive at

$$\dot{r}_{21}\dot{r}_{23} \, e^{2ik_{2y}h} = 1 \quad \text{or} \quad \dot{r}_{21}\dot{r}_{32} \, e^{2ik_{2y}h} + 1 = 0 \tag{B.23}$$

This is the thin metal film dispersion eqn.

Now we need to express A_2 interms of A_3 using eqn. (B.20) in the 2nd of eqn. (B.16), and also using eqn. (B.23), we have

$$A_2 = \frac{\dot{r}_{23}\dot{A}_3 \, e^{i(\dot{k}_{2y} + \dot{k}_{3y})h}}{\dot{r}_{23} + 1} \tag{B.24}$$

and using eqn. (B.20) $\dot{B}_2$ can be written as

$$B_2 = \frac{A_3 \, e^{i(\dot{k}_{3y} - \dot{k}_{2y})h}}{\dot{r}_{23} + 1} \tag{B.25}$$

Using eqn. (B.15) $\dot{A}_1$ can be written as

$$\dot{A}_1 = \frac{\dot{A}_3 \, e^{i(\dot{k}_{2y} + \dot{k}_{3y})h}}{\dot{r}_{23} + 1} \left[\dot{r}_{23} + e^{-2i\dot{k}_{2y}h} \right] \tag{B.26}$$

In the expressions for the power flows we frequently come across terms like $|\dot{H}_{zi}|^2$, $i = 1,2,3$.

For medium 1 (air)

$$|\dot{H}_{z1}|^2 = |\dot{A}_1|^2 \; e^{-2k''_{1y}y - 2k''_x x} \tag{B.27}$$

For metal film (2)

$$|\dot{H}_{z2}|^2 = \left[|\dot{A}_2|^2 \, e^{-2k''_{2y}y} + |\dot{B}_2|^2 \, e^{2k''_{2y}y} + \dot{A}_2\dot{B}_2^* \, e^{2ik'_{2y}y} \right.$$

$$\left. + \dot{B}_2\dot{A}_2^* \, e^{-2ik'_{2y}y} \right] \cdot e^{-2k''_x x} \tag{B.28}$$

For Prism (3)

$$|\dot{H}_{z3}|^2 = |\dot{A}_3|^2 \; e^{2k''_{3y}y - 2k''_x x} \tag{B.29}$$

Putting eqns. (B.27) through (B.29) in eqns. (B.9), B.10), and B.12), we have for the x-components

$$\langle s_{x1} \rangle = \frac{1}{2} R_e \frac{k'_x}{\omega\varepsilon_1} |\dot{A}_1|^2 \; e^{-2k''_{1y}y - 2k''_x x} \tag{B.30}$$

$$\langle s_{x2} \rangle = \frac{1}{2} R_e \frac{k'_x}{\omega\varepsilon_2} \left[|\dot{A}_2|^2 \, e^{-2k''_{2y}y} + |\dot{B}_2|^2 \, e^{2k''_{2y}y} + \right.$$

$$\left. + \dot{A}_2\dot{B}_2^* \, e^{2ik'_{2y}y} + \dot{B}_2\dot{A}_2^* \; e^{-2ik'_{2y}y} \right] \cdot e^{-2k''_x x} \tag{B.31}$$

$$\langle s_{x3} \rangle = \frac{1}{2} R_e \frac{k_x}{\omega\varepsilon_3} |\dot{A}_3|^2 \; e^{2k''_{3y}y - 2k''_x x} \tag{B.32}$$

and for the y - components, we get

$$\langle s_{y1} \rangle = \frac{1}{2} R_e \frac{\dot{k}_{1y}}{\omega \varepsilon_1} |\dot{A}_1|^2 \; e^{-2k''_{1y} y - 2k''_x x} \tag{B.33}$$

$$\langle s_{y2} \rangle = -\frac{1}{2} R_e \frac{\dot{k}_{2y}}{\omega \dot{\varepsilon}_2} \Big[-|\dot{A}_2|^2 \, e^{-2k''_{2y} y} + |\dot{B}_2|^2 e^{2k''_{2y} y}$$

$$+ \dot{B}_2 \dot{A}_2^* \, e^{-2ik'_{2y} y} - \dot{A}_2 \dot{B}_2^* \, e^{2ik'_{2y} y} \Big] \cdot e^{-2k''_x x} \tag{B.34}$$

$$\langle s_{y3} \rangle = -\frac{1}{2} R_e \frac{\dot{k}_{3y}}{\omega \varepsilon_3} |\dot{A}_3|^2 \; e^{2k''_{3y} y - 2k''_x x} \tag{B.35}$$

The next step is to replace $\dot{A}_1$, $\dot{A}_2$ and $\dot{B}_2$ by their expressions interms of $\dot{A}_3$, eqns. (B.24) through (B.26). Hence

$$|\dot{A}_2|^2 = \frac{|\dot{r}_{23}|^2 \, |\dot{A}_3|^2 \, e^{-2k''_{2y} h - 2k''_{3y} h}}{|\dot{r}_{23}|^2 + 2r'_{23} + 1} \tag{B.36}$$

$$|\dot{B}_2|^2 = \frac{|\dot{A}_3|^2 \, e^{(-2k''_{3y} h + 2k''_{2y} h)}}{|\dot{r}_{23}|^2 + 2r'_{23} + 1} \tag{B.37}$$

$$\dot{A}_2 \cdot \dot{B}_2^* = \frac{\dot{r}_{23} \, |\dot{A}_3|^2 e^{-2k''_{3y} h + 2ik'_{2y} h}}{|\dot{r}_{23}|^2 + 2r'_{23} + 1} \tag{B.38}$$

$$\dot{B}_2 \cdot \dot{A}_2^* = \frac{\dot{r}_{23}^* \, |\dot{A}_3|^2 \, e^{-2k''_{3y} h - 2ik'_{2y} h}}{|\dot{r}_{23}|^2 + 2r'_{23} + 1} \tag{B.39}$$

$$|A_1|^2 = \frac{|A_3|^2 e^{-2k''_{3y}h}}{|\dot{r}_{23}|^2+2r'_{23}+1}\left[|\dot{r}_{23}|^2 e^{-2k''_{2y}h} + e^{2k''_{2y}h} + \right.$$

$$\left. 2(r'_{23}\cos(2k'_{2y}h) - r''_{23}\sin(2k'_{2y}h))\right] \qquad (B.40)$$

Eqns. (B.38) and B.39) should be resolved into Re and Im parts.

The complex term in eqn. (B.38) is

$$\dot{r}_{23}e^{2ik'_{2y}h} = (r'_{23} + ir''_{23}) \cdot (\cos(2k'_{2y}h) + i\sin(2k'_{2y}h))$$

$$= r'_{23}\cos(2k'_{2y}h) - r''_{23}\sin(2k'_{2y}h) + i[r'_{23}\sin(2k'_{2y}h) + r''_{23}\cos(2k'_{2y}h)]$$

This implies

$$\mathrm{Re}(\dot{A}_2 \cdot \dot{B}_2^*) = \frac{|A_3|^2 e^{-2k_{3y}''h}[r'_{23}\cos(2k'_{2y}h) - r''_{23}\sin(2k'_{2y}h)]}{|\dot{r}_{23}|^2 + 2r'_{23} + 1} \qquad (B.41)$$

$$\mathrm{Im}(\dot{A}_2 \cdot \dot{B}_2^*) = \frac{|A_3|^2 e^{-2k''_{3y}h}[r'_{23}\cos(2k'_{2y}h) + r''_{23}\sin(2k'_{2y}h)]}{|r_{23}|^2 + 2r'_{23} + 1} \qquad (B.42)$$

The complex term in eqn. (B.39) is

$$\dot{r}^*_{23} e^{-2ik'_{2y}h} = [r'_{23}\cos(2k'_{2y}h) - r''_{23}\sin(2k'_{2y}h)] - i[r'_{23}\sin(2k'_{2y}h) + r''_{23}\cos(2k'_{2y}h)]$$

That is

$$R_e(\dot{A}_2 \cdot \dot{B}_2^*) = R_e(\dot{B}_2 \cdot \dot{A}_2^*)$$

$$Im(\dot{A}_2 \dot{B}_2^*) = -Im(\dot{B}_2 \cdot \dot{A}_2^*) \qquad (B.43)$$

Using eqn. (B.43) for the last two terms in eqn. (B.31)

$$\dot{A}_2 \cdot \dot{B}_2^* \; e^{2ik'_{2y}Y} + \dot{B}_2\dot{A}_2^* \; e^{-2ik'_{2y}Y} = 2\,R_e(A_2 \cdot B_2^*)\cos(2k'_{2y}Y) - 2\,Im(A_2 \cdot B_2^*)\sin(2k'_{2y}Y) \qquad (B.44)$$

Similarly, for the last two terms in eqn. (B.34)

$$\dot{A}_2\dot{B}_2^* \; e^{2ik'_{2y}Y} - \dot{B}_2\dot{A}_2^* \; e^{-2ik'_{2y}Y} = 2i\left[R_e(A_2 \cdot B_2^*)\sin(2k'_{2y}Y) + Im(A_2 \cdot B_2^*)\cos(2k'_{2y}Y)\right] \qquad (B.45)$$

Using eqns. (B.36) through (B.45) in eqns. (B.30) through (B.35), and also using the trigonometric relations

$$\sin(\alpha + \beta) = \sin\alpha\cos\beta + \cos\alpha\sin\beta$$

$$\cos(\alpha + \beta) = \cos\alpha\cos\beta - \sin\alpha\sin\beta \qquad (B.46)$$

We are also resolving the terms in eqns. (B.30) through (B.35). into Re and Im parts.

In eqn. (B.30), the term

$$\dot{k}_x = k'_x + ik''_x, \quad \text{i.e.,} \quad R_e(\dot{k}_x) = k'_x \qquad (B.47)$$

In eqn. (B. 31), the term

$$\frac{\dot{k}_x}{\dot{\epsilon}_2} = \frac{k'_x + ik''_x}{\epsilon'_2 + i\epsilon''_2} \cdot \frac{\epsilon'_2 - i\epsilon''_2}{\epsilon'_2 - i\epsilon''_2} = \frac{k'_x \epsilon'_2 + k''_x \epsilon''_2}{|\dot{\epsilon}_2|^2} + \frac{i[k''_x \epsilon'_2 - \epsilon''_2 k'_x]}{|\dot{\epsilon}_2|^2} \qquad (B.48)$$

In eqn. (B.32), the term

$$\dot{k}_x = k'_x + ik''_x \qquad (B.49)$$

In eqn. (B.33), the term

$$\dot{k}_{1y} = k'_{2y} + ik''_{1y} \qquad (B.50)$$

In eqn. (B. 34), the term

$$\frac{\dot{k}_{2y}}{\dot{\epsilon}_2} = \frac{k'_{2y} + ik''_{2y}}{\epsilon'_2 + i\epsilon''_2} \cdot \frac{\epsilon'_2 - i\epsilon''_2}{\epsilon'_2 - i\epsilon''_2} = \frac{k'_{2y}\epsilon'_2 + k''_{2y}\epsilon''_2}{|\dot{\epsilon}_2|^2} +$$

$$i \frac{(k''_{2y}\epsilon'_2 - k'_{2y}\epsilon''_2)}{|\dot{\epsilon}_2|^2} \qquad (B.51)$$

In eqn. (B.35), the term

$$\dot{k}_{3y} = k'_{3y} + ik''_{3y} \qquad (B.52)$$

Now eqns. (B.30) through (B.35) can be written as.

$$\langle s_{x1} \rangle = \frac{k'_x \, e^{-2k''_{3y}h}}{2\omega\varepsilon_4 \left[|r_{23}|^2 + 2r'_{23} + 1 \right]} \left[|\dot{r}_{23}|^2 \, e^{-2k''_{2y}h} + e^{2k''_{2y}h} \right.$$

$$\left. + 2(r'_{23} \cos(2k'_{2y}h) - r''_{23} \sin(2k'_{2y}h)) \right] \cdot e^{-2k''_{1y}y} \qquad \text{(B.53)}$$

$$\langle s_{x2} \rangle = \frac{(k'_x\varepsilon'_2 + k''_x\varepsilon''_2) \, e^{-2k''_{3y}h}}{2\omega|\dot{\varepsilon}_2|^2(|\dot{r}_{23}|^2 + 2r'_{23} + 1)} \left[|\dot{r}_{23}|^2 \, e^{-2k''_{2y}(h+y)} \right.$$

$$\left. + e^{2k''_{2y}(h+y)} + 2(r'_{23} \cos[2k'_{2y}(h+y)] - r''_{23} \sin[2k'_{2y}(h+y)]) \right] \qquad \text{(B.54)}$$

$$\langle s_{x3} \rangle = \frac{k'_x \, e^{2k''_{3y}y}}{2\omega\varepsilon_3} \qquad \text{(B.55)}$$

Assuming $|A_3|^2 = 1$ and at $x = 0$. with the same assumption for the y - components.

$$\langle s_{y1} \rangle = \left(\frac{k'_{1y} \, e^{-2k''_{3y}h}}{2\omega\varepsilon_1 \left[|\dot{r}_{23}|^2 + 2r'_{23} + 1 \right]} \right) \left[|\dot{r}_{23}|^2 \, e^{-2k''_{2y}h} + \right.$$

$$\left. + e^{2k''_{2y}h} + 2(r'_{23} \cos(2k'_{2y}h) - r''_{23} \sin(2k'_{2y}h)) \right] \cdot e^{-2k''_{1y}y} \qquad \text{(B.56)}$$

$$\langle S_{y2} \rangle = \frac{e^{-2k''_{3y}h}}{2\omega|\dot{\varepsilon}_2|^2 \left[|\dot{r}_{23}|^2 + 2r'_{23} + 1 \right]} \left[(k'_{2y}\varepsilon'_2 + k''_{2y}\varepsilon''_2) \right.$$

$$\cdot \left(|r_{23}|^2 \, e^{-2k''_{2y}(h+y)} - e^{2k''_{2y}(h+y)} \right) + 2 (k'_{2y}\varepsilon''_2 - k''_{2y}\varepsilon'_2)$$

$$\left. \cdot (r'_{23} \sin \left[2k'_{2y}(h+y) \right] + r''_{23} \cos \left[2k'_{2y}(h+y) \right]) \right] \qquad (B.57)$$

$$\langle S_{y3} \rangle = \frac{-k'_{3y} \, e^{2k''_{3y}y}}{2\omega\varepsilon_3} \qquad (B.58)$$

Integrating, over y from $-\infty$ upto $+\infty$, the x - components of the power flow, the total cycle-average power flow in each medium comes out as

$$\langle P_{1x} \rangle = \int_0^\infty \langle S_{1x} \rangle dy$$

$$= \frac{k'_x \, e^{-2k''_{3y}h}}{4\omega\varepsilon_1 k''_{1y} \left[|\dot{r}_{23}|^2 + 2r'_{23} + 1 \right]} \left[|\dot{r}_{23}|^2 \, e^{-2k''_{2y}h} + \right.$$

$$\left. + e^{2k''_{2y}h} + 2 \left(r'_{23} \cos(2k'_{2y}h) - r''_{23} \sin(2k'_{2y}h) \right) \right] \qquad (B.59)$$

$$\langle P_{2x} \rangle = \int_h^0 \langle S_{2x} \rangle \, dy$$

$$= \frac{(k'_x\varepsilon'_2 + k''_x\varepsilon''_2) \, e^{-2k''_{3y}h}}{2\omega|\dot{\varepsilon}_2|^2 \left[|\dot{r}_{23}|^2 + 2r'_{23} + 1 \right]} \left[\frac{1}{2k''_{2y}} \left(e^{2k''_{2y}h} - 1 \right) \right.$$

$$\left. - |\dot{r}_{23}|^2 \left(e^{-2k''_{2y}h} - 1 \right) \right] + \frac{1}{k'_{2y}} \left[r'_{23} \sin(2k'_{2y}h) + r''_{23} \right.$$

$$\left. \cdot \left(\cos(2k'_{2y}h) - 1 \right) \right] \right] \qquad (B.60)$$

$$\langle P_{3x} \rangle = \int_{-\infty}^{-h} \langle s_{3x} \rangle \, dy$$

$$= \frac{k'_x \, e^{-2k''_{3y} h}}{4\omega\epsilon_3 k''_{3y}} \qquad \text{(B.61)}$$

REFERENCES

1) C.j. Powell, J.B. Swan: Phys. Rev. 118,640 (1960)

2) W.P. Chen, J.M. Chen: JOSA 71, 189 (1981)

3) F. Yang, Zh.Coo, J. Fang; Appl. Opt., V.27, Vl, 11(1988)

4) I. Pockrand: Surf. Science 72, 577 (1978)

5) W.P. Chen, J.M. Chen: Surf. Science, V.91, 601 (1980)

6) D.SArid, Long-range surface Plasma waves on very thin metal films; Phys. Rev. Lett; V.47, N26, 1927 (1981)

7) J.C. Quail, J.G. Rako, J.J. Simon: Phys. Rev. Lett. 50, 1987 (1983)

8) Kovener G.S., Alexander R.W., Bell R.J.: Phys. Rev. B - Solid State, Vol. 14, 1458 (1976)

9) H. Raether: " Surface Plasmons on Smooth and Rough Surfaces and on Gratings", Springer Tracts in Modern Physics, Vol. 111 (Springer - verlag, Berlin, Heidelberg, New York, London, Paris, Tokyo, 1988)

10) R.F. Wallis and G.I. Stegeman (Editors): "Electromagnetic Surface Excitations", Springer Series on wave phenomena 3; Proceedings of an International Summer School at the Ettore

Majorana Centre, Erice, Italy, July 1-13, 1985 (Springer - Verlag, Berlin, Heidelberg, New York, TOKYO 1986)

11) T. Lopez - Rios, G. Vuye: "Use of Surface Plasmon excitation for determination of the thickness and Optical constants of very thin surface layers", Surf. Sci. 81, 529 (1978).

12) R.H. Ritchie: Phys. Rev 106, 874 (1957)

13) Abdurahman Ahmed, D.Letov : M.Sc. Thesis (Unpublished), Addis Ababa University (1989).

14) E.T. Arakawa, M.W. Williams, R.N. Hamm, R.H. Ritchie: Phys. Rev. Lett., v.31, N18, 1127 (1973)

15) M. VanExter, A. Lageudijh: Phys. Rev. Lett., v. 60, N1, 49 (1988)